

IRIDIUM CARBONYL COMPLEXES AS MODEL HOMOGENEOUS CATALYSTS

by

ILANA ENGELBRECHT

A dissertation submitted to meet the requirements for the degree of

MAGISTER SCIENTIAE

in the

DEPARTMENT OF CHEMISTRY

FACULTY OF NATURAL- AND AGRICULTURAL SCIENCES

at the

UNIVERSITY OF THE FREE STATE

SUPERVISOR: PROF. ANDREAS ROODT

CO-SUPERVISOR: PROF. HENDRIK G. VISSER

MAY 2010

ACKNOWLEDGEMENTS

Firstly all the glory and honour to my Heavenly Father who equipped me with wisdom, insight and perseverance to make my success possible. Thank you for the countless blessing that You have bestowed on me for I am nothing without You.

Thank you to Prof. Roodt for all the opportunities, patience and endless enthusiasm for chemistry inspiring me to learn as much as I can. It is truly an honour to be known as one of your students.

To Prof. Deon Visser, thank you for all your guidance and encouragement. Your never-ending patience and willingness to give advice is what kept me motivated throughout my studies.

Thank you to all my colleagues in the Inorganic group for all the laughter and jokes. Thank you for sharing your knowledge and for your patience when having to explain something several times! Every one of you contributed to this study in some way and for that I thank you!

To my parents, Barend and Salomé Engelbrecht, without your love, continuous encouragement and sacrifices none of this would be possible. I am truly grateful for everything you have done for me over the years. To my sister, Sarina, your eccentric personality and enthusiasm has made my life an absolute adventure and without your support and “full moon” character trait I would not be the person I am today. Thank you to my grandmother, Sarah Nel, for all your motivational messages and teaching me never to lose faith.

Financial assistance from the Department of Science and Technology (DST) of South Africa, NRF (National Research Foundation), DST-NRF centre of excellence (c*change) and the University of the Free State are gratefully acknowledged.

- The distance between insanity and genius is measured only by success -

TABLE OF CONTENTS

Abbreviations and Symbols	V
Abstract	VI
Opsomming	VIII

Chapter 1

Introduction and Aim

1.1 Introduction	1
1.2 Ligand Systems in Homogeneous Catalysis	3
1.3 Aim of Study	4

Chapter 2

Theoretical Aspects of Homogeneous Catalysis

2.1 Introduction	6
2.2 Transition Metal Catalysts	7
2.3 Iridium in Organometallic Chemistry	8
2.4 Homogeneous Catalysis	9
2.5 General Steps in Homogeneous Catalytic Cycle Mechanisms	11
2.5.1 Creating a “vacant site”	11
2.5.2 Oxidative Addition and Reductive Elimination	12
2.5.2.1 Three-centre Concerted Process	14
2.5.2.2 S _N ² -type Mechanism	14
2.5.2.3 Radical Mechanism	15
2.5.2.4 Ionic Mechanism	16
2.5.3 Migratory Insertion	16
2.6 Ligand Effects	17
2.6.1 Electronic Effect, ν	17
2.6.2 Steric Effect, θ	18
2.7 Homogeneous Catalytic Systems	19
2.7.1 Hydroformylation	19

TABLE OF CONTENTS

2.7.2	Hydrogenation	24
2.7.2.1	Rhodium as Catalyst	24
2.7.2.2	Iridium as Catalyst	26
2.7.3	Carbonylation	31
2.7.3.1	Cobalt Catalysed BASF Process	33
2.7.3.2	Rhodium Catalysed Monsanto Process	36
2.7.3.3	Iridium Catalysed CATIVA™ Process	38

Chapter 3

Basic Theory of Solid and Solution State Characterisation

3.1	Introduction	41
3.2	Infrared Spectroscopy (IR)	41
3.3	Ultraviolet-visible Spectroscopy (UV-vis)	43
3.4	X-Ray Diffraction (XRD)	44
3.4.1	Bragg's Law	45
3.4.2	Structure Factor	47
3.4.3	'Phase Problem'	48
3.4.3.1	Direct Method	48
3.4.3.2	Patterson Function	48
3.4.4	Least Square Refinement	49
3.5	Theoretical Aspects of Chemical Kinetics	50
3.5.1	Introduction	50
3.5.2	Reaction Rates and Rate Laws	50
3.6	Nuclear Magnetic Resonance (NMR) Spectroscopy	53

Chapter 4

Syntheses of Iridium(I) Compounds

4.1	Introduction	57
4.2	Chemicals and Apparatus	58
4.3	Synthetic Procedures	58
4.3.1	Syntheses of Starting Compounds	59

TABLE OF CONTENTS

4.3.1.1	Synthesis of di- μ -chlorido-bis(1,5-cyclooctadiene) diiridium(I) ($[\text{Ir}(\text{Cl})(\text{cod})_2]_2$)	59
4.3.1.2	Synthesis of (acetylacetonato)(1,5-cyclooctadiene) iridium(I) ($[\text{Ir}(\text{acac})(\text{cod})]$)	59
4.3.1.3	Synthesis of (acetylacetonato)(dicarbonyl)iridium(I) ($[\text{Ir}(\text{acac})(\text{CO})_2]$)	60
4.3.2	Syntheses of <i>trans</i> - $[\text{Ir}(\text{acac})(\text{CO})(\text{PR}_3)_2]$ Compounds	60
4.3.2.1	Synthesis of <i>trans</i> - $[\text{Ir}(\text{acac})(\text{CO})(\text{PPh}_3)_2]$	60
4.3.2.2	Synthesis of <i>trans</i> - $[\text{Ir}(\text{acac})(\text{CO})(\text{PPh}_2\text{Cy})_2]$	61
4.3.2.3	Synthesis of <i>trans</i> - $[\text{Ir}(\text{acac})(\text{CO})(\text{PPhCy}_2)_2]$	61
4.3.2.4	Synthesis of <i>trans</i> - $[\text{Ir}(\text{acac})(\text{CO})(\text{PCy}_3)_2]$	62
4.4	Discussion	62

Chapter 5

Crystal Structure Determination of Complexes

5.1	Introduction	67
5.2	Experimental	67
5.3	Crystal Structure Determination of <i>trans</i> - $[\text{Ir}(\text{acac}-\kappa\text{O})(\text{CO})(\text{PPhCy}_2)_2]$	70
5.4	Crystal Structure Determination of <i>trans</i> - $[\text{Ir}(\text{acac}-\kappa^2\text{O},\text{O})(\text{CO})(\text{PCy}_3)_2]$	76
5.5	Discussion	84

Chapter 6

Kinetics of Rapid Substitution of CO by Tertiary Phosphine Ligands

6.1	Introduction	88
6.2	General Considerations	89
6.3	Calculations	89
6.4	Results and Discussion	91
6.4.1	Experimental Procedures	91
6.4.2	Preliminary Analysis of Rate Data Obtained <i>via</i> Stopped-Flow Techniques	96
6.5	Overall Reaction Mechanism	102
6.6	Conclusion	103

TABLE OF CONTENTS

Chapter 7*Evaluation of Study*

7.1	Introduction	106
7.2	Scientific Relevance and Results Obtained	106
7.3	Future Research	107
Appendix I: <i>Supplementary Data to the Crystal Structures</i>		109
Appendix II: <i>Supplementary Data to the Kinetic Study</i>		136

ABBREVIATIONS AND SYMBOLS

Abbreviation	Meaning
L,L'-Bid	Bidentate ligand
acac	Acetylacetonate
Cod	1,5-cyclooctadiene
Z	Number of molecules per unit cell
Å	Angstrom
XRD	X-ray diffraction
NMR	Nuclear magnetic resonance
KMR	Kern magnetise resonance
ppm	(Unit of chemical shift) parts per million
δ	Chemical shift
BP	British Petroleum
TM	Trade mark
IR	Infrared spectroscopy
ν	Stretching frequency on IR
MO	Molecular orbital
μ	Description of bridging
π	Pi
σ	Sigma
α	Alpha
β	Beta
γ	Gamma
σ^*	Sigma anti-bonding
λ	Wavelength
θ	Theta
$^\circ$	Degrees
M	(mol.dm ⁻³)
mM	millimol
(OPh) ₃	Triphenylphosphite
ΔH^\ddagger	Enthalpy of activation
ΔS^\ddagger	Entropy of activation
CO	Carbonyl
h	Planck's constant
k _B	Boltzman's constant
A	Absorbance
A _{obs}	Observed absorbance
k _x	Rate constant for a forward reaction
k _{-x}	Rate constant for a reverse reaction
K _x	Equilibrium constant for an equilibrium reaction
k _{obs}	Observed rate constant
Me	Methyl
Ph	Phenyl
Cy	Cyclohexyl
T or temp.	Temperature
UV	Ultraviolet region in light spectrum
Vis	Visible region in light spectrum
C ₆ D ₆	Deuterated benzene
C ₇ D ₈	Deuterated toluene

ABSTRACT

Key words: Iridium; Acetylacetonate; Phosphine; Substitution; Kinetics

The aim of this study was to investigate model iridium carbonyl complexes as homogeneous catalyst precursors for processes such as olefin hydroformylation. The hydroformylation of alkenes is one of the most important applications of transition metal based homogeneous catalysis. The coordination chemistry of rhodium and iridium phosphine complexes plays a major role in the understanding of basic organometallic reactions and homogenous catalytic processes.¹ The diversity of tertiary phosphines in terms of their Lewis basicity and bulkiness render them excellent candidates to tune the reactivity of square-planar complexes towards a variety of chemical processes, such as oxidative addition and substitution reactions.²

Iridium(I) complexes of the type *trans*-[Ir(acac)(CO)(PR₃)₂] (acac = acetylacetonate, PR₃ = PPh₃, PPh₂Cy, PPhCy₂, PCy₃) were synthesized and characterized by infrared (IR) and nuclear magnetic resonance spectroscopy (NMR). The X-ray crystallographic determinations of *trans*-[Ir(acac-κO)(CO)(PPhCy₂)₂] and *trans*-[Ir(acac-κ²O,O)(CO)(PCy₃)₂] were successfully completed and are compared with literature. Both complexes crystallize in monoclinic crystal systems, *C2/c*. Only *trans*-[Ir(acac-κO)(CO)(PPhCy₂)₂] co-crystallized with solvent molecules as part of the basic molecular unit cell, though these solvent molecules show no apparent impact on the steric packing of the basic organometallic group. This delivered information as to the identification of products formed during the kinetic studies and increased the available information of these rare compounds in literature.³

Two reactions were observed when rapid substitution of CO for PPh₃ in [Ir(acac)(CO)₂] was investigated in methanol as solvent by use of cryo temperature photo-multiplier Stopped-flow spectrophotometry. The first reaction followed the general rate law for square planar substitution reactions where rate = ($k_s + k_1[L]$)([substrate]) with *pseudo* first-order rate constant $k_{obs1} = k_s + k_1[L]$ and k_1 the second-order rate constant for the substitution reaction.

¹ R.S. Dickson, *Homogenous Catalysis with Compounds of Rhodium and Iridium*, Dordrecht, Holland: D. Reidel Publishing Co., 1985.

² W.A. Herrmann, *Applied Homogeneous Catalysis with Organometallic Compounds*, Weinheim: VCH, 1995.

³ Cambridge Structural Database (CSD), Version 5.30, May 2009 update, F.H. Allen, *Acta Cryst.*, 2002, **B58**, 380.

ABSTRACT

This indicated that the first step involves the substitution of one carbonyl group forming $[\text{Ir}(\text{acac})(\text{CO})(\text{PPh}_3)]$. Linear plots of k_{obs} against concentration of the incoming PPh_3 ligand passed through the origin implying that $k_s \approx 0$, signifying that the solvent does not significantly contribute to the reaction rate and the rate law simplifies to $k_{\text{obs}1} = k_1[\text{L}]$, with $k_1 = 92.5(3) \times 10^3$, $77(3) \times 10^3$, $66(1) \times 10^3$ and $58(2) \times 10^3 \text{ M}^{-1} \text{ s}^{-1}$ at -10 , -20 , -30 and -40 °C, respectively. The temperature dependence was determined with $\Delta H_{k_1}^\ddagger = 5.8(6) \text{ kJ mol}^{-1}$ and the large negative values obtained for standard entropy change of activation, $\Delta S_{k_1}^\ddagger = -127(2) \text{ J K}^{-1} \text{ mol}^{-1}$, suggests an associative substitution mechanism.

The second reaction is defined by limiting kinetic behaviour and is indicative of a two-step process involving the stepwise rapid formation of *trans*- $[\text{Ir}(\text{acac})(\text{CO})(\text{PPh}_3)_2]$ with pre-equilibrium $K_2 = 1(3) \times 10^2$, $4(1) \times 10^2$, $7(2) \times 10^2 \text{ M}^{-1}$ at -20 , -30 and -40 °C, respectively and rate-determining second step being the ring opening of the acac^- ligand to yield *trans*- $[\text{Ir}(\text{acac-}\kappa\text{O})(\text{CO})(\text{PPh}_3)_2]$ with $k_3 = 18(5) \times 10^1$, $10(1) \times 10^1$, $4.7(4) \times 10^1 \text{ M}^{-1} \text{ s}^{-1}$ at -20 , -30 and -40 °C, respectively. The temperature dependence for the second reaction was determined with $\Delta H_{k_3}^\ddagger = 30.8(3) \text{ kJ mol}^{-1}$ and $\Delta S_{k_3}^\ddagger = -79(1) \text{ J K}^{-1} \text{ mol}^{-1}$.

OPSOMMING

Sleutelwoorde: *Iridium; Asetielasetonaat; Fosfien; Substitusie; Kinetika*

Die doel van hierdie studie was om model iridium-karboniel komplekse as homogene katalisvoorlopers in prosesse soos olefien hidroformilering te ondersoek. Die hidroformilering van alkene is een van die belangrikste toepassings van oorgangsmetaalgebaseerde homogene katalise. Die koördinasiechemie van rodium- en iridium-fosfien komplekse speel 'n belangrike rol in die verstaan van basiese organometaliese reaksies vir homogene katalitiese prosesse. Die verskeidenheid van tersiêre fosfiene in terme van hulle Lewis basisiteit en bonkigheid maak hulle uitstekende kandidate om die reaktiwiteit van vierkantig-planêre komplekse te verstel ten opsigte van 'n verskeidenheid chemiese prosesse soos oksidatiewe addisie en substitusie reaksies.

Iridium(I) komplekse van die tipe $trans\text{-}[\text{Ir}(\text{acac})(\text{CO})(\text{PR}_3)_2]$ (acac = asetielasetonaat, PR_3 = PPh_3 , PPh_2Cy , PPhCy_2 , PCy_3) is gesintetiseer en gekarakteriseer deur infrarooi (IR) en kern magnetiese resonans spektroskopie (KMR). Die X-straal kristallografiese bepaling van $trans\text{-}[\text{Ir}(\text{acac-}\kappa\text{O})(\text{CO})(\text{PPhCy}_2)_2]$ en $trans\text{-}[\text{Ir}(\text{acac-}\kappa^2\text{O,O})(\text{CO})(\text{PCy}_3)_2]$ is suksesvol voltooi en vergelyk met literatuur. Beide komplekse kristalliseer in monokliniese kristalstelsels, $C2/c$. Slegs $trans\text{-}[\text{Ir}(\text{acac-}\kappa\text{O})(\text{CO})(\text{PPhCy}_2)_2]$ ko-kristalliseer met oplosmiddel molekule as deel van die basiese molekulêre eenheidsel; hierdie oplosmiddel molekule het egter geen ooglopende impak op die steriese pakking van die basiese organometaliese groep nie. Dit lewer inligting ten opsigte van die identifisering van produkte wat gedurende die kinetiese studies gevorm is en verhoog die beskikbare inligting van hierdie skaars verbindings in die literatuur.

Twee reaksies is waargeneem tydens die ondersoeke van vinnige substitusie van CO met PPh_3 in $[\text{Ir}(\text{acac})(\text{CO})_2]$ in metanol as oplosmiddel deur middel van lae temperatuur foto-vermenigvuldiger gestopde-vloei spektrofotometrie. Die eerste reaksie volg die algemene tempowet vir vierkantig-planêre substitusiereaksies waar $Tempo = (k_s + k_1[\text{L}])([\text{substraat}])$ met *pseudo* eerste-orde tempokonstante $k_{\text{obs1}} = k_s + k_1[\text{L}]$ en k_1 die tweede-orde tempokonstante vir die substitusiereaksie. Dit dui aan dat die eerste stap die substitusie van een karbonielgroep om $[\text{Ir}(\text{acac})(\text{CO})(\text{PPh}_3)]$ te vorm behels. Liniêre grafieke van k_{obs}

OPSOMMING

teenoor konsentrasie van die inkomende PPh_3 ligand gaan deur die oorsprong, wat impliseer dat $k_s \approx 0$ en aandui dat die oplosmiddel nie beduidend bydra tot die reaksietempo nie en dat die tempowet vereenvoudig na $k_{\text{obs1}} = k_1[\text{L}]$, met $k_1 = 92.5(3) \times 10^3$, $77(3) \times 10^3$, $66(1) \times 10^3$ en $58(2) \times 10^3 \text{ M}^{-1} \text{ s}^{-1}$ by -10 , -20 , -30 en -40 °C, onderskeidelik. Die temperatuurafhanklikheid is bepaal met $\Delta H_{k_1}^\ddagger = 5.8(6) \text{ kJ mol}^{-1}$ en die groot negatiewe waardes verkry vir standaard verandering van aktiveringsentropie, $\Delta S_{k_1}^\ddagger = -127(2) \text{ J K}^{-1} \text{ mol}^{-1}$, stel 'n assosiatiewe substitusie meganisme voor.

Die tweede reaksie word gedefinieer deur beperkende kinetiese gedrag en is aanduidend van 'n twee-stap proses wat betrokke is by die stapsgewyse vinnige vorming van *trans*- $[\text{Ir}(\text{acac})(\text{CO})(\text{PPh}_3)_2]$ met pre-ekwilibrium $K_2 = 1(3) \times 10^2$, $4(1) \times 10^2$, $7(2) \times 10^2 \text{ M}^{-1}$ teen onderskeidelik -20 , -30 en -40 °C en 'n tempobepalende tweede stap wat die ring-opening van die *acac*⁻ ligand behels om te lei tot *trans*- $[\text{Ir}(\text{acac-}\kappa\text{O})(\text{CO})(\text{PPh}_3)_2]$ met $k_3 = 18(5) \times 10^1$, $10(1) \times 10^1$, $4.7(4) \times 10^1 \text{ M}^{-1} \text{ s}^{-1}$ teen onderskeidelik -20 , -30 en -40 °C. Die temperatuurafhanklikheid vir die tweede reaksie is bepaal met $\Delta H_{k_3}^\ddagger = 30.8(3) \text{ kJ mol}^{-1}$ en $\Delta S_{k_3}^\ddagger = -79(1) \text{ J K}^{-1} \text{ mol}^{-1}$.

1

INTRODUCTION AND AIM

1.1 INTRODUCTION

Iridium (Ir), named after *iris*, the Greek term meaning *rainbow*, due to its highly coloured salts, is a transition metal with atomic number 77. It was discovered by Smithson Tennant in 1803 when he studied the black *aqua regia* insoluble residue of crude platinum.¹ Iridium is not attacked by *aqua regia* nor by any of the acids, but certain molten salts, such as NaCl and NaCN, are corrosive towards iridium. It is extremely hard and the most corrosion-resistant metal known, making it very hard to machine, form, or to work with.

Iridium occurs uncombined in nature with platinum and other metals of this family and is recovered as a by-product from the nickel mining industry. Natural iridium contains two stable isotopes, ¹⁹¹Ir and ¹⁹³Ir with a natural abundance of 37.3 % and 62.7 %, respectively. Iridium is the densest element known apart from osmium and many applications of this metal rely on its inertness. Iridium has found use in making crucibles and apparatus for application at high temperatures, electrical coating and as a hardening agent for platinum.² The inert alloy with osmium is traditionally used in fountain pen nibs. Other applications include the nuclear, defence and space industries.

Iridium can exist in a variety of oxidation states from -1 ($[\text{Ir}(\text{CO})_3(\text{PPh}_3)]^-$) to +6 ($[\text{IrF}_6]$), with the most common oxidation states being +3 and +4.³ Ir(I) oxidation state has a d^8 electron configuration and usually forms either square-planar 4-coordinated or trigonal bipyramidal 5-coordinated complexes that are stabilized by π -bonding ligands such as tertiary phosphines or carbonyl groups. The vast majority of the Ir(III) oxidation state, with d^6 electron configuration, have 6-coordinated octahedral geometries¹ and are commonly the product of

¹ D.N. MacLennan, E.J. Simmonds, *Chemistry of Precious Metals*, Weinheim: Chapman & Hall, 1992.

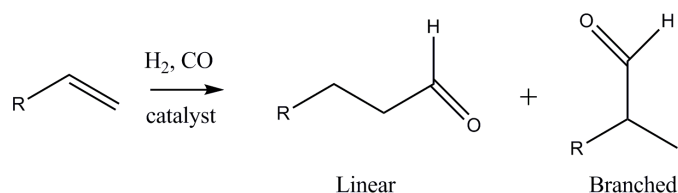
² D.R. Lide, *Handbook of Chemistry and Physics*, Boca Raton, FL: CRC Press, 2005.

³ N.N. Greenwood, *Chemistry of the Elements*, 2nd Ed., Oxford: Butterworth-Heinemann, 1997.

oxidative addition of Ir(I) complexes. Rhodium was discovered in the same year as iridium and share many resemblances in their chemistry.

Catalysis is relevant in many processes of the industrial production of liquid fuels and bulk chemicals, whilst the number of homogeneously catalysed processes has been steadily growing in the eighties and nineties. A commercially essential example of homogeneous catalysis is the synthesis of acetic acid *via* carbonylation of methanol. Earlier processes were based on primarily cobalt as metal catalyst⁴, $[\text{HCo}(\text{CO})_4]$, which reacted under harsh reaction conditions. The process evolved from using cobalt (BASF process) to rhodium,^{5,6} $[\text{RhI}_2(\text{CO})_2]^-$, (Monsanto process) and was then further developed to the iridium CativaTM process, $[\text{IrI}_2(\text{CO})_2]^-$.⁷ The variation of metals combined with ligand modification, resulted in milder reaction conditions and increasing yield and selectivity for the formation of the desired products.⁸

Another large-scale industrial process is hydroformylation, discovered by Otto Roelen in 1938, which comprises the functionalisation of hydrocarbons to aldehydes by addition of a hydrogen atom and formyl (CHO) group to a C=C double bond of an olefin; the reaction is also referred to as the *oxo reaction* in older literature.^{9,10}



Scheme 1-1: Hydroformylation reaction comprising of the addition of a hydrogen atom and CHO group to a C=C double bond of an olefin.

The ratio of linear and branched product formation is of particular interest and factors such as kinetic manipulation or ligand choice, which control the linearity and selectivity, are often

⁴ D. Forster, M. Singleton, *J. Mol. Catal.*, 1982, **17**, 299.

⁵ P.M. Maitlis, A. Haynes, G.J. Sunley, M.J. Howard, *J. Chem. Soc., Dalton Trans.*, 1996, 2187.

⁶ F.E. Paulik, J.F. Roth, *J. Chem. Soc., Chem. Commun.*, 1968, 1578.

⁷ G.J. Sunley, D.J. Watson, *Catalysis Today*, 2000, **58** (4), 293.

⁸ B. Cornils, W.A. Herrmann, *Applied Homogeneous Catalysis with Organometallic Compounds*, New York: VCH publishers, 1996.

⁹ F.A. Cotton, G. Wilkinson, C.A. Murillo, M. Bockmann, *Advanced Inorganic Chemistry*, 6th Ed, New York: John Wiley & Sons, Inc., 1999.

¹⁰ P.W.N.M. Van Leeuwen, *Homogeneous Catalysis: Understanding the Art*, Dordrecht: Kluwer Academic Publishers, 2004.

investigated extensively.¹¹ The catalysts applied in hydroformylation are based, as in methanol carbonylation, on cobalt and rhodium. The original reaction used cobalt as catalyst which resembles the one described for the methanol carbonylation process. A Shell modification adding trialkylphosphine to the cobalt catalyst increased selectivity for linear aldehydes and allowed lower reaction pressures, but gave lower activity and increased hydrogenation. Rhodium is most active as catalyst and has completely replaced cobalt in the hydroformylation process. The rhodium catalyst is distinctly different from the Monsanto catalyst, with the key to selectivity towards linear products being the use of high concentrations of triphenylphosphine with the Rh catalyst, $[\text{RhH}(\text{CO})(\text{PPh}_3)_3]$.^{12,13}

Relatively few hydroformylation studies utilize iridium complexes as active catalysts, nevertheless such systems are of use as stable models for studying reaction intermediates.^{14,15,16,17,18,19} These are just a few examples of catalysts which use iridium and phosphorus ligands as an essential part of the catalytic system.

1.2 LIGAND SYSTEMS IN HOMOGENEOUS CATALYSIS

β -diketonato systems form a wide variety of complexes, for example the oxygen donor atoms of which the acetylacetonato bidentate ligand is very common. Carbon monoxide has strong π -accepting and moderate σ -donor properties and can therefore act both as a ligand and a reactant. A very useful property of carbon monoxide as a ligand is that it can be studied by infrared spectroscopy (IR), and *in situ* IR, in a frequency between 1800 – 2200 cm^{-1} .

The steric and electronic properties of phosphine ligands can be altered over a wide range by changing the substituents on the ligand. Phosphorus ligands can electronically either be strong π -acceptors (e.g. fluoroalkoxide substituents) or strong σ -donors (e.g. t-Bu

¹¹ B.J. Fisher, R. Eisenberg, *Inorg. Chem.*, 1984, **23**, 3216.

¹² F.H. Jardine, J.A. Osborn, G. Wilkinson, J.F. Young, *Chem. Ind. (London)*, 1965, 560; *J. Chem. Soc. (A)*, 1966, 1711.

¹³ T. Matsubara, N. Koga, Y. Ding, D.G. Musaev, K. Morokuma, *Organometallics*, 1997, **16**, 1065.

¹⁴ M.A. Moreno, M. Haukka, T.A. Pakkanen, *J. Catal.*, 2003, **215**, 326.

¹⁵ R. Whyman, *J. Organomet. Chem.*, 1975, **94**, 303.

¹⁶ C. Godard, S.B. Duckett, C. Henry, S. Polas, R. Toose, A.C. Whitwood, *Chem. Commun.*, 2004, 1826.

¹⁷ R. Eisenberg, D.J. Fox, S.B. Duckett, C. Flaschenriem, W.W. Brennessel, J. Schneider, A. Gunay, *Inorg. Chem.*, 2006, **45**, 7197.

¹⁸ C.M. Crudden, H. Alper, *J. Org. Chem.*, 1994, **59**, 3091.

¹⁹ E. Mieczynska, A.M. Trzeciak, J.J. Ziołkowski, I. Kownacki, B. Marciniak, *J. Mol. Catal. A*, 2005, **237**, 246.

substituents). Phosphines PR_3 ($\text{R} = \text{C}_6\text{H}_5, n\text{-C}_4\text{H}_9$), triphenylphosphine oxide and in some special cases organophosphites are the predominant ligands used in industrial hydroformylation reactions. Organophosphites are strong π -acceptors and form stable complexes with electron rich transition metals. Lower reaction rates in the oxo reaction were observed with nitrogen-containing ligands such as amides, amines or isonitrils, due to their stronger coordination to the metal centre.⁸ Nitrogen groups containing electron-withdrawing acyl- or sulfone groups form good π -acceptor phosphorus amidites.²⁰ An electron-poor phosphorus ligand can be formed when pyrrole is used as a substituent at the phosphorus atom.²¹ In general, phosphites and phosphorus amidites are more easily prepared than phosphines and they allow a greater variation in structure and properties.²²

It is clear that by changing the substituents at the phosphorus atom the electronic and steric properties of the coordinating ligand can be altered significantly. Approximately 250 papers and patent applications appear annually in the area of hydroformylation, most dealing with new phosphine structures and their catalytic results.⁸ It is then understandable that phosphine ligands play a key role in understanding and constructing new catalytic systems.

1.3 AIM OF STUDY

It is clear from available literature that iridium(I) complexes play an important role in catalytic cycles, especially those containing phosphorus ligands. The magnitude of several tons of acetic acid produced by the CativaTM iridium process annually is evidence enough to clarify the importance of understanding the mechanism of iridium(I) reactions. In most cases a pre-catalyst is added in different metal to phosphorus ligand ratios which influences the formation of certain species in order for the more kinetically favourable catalysts to dominate. It is important to understand the delicate balance between different starting materials to ultimately identify the active species in the catalytic cycle.

In this study, model complexes of the general formula *trans*-[Ir(acac)(CO)(PR_3)₂] ($\text{PR}_3 = \text{PPh}_3, \text{PPh}_2\text{Cy}, \text{PPhCy}_2, \text{PCy}_3$) with possible catalytic properties were selected. The

²⁰ S.C. Van der Slot, P.C.J. Kamer, P.W.N.M. Van Leeuwen, J. Van Leeuwen, K. Goubitz, M. Lutz, A.L. Spek, *Organometallics*, 2000, **19**, 2504.

²¹ K.G. Moloy, J.L. Petersen, *J. Am. Chem. Soc.*, 1995, **117**, 7696.

²² D. Peña, A.J. Minnaard, J.G. de Vries, B.L. Feringa, *J. Am. Chem. Soc.*, 2002, **124**, 14552.

acetylacetonato moiety will limit isomers from forming due to the symmetrical nature of the bidentate ligand. A better understanding into the properties and coordination of the iridium(I) species was one of the overarching aims of this study.

With the above in mind, the following stepwise project goals were set for this study:

- Synthesis of model complexes with general formula *trans*-[Ir(acac)(CO)(PR₃)₂] (PR₃ = PPh₃, PPh₂Cy, PPhCy₂, PCy₃) to study the solid and solution state properties thereof.
- The crystallographic characterisation of *trans*-[Ir(acac-κO)(CO)(PPhCy₂)₂] and *trans*-[Ir(acac-κ²O,O)(CO)(PCy₃)₂] complexes to study the coordination mode, bond lengths and distortion of the phosphine moieties.
- Kinetic mechanistic investigation of the carbonyl substitution- and addition reactions in [Ir(acac)(CO)₂] as starting complex with PPh₃ as entering ligand.
- Analysis of results with respect to coordinating ability and comparison to other phosphine systems available in literature.

2

THEORETICAL ASPECTS OF HOMOGENEOUS CATALYSIS

2.1 INTRODUCTION

Thermodynamically favourable reactions may take place at room temperature, but might be too slow for commercial application. If that is the case it is ideal to use a catalyst, which increases the rate at which a chemical reaction approaches equilibrium without becoming itself permanently involved. A catalyst lowers the activation energy of the chemical reaction by providing an alternative pathway by which the reaction can proceed.

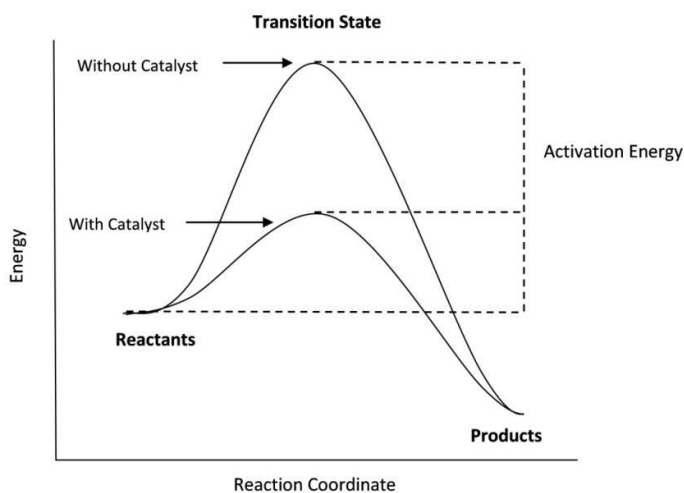


Figure 2-1: Reaction profile exemplifying the goal of a catalyst: the lowering of the activation energy of a process.

Homogeneous catalysis is a sequence of reactions that involve a catalyst in the same phase as the reactants. The organometallic catalyst consists of a central metal surrounded by organic and/or inorganic ligands. Catalyst properties are tailored by changing the ligand environment that in change effect crucial reaction properties such as the rate of the reaction and selectivity towards certain products.

Homogeneous transition metal catalysts draw great interest due to the combination of mild reaction conditions, high efficiency and great selectivity in the industrial and economic setting. It plays an important role in industrial processes such as hydrogenation, hydroformylation and carbonylation reactions.

2.2 TRANSITION METAL CATALYSTS

The metal centre and ligand/s used for a specific process in homogeneous catalysis need to be planned vigilantly. In changing the metal, the electronic character and size of the specific metal atom is altered. This implicates that different catalytic behaviours can be induced by utilising different metal atoms and that the same catalytic reaction can be promoted by different metals. Ligands thus also play a crucial role in complex design to direct certain properties of the metal complex.

The platinum group metals (PGM's)¹ – platinum, ruthenium, rhodium, palladium, osmium, iridium – are “d” block elements with partly filled *d* or *f* shells in any of their chemically important oxidation states. The empty *d* orbitals offer the possibility of binding suitable neutral molecules to the metal centre. The outstanding properties of these PGMs include high melting points, high lustre, resistance to corrosion as well as catalytic tendencies used in the chemical, electrical and petroleum refining industries.

The earliest commercial premier location of these PGM sources was in the Urals near Ekaterinburg, with major source today in South Africa.² The platinum metals tend to occur in the same mineral desposits,³ and generally with small amounts of gold, copper, silver, nickel, iron, and other metals. They often occur as natural alloys such as osmiridium which consists of iridium, osmium and small amounts of the other metals. The ore is concentrated by gravitation and flotation and then smelted with coke, lime and sand. The resulting Ni-Cu sulphide “matte” is cast into anodes. Upon electrolysis in sulphuric acid solution, copper is deposited at the cathode while nickel remains in solution. Nickel is recovered by electrodeposition and a mixture of PGMs, silver and gold collect in the anode slime.

¹ L.B. Hunt, F.M. Lever, *Platinum Metals Rev.*, 1969, **13** (4), 126.

² H.V. Eales, *A First Introduction to the Geology of the Bushveld Complex*, Pretoria: Council of GeoScience, 2001, 73.

³ D.C. Harris, L.J. Cabri, *The Canadian Mineralogist*, 1991, **29**, 231.

Ruthenium, osmium, rhodium and iridium are collected in the *aqua regia* insoluble residue and upon further complex separation procedures, rhodium and iridium are collected as pure compounds. Iridium is a very hard, lustrous, silvery-white metal and is the second densest element after osmium.⁴

The interest of iridium coordination compounds remain in the catalysis field and in its luminescent properties. Iridium compounds are in some instances the most active catalysts available and in the cases where it may not yield the most active catalysts, iridium complexes nevertheless yield important information about the structure and reactivity of important catalytic intermediates.

2.3 IRIDIUM IN ORGANOMETALLIC CHEMISTRY

Iridium is a third-row d-block metal and the heaviest element in group 9. In many respects, the chemistry of its compounds resembles that of rhodium. Iridium ranges in oxidation states from -1 [Ir(CO)₃(PPh₃)⁻] to +6 [IrF₆]. The most common oxidation states for rhodium and iridium are +1 and +3 and also substantially in +4 for iridium.⁵ Low oxidation state iridium species are usually stabilised by π -acceptor ligands such as CO ligands or P donor atoms, whereas high oxidation number coordination compounds are predominantly hexahalide ones. Ir(I) oxidation state with d^8 configuration is a 16-electron, “coordinatively unsaturated” species which predominantly favours a four-coordinate, square-planar stereochemistry, *trans*-[IrCl(CO)(PPh₃)₂]. Saturation requires five ligands, i.e. ten electrons, to the metal ion therefore five-coordinate, trigonal bipyramidal, [Ir(dppe)₂(CNMe)]⁺, species also occur. The majority of donor atoms bind to Ir(I) and oxidative addition reactions feature regularly. Complexes of Ir(III) oxidation state has a d^6 electron configuration with a six-coordinate, octahedral geometry. All the compounds have low-spin (t_{2g})⁶ configurations and a majority are colourless or pale yellow.

These complexes are usually prepared by the reduction of compounds such as RhCl₃·3H₂O and K₂IrCl₆ in the presence of the desired ligand. The use of a specific reductant is unnecessary since the ligand itself or alcoholic solvent is generally adequate. A substantial

⁴ F.R. Hartley, *Chemistry of the Platinum Group Metals: Recent Developments*, Amsterdam: Elsevier, 1991.

⁵ D.N. MacLennan, E.J. Simmonds, *Chemistry of Precious Metals*, Chapman & Hall, 1992.

quantity of Ir(I) and Rh(I) complexes are phosphines of which two in particular demand attention. They are Wilkinson's catalyst, $[\text{RhCl}(\text{PPh}_3)_3]$,^{6,7,8} and Vaska's compound, *trans*- $[\text{IrCl}(\text{CO})(\text{PPh}_3)_2]$,⁹ both essentially square planar.

Vaska's compound was first prepared by Angoletta¹⁰ and later correctly put together by Vaska and DiLuzio¹¹. It played a major role in the development and research of new homogeneous catalysts since the 1960s, because it readily undergoes oxidative addition with numerous substrates, such as H_2 , Cl_2 , HX , MeI and RCO_2H , to yield six-coordinated, octahedral Ir(III) complexes wherein the phosphine ligands are *trans* to each other in all cases. Vaska's compound subsequently became the ideal model compound for the study of transition metal complexes undergoing oxidative addition reactions.^{12,13} Replacing the Cl of Vaska's compound with H, Me or Ph, delivers products in which the phosphines are now *cis*. Various theoretical models have been suggested to account for this.¹⁴ Although addition of an uncharged ligand is unusual, with ligands such as CO and SO_2 no oxidation occurs and five-coordinated 18-electron Ir(I) products are formed.

2.4 HOMOGENEOUS CATALYSIS

The chemical industry is primarily based on the production of economically important chemicals through the catalytic combination of small molecules (C_2H_4 , CO, H_2 , H_2O and NH_3) to produce larger molecules (ethylene glycol, acetaldehyde, acetic acid and acrylonitrile)¹⁵. Homogeneous catalysis refers to a catalytic system in which the reactants and catalyst of the reaction is in the same phase, most often the liquid phase. Phase boundaries however do exist in heterogeneous catalysis.^{16,17} Homogeneous catalysis is more

⁶ J.A. Osborn, G. Wilkinson, J.F. Young, *Chem. Commun.*, 1965, 17.

⁷ J.A. Osborn, F.H. Jardine, J.F. Young, G. Wilkinson, *J. Chem. Soc. (A)*, 1966, 1711.

⁸ M.A. Bennett, P.A. Longstaff, *Chem. Ind. (London)*, 1965, 846.

⁹ L. Vaska, D. Rhodes, *J. Am. Chem. Soc.*, 1965, **87**, 4970.

¹⁰ M. Angoletta, *Gazz. Chim. Ital.*, 1959, **89**, 2359.

¹¹ L. Vaska, J.W. DiLuzio, *J. Am. Chem. Soc.*, 1961, **83**, 2784.

¹² L. Vaska, *Acc. Chem. Res.*, 1968, **1**, 335.

¹³ L. Vaska, J.W. Diluzio, *J. Am. Chem. Soc.*, 1962, **84**, 679.

¹⁴ M.J. Burk, M.P. McGrath, R. Wheeler, R.H. Crabtree, *J. Am. Chem. Soc.*, 1988, **110**, 50349.

¹⁵ K.F. Purcell, J.C. Kotz, *An Introduction to Inorganic Chemistry*, Philadelphia: Saunders College Publishing, 1980.

¹⁶ G.C. Bond, *Heterogeneous catalysis*, Oxford: Clarendon Press, 1974.

¹⁷ J.T. Richardson, *Principles of Catalyst Development*, New York: Plenum Press, 1989.

stereoselective, but heterogeneous catalysis is still used for most petrochemical processes.¹⁸ This is because heterogeneous catalysts are more stable at higher temperatures and are easily separated from the substrate phase. In homogeneous catalysis the catalytic cycle mechanism can be studied in much detail to deliberate the influencing steric and electronic properties of the catalyst, unlike heterogeneous catalysis. It is therefore possible to optimize the homogeneous catalyst by tailoring it through its chemical and structural basis.

Coordinative unsaturated square planar group 9 and 10 complexes can partake in a series of elementary reactions that are key steps in the catalytic synthesis of organic products.^{19,20}

In general, the key reactions of a catalytic cycle include:^{21,22}

- Creation of a “vacant site”.
- Olefin insertion.
- Carbonyl insertion.
- β -hydrogen elimination.
- Nucleophilic addition to coordinated ligands.
- Oxidative addition.
- Reductive elimination.
- *Cis* migration.

Some well-known examples of homogeneous catalytic processes are listed below and a few will be discussed in detail:

- The making of sulphuric acid *via* the old catalytic “lead chamber process”.²³
- Wacker synthesis of acetaldehyde from olefins using a PdCl₂ catalyst and air.^{24,25,26}
- Hydrocyanation of alkenes using nickel phosphite complexes.²⁷
- The BASF, Monsanto and Cativa catalysed carbonylation of methanol.^{28,29}

¹⁸ G.W. Parshall, R.E. Putscher, *J. Chem. Educ.*, 1986, **63**, 189.

¹⁹ F.A. Cotton, G. Wilkinson, *Advanced Inorganic Chemistry*, 5th Ed., New York: John Wiley & Sons, Inc., 1980.

²⁰ J. Halpern, *Inorg. Chim. Acta.*, 1980, **50**, 11.

²¹ W. Koga, K. Morokuma, *Chem. Rev.*, 1991, **91**, 823.

²² D.F. Schriver, P.W. Atkins, C.H. Langford, *Inorganic Chemistry*, 2nd Ed., Oxford University, Oxford, 1994.

²³ P.W.N.M. Van Leeuwen, *Homogeneous Catalysis: Understanding the Art*, Dordrecht: Kluwer Academic Publishers, 2004.

²⁴ J. Smidt, W. Hafner, R. Jira, J. Sedlmeier, R. Sieber, R. Rüttinger, H. Kojer, *Angew. Chem.*, 1959, **71**, 176.

²⁵ J. Smidt, W. Hafner, R. Jira, R. Sieber, J. Sedlmeier, A. Sabel, *Angew. Chem.*, 1962, **74**, 93.

²⁶ J.E. Baeckvall, B. Akermarck, S.O. Ljunggren, *J. Am. Chem. Soc.*, 1979, **101**, 2411.

²⁷ F.A. Cotton, G. Wilkinson, P.L. Gaus, *Basic Inorganic Chemistry*, 3rd Ed., New York: John Wiley & Sons, Inc., 1995.

- The hydrogenation of unsaturated compounds using Wilkinson's catalyst $\text{RhCl}(\text{PPh}_3)_3$, $\text{RhCl}_3(\text{Py})_3$ etc.³⁰
- Metathesis of alkenes with Schrock's and Grubbs' catalysts.^{31,32,33}

2.5 GENERAL STEPS IN HOMOGENEOUS CATALYTIC CYCLE MECHANISMS

2.5.1 Creating a "vacant site"

In a catalytic reaction the catalyst brings the reactants together and lowers the activation barrier of the reaction. In order to bring the reactants together a metal centre must have a vacant site. Catalysis thus begins with the creation of such a vacant site. In homogeneous catalysis solvent molecules will always be co-ordinated to the metal ion and the term "vacant site" is an inaccurate description.

A competition in complex formation arises between the substrate and other potential ligands present in the solution for they are both in excess. Often a negative order in one of the concentrations of the ligands present can be found in the rate expression of product formation. A way of looking at the creation of a vacant site and coordination of the substrate is the way by which substitution reactions are described. Two mechanisms are distinguished, associative and dissociative mechanisms. In the dissociative mechanism (Scheme 2-1) the bond between the metal and leaving ligand is broken and is the rate determining step. A solvent molecule then occupies the vacant site and is quickly replaced by the substrate molecule. In the associative ($\text{S}_{\text{N}}2$) mechanism (Scheme 2-2) a simultaneous bond breaking of the leaving ligand and bond formation of the metal and substrate occurs and is the most common mechanism in square planar group 9 and 10 complexes.

²⁸ C.E. Hickey, P.M. Maitlis, *J. Chem. Soc. Chem. Commun.*, 1984, 1609.

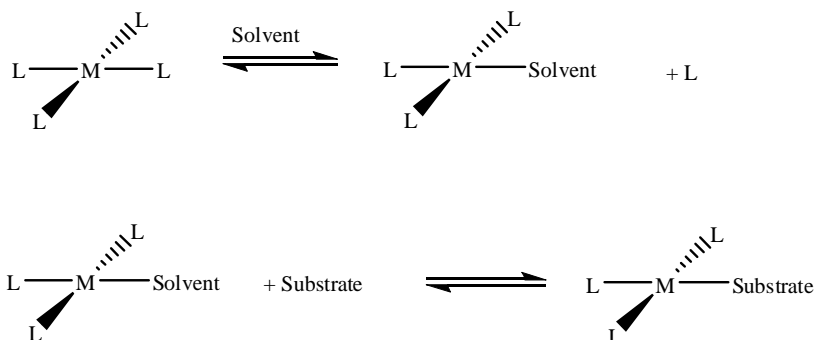
²⁹ C.M. Lukehart, *Fundamental Transition Metal Organometallic Chemistry*, California: Brooks/Cole Publishing Company, 1985.

³⁰ R.H. Crabtree, *The Organometallic Chemistry of the Transition Metals*, New York, John Wiley & Sons., 1988.

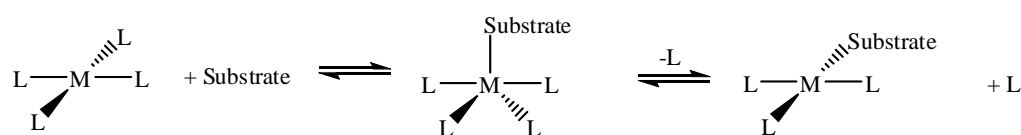
³¹ R.R. Schrock, J.S. Murdzek, G.C. Bazan, J. Robbins, M. DiMare, M. O'Regan, *J. Am. Chem. Soc.*, 1990, **112**, 3875.

³² R.H. Grubbs, *Tetrahedron*, 2004, **60**, 7117.

³³ R.H. Grubbs, S. Chang, *Tetrahedron*, 1998, **54**, 4413.



Scheme 2-1: Dissociative ligand exchange in square planar substitution reactions.



Scheme 2-2: Associative ligand exchange in square planar substitution reactions.

2.5.2 Oxidative Addition and Reductive Elimination

An oxidative addition (O.A.) reaction is a reaction where a substrate molecule XY adds to a metal complex. The original XY bond dissociates and two new bonds are formed, metal-X and metal-Y. X and Y are reduced and both have a -1 charge, therefore the formal oxidation state as well as the co-ordination number of the metal is raised by two. The substrate molecule usually has a highly polarized X-Y bond, or a very reactive, low-energy bond between highly electronegative atoms.²⁹

A number of computational studies on transition state geometries for addition of H₂, H-C and C-C bonds to transition metal complexes have been done.³⁴ A 16-electron square planar complex can thus be converted into an octahedral 18-electron species.²⁸ The most recognizable bond types that can undergo oxidative addition to low valence transition metal complexes are: H-H, C-H, Si-H, S-H, X-H (X = halogen), N-H, O-H, C-C, C-X, X-X and C-O. Oxidative addition is the initiating step for many catalytic reactions.

³⁴ C.L. Randolph, M.S. Wrighton. *J. Am. Chem. Soc.*, 1986, **108**, 3366.

Nonbonding electron density must be present on the metal along with two vacant coordination sites in order for oxidative addition reactions to proceed. The metal must also have stable oxidation states separated by two oxidation numbers. Metal complexes with d^8 and d^{10} electron configuration are the most intensively studied reactions for transition metals, notable Fe^0 , Ru^0 , Os^0 , Rh^I , Ir^I , Ni^0 , Pd^0 , Pt^0 , Pd^{II} and Pt^{II} . Square-planar type *trans*- $[\text{IrX}(\text{CO})(\text{PR}_3)_2]$ complexes are one of the most studied species because the equilibria lies well to the oxidised side and the resulting octahedral compounds are stable.

Ligands have tremendous influence on oxidative addition reactions. Ligands increasing the electron density of the metal, therefore σ -donating ligands, increases the rate of oxidative addition and better π -accepting ligands, slows down the oxidative addition rate. Sterically bulky ligands, e.g. $\text{PEt}(\text{t-Bu})_2$ tend to favour the forward reaction, but the substitution of an *o*-methoxy group on a phenylphosphine increases the nucleophilicity of the metal by donation.³⁵

A variety of mechanisms for oxidative addition to four-coordinate d^8 metal complexes exist and no straightforward generalisations can be made. Numerous reaction conditions may influence oxidative addition reactions, e.g. solvent polarity, temperature and trace amounts of oxidising impurities. A particular substrate can also react *via* a different pathway with different metal complexes. The following mechanisms are most commonly proposed:

- Three-centre concerted processes.
- $\text{S}_{\text{N}}2$ -type mechanism.
- Free radical mechanism.
- Ionic mechanism.

Reductive elimination (R.E.) is the reverse of oxidative addition, namely the formal valence state of the metal and total electron count of the complex is reduced by two with the elimination of ligands.³⁶ Reductive eliminations can be promoted by stabilisation of the low-valent state of the product by means of ligands that are good π -acceptors or sterically bulky.

³⁵ E.M. Miller, B.L. Shaw, *J. Chem. Soc., Dalton Trans.*, 1974, 480.

³⁶ J.F. Young, J.A. Osborn, F.H. Jardine, G. Wilkinson, *Chem. Commun.*, 1965, 131.

2.5.2.1 Three-centre Concerted Process

The oxidative addition of non-polar molecules such as H_2 , Cl_2 etc., tend to react according to the three-centre concerted mechanism whereby the *cis* isomer is formed.³⁷ An example is the stable d^6 complex formed when dihydrogen is added to a metal complex such as Vaska's complex, $[\text{IrCl}(\text{CO})\text{L}_2]$.¹²

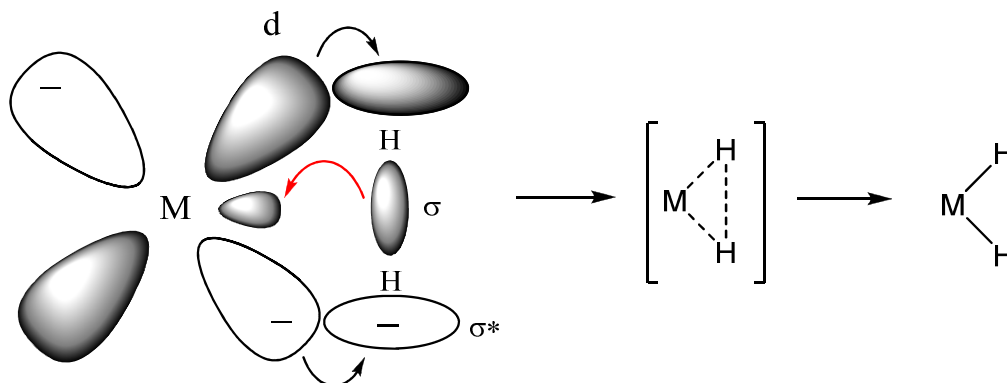


Figure 2-2: Three-centre concerted addition of H_2 forming the *cis*-dihydrido product.

Electron density is transferred from a filled d orbital on the metal into the empty σ^* molecular orbital (MO) of H_2 . Back-donation of electron density from the occupied σ MO of H_2 into an empty valence orbital on the metal atom occurs. The three-centered transition state is formed from the simultaneous formation of two M-H bonds while weakening the H-H bond.^{38,39} Two M-H single bonds are formed and the H-H bond is cleaved.

2.5.2.2 $\text{S}_{\text{N}}2$ -Type Mechanism

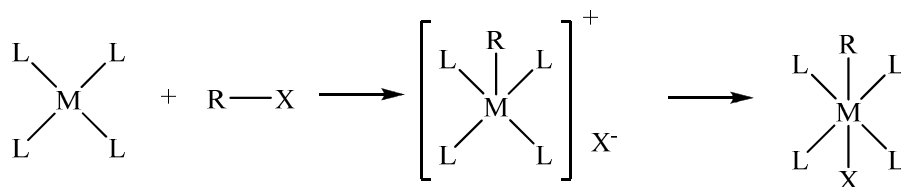
The $\text{S}_{\text{N}}2$ -type mechanisms usually occur when molecules like alkyl, acyl and benzyl halides react with transition metal compounds such as Vaska's complex. These reactions show large negative activation entropies and are first order in metal and first order in substrate. Typical $\text{S}_{\text{N}}2$ -type mechanisms in organometallic catalysis closely resemble the $\text{S}_{\text{N}}2$ -type mechanisms

³⁷ R.J. Cross, *Chem. Soc. Rev.*, 1985, **14**, 197.

³⁸ C.E. Johnson, B.J. Fisher, R. Eisenberg, *J. Am. Chem. Soc.*, 1983, **105**, 7772; C.E. Johnson, R. Eisenberg, *J. Am. Chem. Soc.*, 1985, **107**, 3148.

³⁹ R.H. Crabtree, R.J. Uriarte, *Inorg. Chem.*, 1983, **22**, 4152.

found in organic chemistry. This is due to the formation of a polar five-coordinated transition state in both cases.⁴⁰

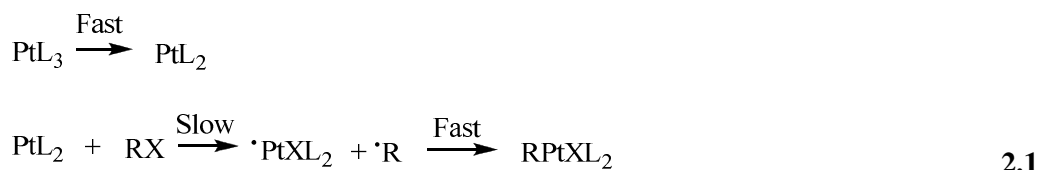


Scheme 2-3: S_N2-type oxidative addition.

Electronic, steric and solvent effects accelerate the rate of the S_N2-type oxidative addition mechanism.³⁰ As the nucleophilicity of the metal increases, the reactivity in the S_N2-type additions are increased.⁴¹

2.5.2.3 Radical Mechanism

Two types of radical mechanisms can be distinguished, namely: non-chain and chain radical mechanisms. An example of the non-chain radical mechanism (Eq. 2.1) is the addition of certain alkyl halides, RX, to [Pt(PPh₃)₃] where (R = Me, Et; X = I); (R = PhCH₂; X = Br).^{42,43}



There is a 1-electron oxidation of the metal by the alkyl halide as X is transferred from RX to the metal. This produces free radicals which combine rapidly to form the product. The reaction rates increase as the stability of the radical, •R, increases.

⁴⁰ J. Halpern, *Acc. Chem. Res.*, 1982, **15**, 238.

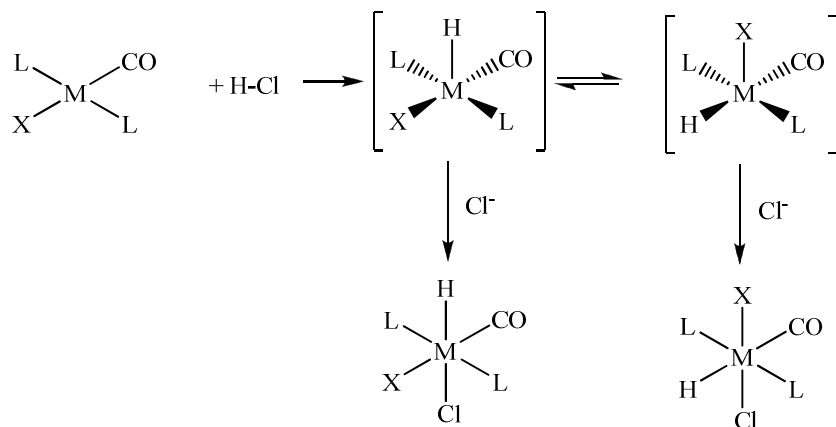
⁴¹ E. Uhlig, D. Walther, *Coord. Chem. Rev.*, 1980, **33**, 3.

⁴² M.F. Lappert, P.W. Lednor, *Chem. Comm.*, 1973, 948.

⁴³ T.L. Hall, M.F. Lappert, P.W. Lednor, *J. Chem. Soc., Dalton Trans.*, 1980, **8**, 1448.

2.5.2.4 Ionic Mechanism

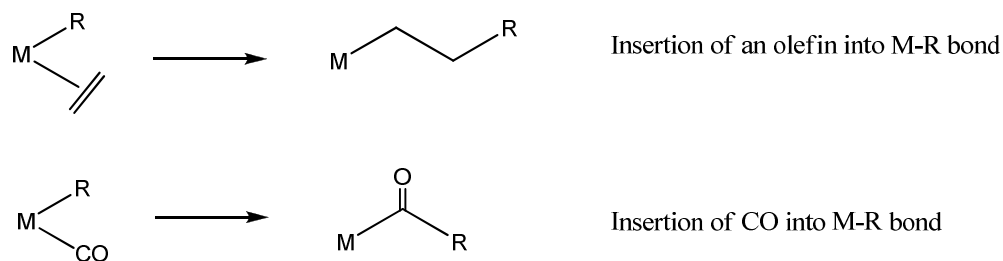
The ionic mechanism is normally found in polar medium where a hydrogen halide (e.g. HCl or HBr) would be dissociated. Protonation of a square complex would first produce a five-coordinate intermediate followed by intramolecular isomerisation and coordination of Cl^- to give the final product.



Scheme 2-4: Ionic mechanism for the oxidative addition of HCl to $[\text{MXL}_2\text{CO}]$.²⁹

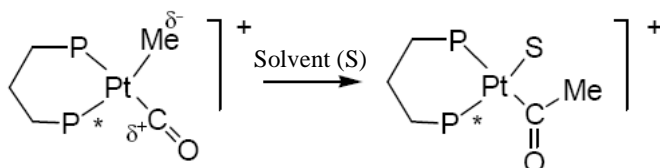
2.5.3 Migratory Insertion

Migratory insertion reactions create the opportunity for the synthesis of many organic molecules, e.g. the migration of a hydride to a coordinated alkene in hydroformylation. Crucial migratory insertion steps in catalytic reactions such as hydrogenation, polymerization and CO-involving processes are illustrated below:



Scheme 2-5: Migratory insertion of different ligands into a Metal-R bond.

Insertion of carbon monoxide proceeds with complete retention of configuration at the migrating carbon atom, thus remaining *trans* to P*.



Scheme 2-6: Migratory insertion of carbon monoxide.

2.6 LIGAND EFFECTS

The reactivity of a transition metal catalyst is largely influenced by ligands. In order to tailor-make a catalytic system to yield the desired product, the parameters of the ligands need to be characterized and fully understood. Phosphine ligated systems still receive a significant amount of attention because of their widespread application in organometallic chemistry. These ligands significantly influence the metal centre *via* both electronic and steric properties.

2.6.1 Electronic Effect, ν

Infrared (IR) frequencies can be used to determine the electronic properties of a series of phosphorus ligands during co-ordination to a particular metal. CO as ligand in catalysts is easily identified on an IR spectrum and is a convenient method to determine the σ -basicity and π -acidity of phosphorus ligands. Strong σ -donor ligands increase the electron density on the metal and hence a substantial back-donation to the CO ligands occurs, lowering the IR frequency. Strong π -acceptor ligands will compete with CO for the electron back-donation and the CO stretching frequencies will remain high.⁴⁴

Tolman⁴⁴ has defined an electronic parameter for phosphorus ligands based upon the vibrational spectra of $[\text{Ni}(\text{CO})_3\text{L}]$ in CH_2Cl_2 where $\text{L} = \text{PR}_3$. Tri-*tert*-butylphosphine,

⁴⁴ C.A. Tolman, *Chem. Rev.*, 1977, **77**, 313.

$P(t\text{-Bu})_3$ was used as reference. The electronic parameter, ν , can be calculated for a variety of ligands using Eq. 2.2.⁴⁵

$$\text{For } P = X_1X_2X_3 \quad \nu = 2056.1 + \sum_{i=1}^3 \chi_i \quad 2.2$$

The value of χ_i (chi) is the individual substituent contribution that was calculated by a number of substituents, X_1 , X_2 and X_3 .

2.6.2 Steric Effect, θ

Tolman's cone angle is the most widely used method in defining a reliable steric parameter that indicates the amount of space a phosphorus based ligand system occupies. Tolman proposed the measurement of the steric bulk of a phosphine ligand by use of CPK models. From the metal centre, 2.28 Å from the phosphorus atom, a cylindrical cone is constructed which just touches the van der Waals radii of the outermost atoms of the model. The cone angle, θ , measured is the desired steric parameter. In the case of non-symmetrical phosphorus ligands this cone angle, θ , can be calculated by the following equation:

$$\theta = (2/3) \sum_{i=1}^3 \theta_i/2 \quad 2.3$$

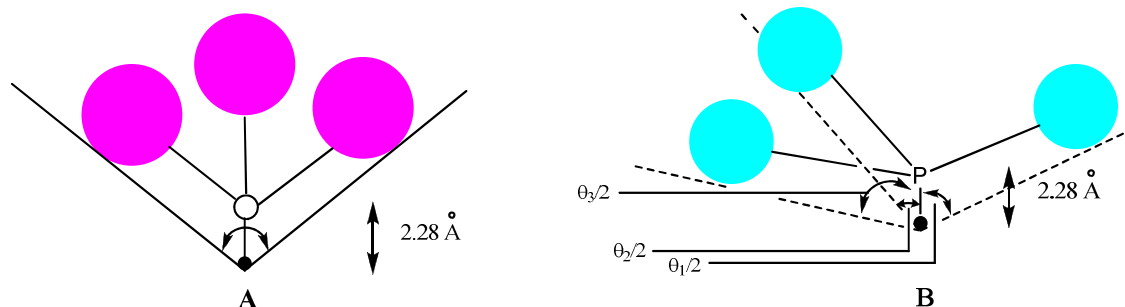


Figure 2-3: Cone angle measurements of symmetrical (A) and unsymmetrical (B) ligands.⁴⁴

⁴⁵ C.A. Tolman, *J. Am. Chem. Soc.*, 1970, **92**, 2953.

2.7 HOMOGENEOUS CATALYTIC SYSTEMS

2.7.1 Hydroformylation

Hydroformylation or “oxo reaction” was discovered by Otto Roelen in 1938. The basic reaction converts alkenes into aldehydes by addition of a hydrogen atom and formyl (CHO) group to a C=C double bond.⁴⁶ The aldehydes can then be converted to alcohols for the production of polyvinylchloride (PVC), polyalkenes and, in the case of the long-chain alcohols, in the production of detergents. High selectivity (> 95%) for the desired isomer of the aldehyde can be achieved through an optimal choice of catalyst, ligand and process conditions. The original cobalt catalyst used in hydroformylation, $[\text{Co}_2(\text{CO})_8]$,⁴⁷ was later replaced by the rhodium catalyst, $[\text{RhHCO}(\text{PPh}_3)_3]$.⁶ In the old process a cobalt salt was used, but was later modified to a cobalt salt plus a tertiary phosphine as the catalyst precursor. The phosphine-modified cobalt-based system was developed by Shell specifically for linear alcohol syntheses. $[\text{Rh}_4(\text{CO})_{12}]$ is another very active Rh catalyst, but has poor selectivity proving that the presence of phosphine ligands increase selectivity. The highly phosphine-substituted rhodium catalyst, $[\text{RhHCO}(\text{PPh}_3)_3]$, is a more active, highly selective catalyst reacting under milder pressures and lower temperatures than the earlier Co-catalyzed reaction.⁴⁸ Some comparisons of hydroformylation process parameters are shown in Table 2-1.

Table 2-1: Process parameters for various catalysts used in hydroformylation.⁴⁹

Process parameters	Cobalt	Cobalt + phosphine	Rhodium + phosphine
Temperature (°C)	140-180	160-200	90-110
Pressure (atm)	200-300	50-100	10-20
Selectivity towards <i>n</i> -butyraldehyde (%)	75-80	85-90	92-95

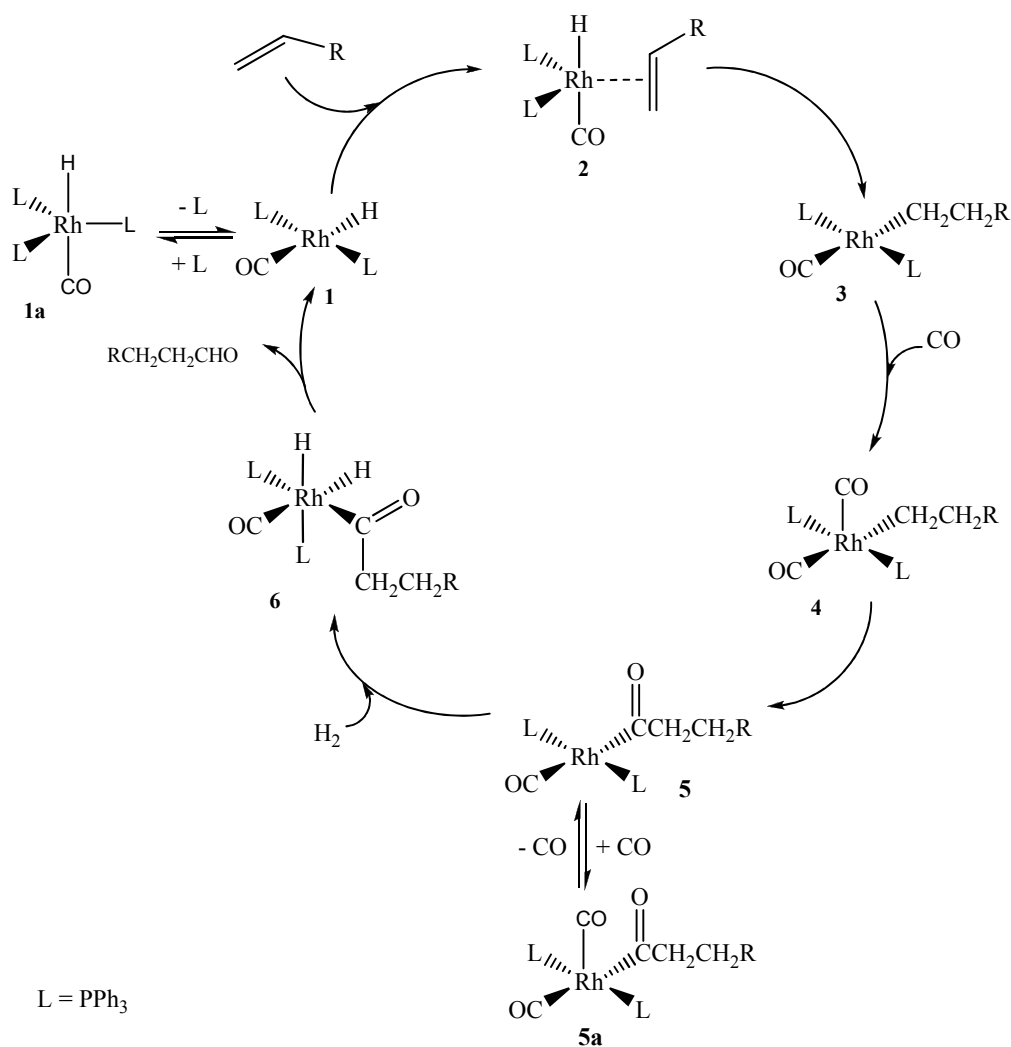
⁴⁶ D.W.A. Sharpe, *The Penguin Dictionary of Chemistry*, 3rd Ed., England: Penguin Books Ltd., 2003.

⁴⁷ C. Elschenbroich, A. Salzer, *Organometallics: A Concise Introduction*, New York: VCH Publishers, 1989.

⁴⁸ R. Ugo, *Aspects of Homogenous Catalysis*, Vol 2, Dordrecht, Holland: D. Reidel Publ. Comp., 1974.

⁴⁹ R.L. Pruett, *J. Chem. Edu.*, 1986, **63**, 196.

The basic catalytic cycle for the rhodium-phosphine based hydroformylation process is shown in Scheme 2-7.



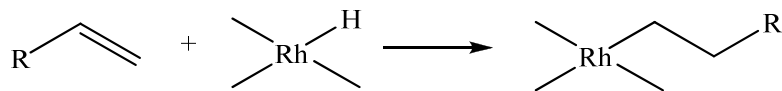
Scheme 2-7: The basic catalytic cycle for the hydroformylation of propylene (only *n*-product pathway shown) using a rhodium-phosphine based catalyst.²³

The rhodium catalyst is based on [RhH(CO)(PPh₃)₃] with the initial step being the generation of a 16-electron square intermediate, **1**, from the 18-electron precursor, **1a**. This is followed by alkene coordination, **2**, and hydrogen transfer to give the alkyl species **3**. CO addition, **4**, and insertion give the acyl derivative, **5**, which subsequently undergoes oxidative addition of molecular hydrogen to give the hydridoacyl complex, **6**. The final steps are another H

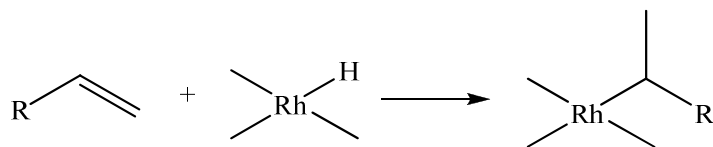
transfer to the carbon atom of the acyl group, i.e., the reductive elimination of aldehyde, and regeneration of **1**.

An excess of CO over H₂ forms five-coordinate dicarbonyl acyl complexes, **5a**, which cannot react with hydrogen, therefore inhibiting the hydroformylation process. The rhodium catalyst can be added as [Rh(acac)(CO)(PPh₃)], [RhH(CO)(PPh₃)₃] or similar complexes. High concentrations of PPh₃ are used so that species of type **1** dominate, although the steric hindrance of the PPh₃ reduces the tendency of alkene binding. It has been argued that at lower [PPh₃] the square planar species, [RhH(CO)₂(PPh₃)], may be more kinetically favourable towards alkene binding. Calculated energy profiles for such a sequence shows that alkyl intermediates of type **4** to be particularly stable. The results also suggest that square intermediates experience strong stabilization through solvation.⁵⁰

There are two different ways of inserting an alkene into a metal-hydrogen bond, namely the anti-Markovnikov (Scheme 2-8) and Markovnikov (Scheme 2-9) addition.^{23,51}



Scheme 2-8: Anti-Markovnikov addition of an alkene into a metal-hydrogen bond.



Scheme 2-9: Markovnikov addition of an alkene into a metal-hydrogen bond.

Very high PPh₃ concentrations increase the selectivity for the linear aldehyde product by suppressing the formation of monophosphine species. The high selectivity is considered to be primarily an effect of steric crowding around the metal centre. The linear alkyl

⁵⁰ K. Morokuma *et al.*, *Organometallics*, 1997, **16**, 1065.

⁵¹ I. Tkatchenko, *Comprehensive Organometallic Chemistry*, Editors: G. Wilkinson, F. G. A. Stone, E. W. Abel, Pergamon Press, Vol. 8, 1982.

intermediate, **3**, requires less space and therefore formed more easily than the branched one in the presence of bulky ligands; the selectivity is therefore promoted by the phosphine cone angle.^{52,53} The balance between sterically demanding ligands and their ability to remain coordinated so that product selectivity could be influenced is a fine one. In Figure 2-4 bulky phosphites, **A**, combine high activity with high regioselectivity for linear aldehydes,^{54,55} whereas others, such as **B**, allow catalytic reactions to be carried out in organic media followed by extraction of the catalyst into aqueous acid by protonation of the amino substituents.⁵⁶ Flexible phosphite ligands, **C**, hydroformylate styrene with very high regioselectivities for the branched aldehyde.⁵⁷

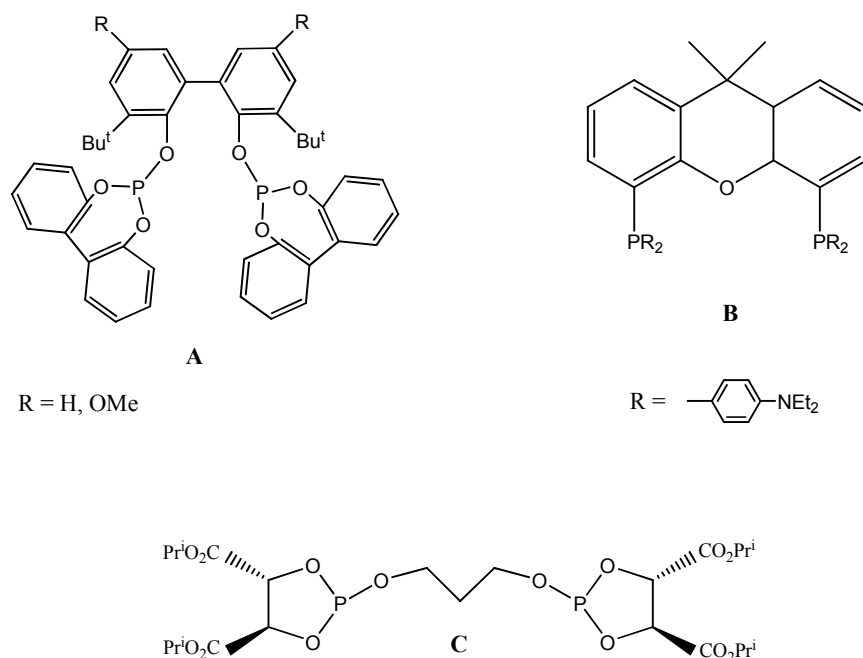


Figure 2-4: Various ligands used in Rh-catalysed hydroformylation.

Rhodium is an expensive metal and the commercial viability of the rhodium-based hydroformylation process crucially depends on the near-complete recovery process of the

⁵² C.A. Tolman, *J. Chem. Edu.*, 1986, **63**, 199.

⁵³ C.A. Tolman, J.W. Faller, *Homogeneous Catalysis with Metal Phosphine Complexes*, Editor: L.H. Pignolet, New York: Plenum Press, 1983.

⁵⁴ G.D. Cuny, S.L. Buchwald, *J. Am. Chem. Soc.*, 1993, **115**, 2066.

⁵⁵ P.W.N.M. van Leeuwen, K. Goubitz, J.N. Veldman, A. van Rooy, P.C.J. Kamer, A.L. Spek, *Organometallics*, 1996, **15**, 835.

⁵⁶ P.W.N.M. van Leeuwen, A. Buhling, P.C.J. Kamer, J.W. Elgersma, K. Goubitz, J. Fraanje, *Organometallics*, 1997, **16**, 3027.

⁵⁷ T.J. Kwok, D.J. Wink, *Organometallics*, 1993, **12**, 1954.

catalyst. In the past, complicated recycle processes and distillation was used, but more recently, catalyst recovery is achieved *via* a separation method based on water-soluble phosphines⁵⁸, notably $P(C_6H_4SO_3)_3^{3-}$,⁵⁹ allowing the hydroformylation process to be conducted by means of a two-phase system designed by Rhône-Poulenc and Ruhrchemie in 1986. The trisulfonated triphenylphosphine ligand is commonly referred to as TPPTS and a pH-dependant equilibrium exists between the water-soluble and the organic-soluble forms of TPPTS as shown in Figure 2-5.

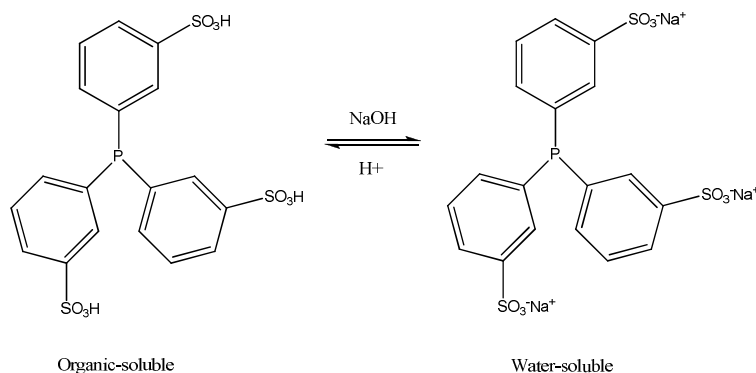


Figure 2-5: Organic- and water-soluble forms of TPPTS.

Between pH 0 and -1 the protonated form is extractable with organic solvents while at higher pH the sodium salt is soluble in water to the extent of 1100 g/liter. The ligand is non-toxic which makes it appealing to use in large-scale industrial processes. The use of a buffer component such as Na_2HPO_4 has been suggested for the control of pH, however the use of such salts influences the reaction rate and product selectivity. The two-phase system contains a water soluble rhodium phosphine catalyst in the aqueous phase with the aldehyde product forming an organic layer, which is separated by decantation from the catalyst containing aqueous phase. This recovery process proves to be highly efficient with Rh losses in parts per billion, however the two-phase process is not suited for higher alkenes because of the low solubility of higher alkenes in water and the first-order dependency of the rate on alkene concentration.⁶⁰

⁵⁸ E. G. Kuntz, *Chemtech*, 1987, **17**, 570.

⁵⁹ B.E. Hanson, H. Ding, T.E. Glass, *Inorg. Chim. Acta*, 1995, **229**, 329.

⁶⁰ C.M. Thomas, G. Süß-Fink, *Coordination Chem. Rev.*, 2003, **243**, 125.

Hydroformylation is truly an exceptional industrial process for a variety of different product syntheses with the use of an array of catalyst systems as illustrated in Table 2-2.

Table 2-2: Hydroformylation reaction processes.⁶¹

Manufacturer	Product	Process
Mitsubishi-Kasei	Isononyl aldehyde for isononyl alcohol used in PVC resin as a plasticizer alcohol	Rh catalyst with triphenyl phosphine oxide as a weakly coordinating ligand; catalyst separated from products by distillation
BASF Hoffman-LaRoche	An intermediate for Vitamin A synthesis	Rh catalyst without phosphorus ligand
ARCO	An intermediate for 1,4-butanediol	Rh catalyst with chelating phosphorus ligand
Kuraray	An intermediate for 3-methyl 1,5-pentanediol	[Rh ₄ (CO) ₁₂] with phosphorus ligand as precursor

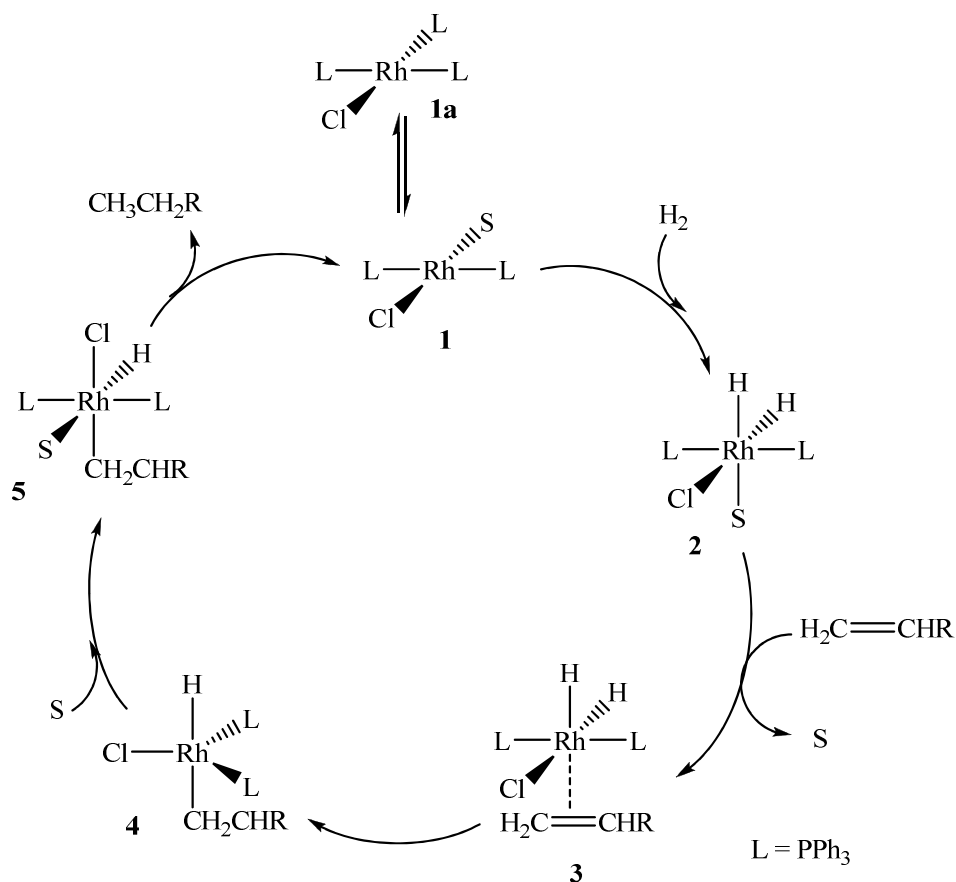
2.7.2 Hydrogenation

2.7.2.1 Rhodium as Catalyst

The general reaction of hydrogenation is the conversion of alkenes and alkynes into alkanes with the use of H₂ and a catalyst at high pressure. Many transition metal complexes have been used as homogeneous catalysts of which the most popular is Wilkinson's catalyst,^{7,62} [RhCl(PPh₃)₃], discovered in the sixties. It is a square planar 16-electron complex with a *d*⁸ configuration. As in many other cases the number of valence electrons switches during the cycle between 16 e and 18 e. A hydrogen reaction cycle using Wilkinson's catalyst follows:

⁶¹ S. Bhaduri, D. Mukesh, *Homogeneous Catalysis: Mechanisms and Industrial Applications*, New York: John Wiley & Sons, Inc., 2000.

⁶² F.H. Jardine, J.A. Osborn, G. Wilkinson, J.F. Young, *Chem, Ind. (London)*, 1965, 560.



Scheme 2-10: Hydrogenation cycle with Wilkinson's catalyst.^{63,64}

Dissociation of one ligand, L, and the replacement thereof by a solvent molecule, S, is the first step (**1a** → **1**). The dissociation of one of the phosphine ligands leaves [RhCl(PPh₃)₂], a very reactive *tris*-coordinate system. Oxidative addition of dihydrogen, **2**, followed by an alkene, **3**, then occurs. Usually *cis* fashion can be promoted by the substitution of more electron-rich phosphines on the rhodium complex. On the other hand, very strong donor ligands can stabilise the trivalent rhodium (III) chloro-dihydride to such an extent that the complex is no longer active. Next is the hydrogen migration, **4**, from the metal to a carbon in the coordinated alkene. Finally, reductive elimination, **5**, of the product completes the cycle. The use of electron-withdrawing ligands can increase the rate of the final step.⁶⁵

⁶³ C. O'Connor, G. Yagupsky, D. Evans, G. Wilkinson, *Chem. Commun.*, 1968, 420.

⁶⁴ C. O'Connor, G. Wilkinson, *J. Chem. Soc. (A)*, 1968, 2665.

⁶⁵ D.J. Drury, *Aspects Homog. Catal.*, 1984, **5**, 197.

Hydrogenation reactions with Wilkinson's catalyst are experimentally simple reactions. They are done at ambient temperature and in many cases 1 atm hydrogen is sufficient. General solvents used are MeOH, EtOH, acetone, THF or benzene.⁶⁶ Chloroform and carbon tetrachloride may undergo H/Cl exchange and therefore should be avoided.⁶⁷

Hydrogenation of terminal olefins is faster than the hydrogenation of double bonds in cyclic systems or internal double bonds. *cis*-Olefins are hydrogenated faster than *trans*-olefins. As the degree of substitution at the double bond increases, reactivity toward hydrogenation with Wilkinson-type catalysts is lowered. Carbonyl compounds are not compatible with Wilkinson-type catalysts. Aldehydes are decarbonylated during hydrogenation reactions⁶⁸ and hydrogenation of ketones is slower than for olefins. An advantage of homogeneous Wilkinson catalysts is its stability towards sulphur compounds which tend to poison heterogeneous catalysts.

2.7.2.2 Iridium as Catalyst

The iridium analogue of Wilkinson's compound, $[\text{IrCl}(\text{PPh}_3)_3]$, illustrates the differences that can arise between two very similar metals. Unlike $[\text{RhCl}(\text{PPh}_3)_3]$, it cannot be made by heating $[\text{IrCl}_3]$ with excess phosphine, using the phosphine as a reducing agent, because hydride complexes are easily formed, a characteristic of iridium. Stable hydrides can also be made by oxidative addition to $[\text{IrCl}(\text{PPh}_3)_3]$. Some reactions of $[\text{IrCl}(\text{PPh}_3)_3]$ are shown in Figure 2-6.

⁶⁶ B.R. James, *Comprehensive Organometallic Chemistry*, Editors: G. Wilkinson, F.G.A. Stone, E.W. Abel, Oxford: Pergamon, 1982.

⁶⁷ H.D. Kaesz, R.B. Saillant, *Chem. Rev.*, 1972, **72**, 231.

⁶⁸ K. Ohno, J. Tsuji, *J. Am. Chem. Soc.*, 1968, **90**, 99.

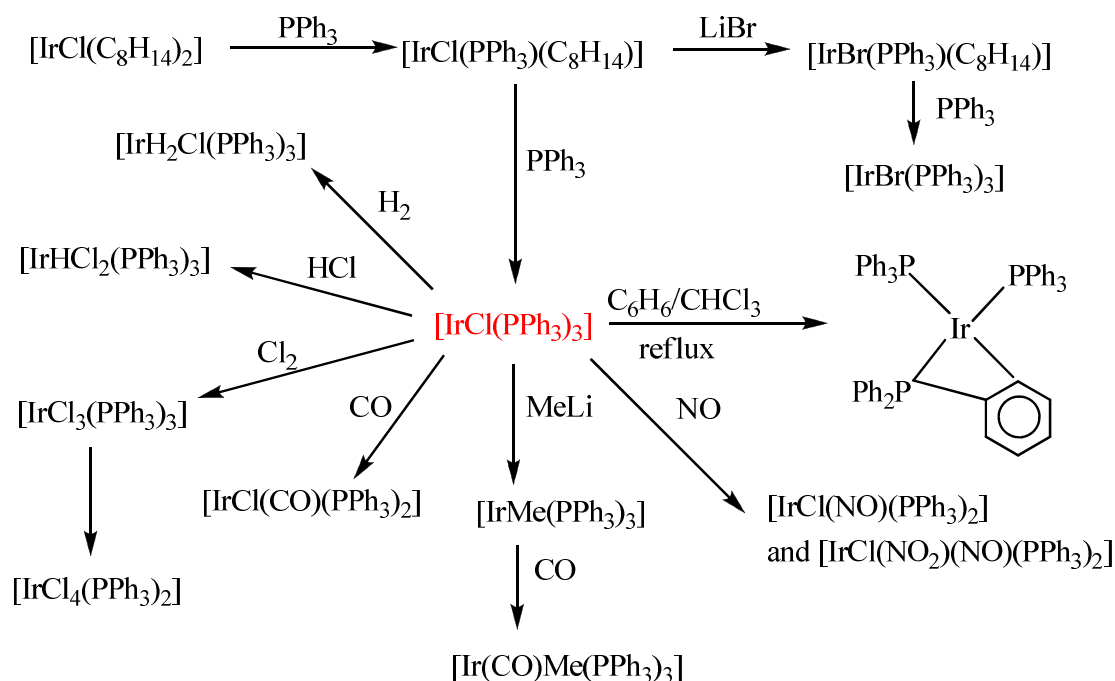


Figure 2-6: Some syntheses and reactions of $[\text{IrCl}(\text{PPh}_3)_3]$.⁶⁹

$[\text{IrCl}(\text{PPh}_3)_3]$ cannot be used as a hydrogenation catalyst because all the ligands are tightly bound. PPh_3 does not dissociate from $[\text{IrH}_2\text{Cl}(\text{PPh}_3)_3]$ so the alkene is unable to bind. Without alkene binding, hydrogen transfer from the metal to the alkene cannot occur.⁷ Iridium analogues of Rh hydrogenation catalysts are less labile and less active than the Rh series and consequently attention was focused on stable hydrides in iridium species for the study of transition intermediates of Rh catalysts.

Later it was found that $[\text{Ir}(\text{cod})(\text{PCy}_3)(\text{pyridine})]\text{BF}_4$, referred to as Crabtree's catalyst,^{70,71} showed high activity for hindered alkenes. Tri- and tetrasubstituted alkenes could be reduced efficiently when employing a low PR_3 to metal ratio and non-bonding solvent.⁷² It was also a widely successful catalyst for directed (diastereoselective) hydrogenation of alkenes (Scheme 2-11),⁶⁷ but application to enantioselective hydrogenation was lacking.

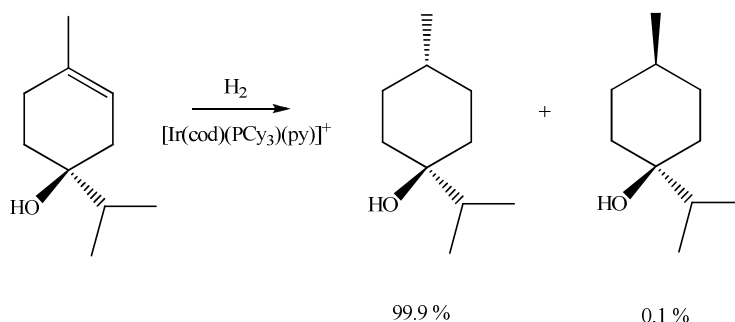
⁶⁹ M.A. Bennett, D.L. Milner, *J. Am. Chem. Soc.*, 1969, **91**, 6983.

⁷⁰ R.H. Crabtree, H. Felkin, G.E. Morris, *J. Organomet. Chem.*, 1977, **141**, 205.

⁷¹ R.H. Crabtree, H. Felkin, T. Fillebeen-Khan, G.E. Morris, *J. Organomet. Chem.*, 1979, **168**, 183.

⁷² R.H. Crabtree, *Acc. Chem. Res.*, 1979, **12**, 331.

The catalyst binds to a substrate's OH or CO and then delivers H₂ almost exclusively from the face of the substrate containing the binding group.^{73,74}



Scheme 2-11: Diastereoselective capability of the Crabtree catalyst for hydrogenation process.

The reason for the efficient directing is due to the low PR₃ to Ir ratio. This allows H₂ and the C=C double bond to bind to the metal simultaneously.⁷³ Based on this catalytic system discovered by Crabtree and co-workers, an efficient method for enantioselective hydrogenation of unfunctionalized olefins was developed by Pfaltz^{75,76} (Figure 2-7) with the use of a [Ir(cod)(P-N)]⁺ catalyst, bearing a chelating phosphino-oxazolidene ligand.

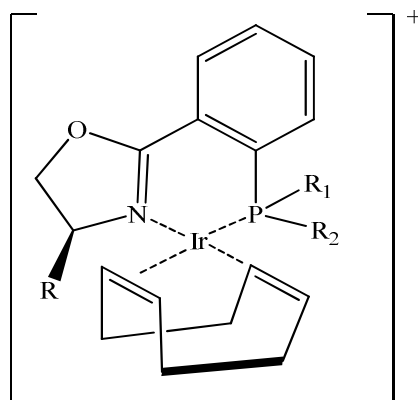


Figure 2-7: Pfaltz's catalyst used for enantioselective hydrogenation of olefins.^{77,78}

⁷³ R.H. Crabtree, M.W. Davis, *Organometallics*, 1983, **2**, 681.

⁷⁴ R.H. Crabtree, M.W. Davis, *J. Org. Chem.* 1986, **51**, 2655.

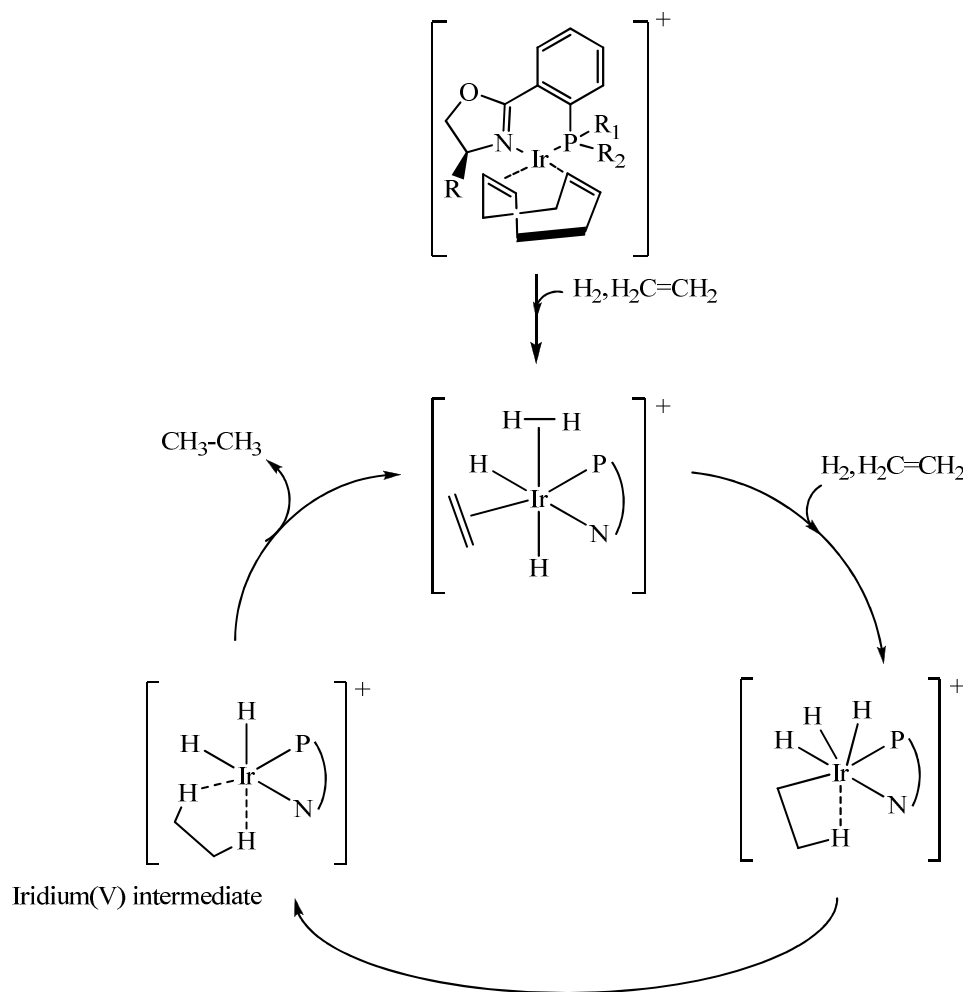
⁷⁵ A. Lightfoot, P. Schneider, A. Pfaltz, *Angew. Chem.*, 1998, **110**, 3047.

⁷⁶ R. Hilgraf, A. Pfaltz, *Synlett*, 1999, 1814.

⁷⁷ P. Brandt, E. Hedberg, P. G. Andersson, *Chem. Eur. J.*, 2003, **9**, 339.

⁷⁸ A. Pfaltz, J. Blankenstein, R. Hilgraf, E. Hormann, S. McIntyre, F. Menges, M. Schonleber, S.P. Smidt, B. Wustenberg, N. Zimmermann, *Adv. Synth. Catal.*, 2003, **345**, 33.

Essential features in the hydrogenation mechanism of ethylene with Pfaltz's catalyst are shown below (Scheme 2-12). The presence of COD in the precatalyst assures irreversible formation of free coordination sites at the metal centre. Formation of the active catalyst takes place by an irreversible hydrogenation of the ligand cyclooctadiene. The ligand is thus released as cyclooctane and displaced by either solvent, dihydrogen, or a substrate alkene.



Scheme 2-12: Hydrogenation of ethylene with the use of Pfaltz's catalyst, $[\text{Ir}(\text{cod})(\text{P-N})]^+$.

Surprisingly, the hydrogenation mechanism proceeds *via* an Ir(III)/Ir(V) cycle rather than the typical Metal(I)/Metal(III) cycle. An olefin is coordinated *trans* to phosphorus and H_2 is coordinated in the remaining axial position. The olefin then undergoes a migratory insertion into the axial Ir-H bond and the resulting Ir(V) species is now extremely labile and reductive elimination occurs. The catalysis is thus taking place without the intervention of Ir(I) in any

step, in contrast to the analogous rhodium systems in which the oxidation state of the metal changes between I and III.⁷⁹ The rate of the reaction is zero-order in alkene concentration due to the strong binding of alkenes to iridium.⁸⁰ The coordination of the alkene is not the rate-determining step. The coordination of H₂ or the migratory insertion step acts as the rate-determining step.

The hydrogenation mechanism using the [Ir(cod)LL']BF₄ systems are difficult to study because of their high activity and the fact that the rates are often limited by the mass transfer of H₂ from the gas phase into solution. It is very likely that a similar Ir(III)/Ir(V) cycle applies to typical [Ir(cod)LL']BF₄ catalysts.

An iridium complex (Figure 2-8) developed by Blaser⁸¹ by means of combining {(cod)Ir}⁺ with an asymmetric ligand of Togni's⁸² is used for the commercial production of the agrochemical metalachlor (Dual Magnum). This is one of the few enantioselective hydrogenation systems in commercial use today.

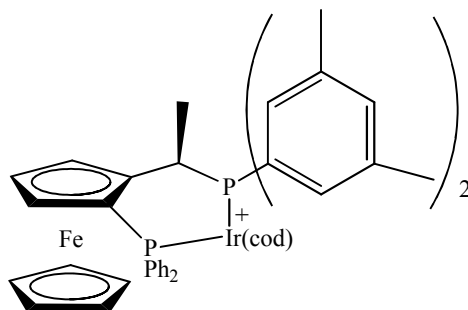


Figure 2-8: Iridium catalyst used in the hydrogenation process for the production of metalachlor.

⁷⁹ C.R. Landis, P. Hilfenhaus, S. Feldgus, *J. Am. Chem. Soc.*, 1999, **121**, 8741.

⁸⁰ D.G. Blackmond, A. Lightfoot, A. Pfaltz, T. Rosner, P. Schnider, N. Zimmermann, *Chirality*, 2000, **12**, 442.

⁸¹ H.U. Blaser, H.P. Buser, K. Coers, R. Hanreich, H.P. Jalett, E. Jelsch, B. Pugin, H.D. Schneider, F. Spindler, A. Wegmann, *Chimia*, 1999, **53**, 275.

⁸² A. Togni, C. Breutel, A. Schnyder, F. Spindler, H. Landert, A. Tijani, *J. Am. Chem. Soc.*, 1994, **116**, 4062.

2.7.3 Carbonylation

Carbonylation is generally the reaction involving the addition of carbon monoxide (CO) to organic compounds with the use of a transition metal catalyst. The formation of the metal-carbon bond is most commonly the first step in the carbonylation reaction mechanism concluding with the liberation of the organic carbonyl product and regenerated catalyst. Examples of catalytic insertion of carbon monoxide include: ethene conversion to propionic acid or its anhydride with the use of $[\text{Mo}(\text{CO})_6]$,⁸³ the carbonylation of methyl isocyanide by reductive coupling to niobium⁸⁴ and palladium-catalysed carbonylation of halide containing alcohols for the production of lactones and lactams.⁸⁵

Although there are many different carbonylation reactions the most important homogeneous catalysed industrial application is the carbonylation of methanol for the production of acetic acid.⁸⁶ The production of vinyl acetate, an important industrial monomer, is one of the largest and fastest growing uses of acetic acid and accounts for 40% of the total global acetic acid consumption.⁸⁷ The majority of the remaining acetic acid production is used to manufacture other acetate esters. Methyl, ethyl, *n*- and *iso*-butylacetates are important industrial solvents. Cellulose acetate is used in the preparation of fibres and photographic films. Inorganic acetates (e.g. Na, Pd, Al and Zn) are used in the textile, leather and paint industries. Acetic acid is also used in the manufacture of chloroacetic acid and terephthalic acid.⁸⁸

Reactions in which carbonyl is involved attracted attention since the late nineteenth century with the discovery of carbon-carbon bond formation reactions by Michail *et al.*⁶⁵ The carbonyl is susceptible to nucleophilic attack on the carbon and electrophilic attack on the oxygen, making it one of the most versatile functionalities available. It is able to stabilise an adjacent carbanion by charge delocalization onto the C=O double bond and for many

⁸³ J.R. Zoeller, E.M. Blakely, R.M. Moncier, T.J. Dickson, *Catal. Today*, 1997, **36**, 227.

⁸⁴ E.M. Carnahan, S.J. Lippard, *J. Am. Chem. Soc.*, 1990, **112**, 3230.

⁸⁵ M.L. Tobe, J. Burgess, *Inorganic Reaction Mechanisms*, England: Addison Wesley Longman Ltd., 1999.

⁸⁶ P.M. Maitlis, A. Haynes, G.J. Sunley, M.J. Howard, *J. Chem. Soc., Dalton Trans.*, 1996, 2187.

⁸⁷ R.P.A. Sneeden, *Comprehensive Organometallic Chemistry*, Editors: G. Wilkinson, F.G.A. Stone, E.W. Abel, Vol.8, Oxford: Pergamon Press, 1982.

⁸⁸ B. Cornils, W.A. Herrmann, *Applied Homogeneous Catalysis with Organometallic Compounds*, New York: VCH Publishers, 1996.

synthetic purposes can be introduced directly onto a number of different sites in an organic molecule.

The electronic structure of carbonyl can be visualized as:

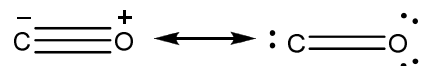


Figure 2-9: Diagram of carbon monoxide in valence bond terms.

Once the ligand possesses a π bond pertaining to the atom bound to the metal it leads to the presence of a π bonding and π^* antibonding orbital on the ligand. When carbon monoxide is bonded to a transition element through σ -donation and π -back donation the carbon atom obtains a positive character making it more susceptible towards a migrating anion at the metal centre or for a nucleophilic attack from outside the co-ordination sphere.

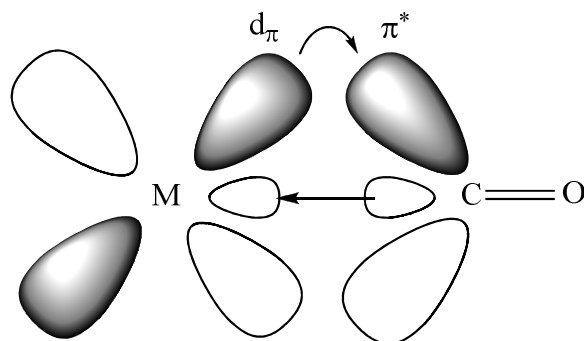


Figure 2-10: Diagram of the formation of the metal-carbonyl bond.⁸⁹

Through the donation of the lone pair electrons on the carbonyl carbon into the empty d_σ orbital on the metal the M-CO σ -bond is formed. A back-donation of electrons take place from filled or half filled metal d orbitals to empty π^* antibonding orbitals of the carbonyl. Ligands *trans* to the carbonyl compete for the electrons of a particular metal d orbital. Weaker π -acceptor ligands cause a strengthening of the *trans* M-CO bond, consequently weakening the C-O bond and *vice versa*.⁹⁰

⁸⁹ R.H. Crabtree, *The Organometallic Chemistry of the Transition Metals*, 4th Ed, New Jersey, John Wiley & Sons, 2005.

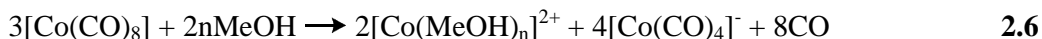
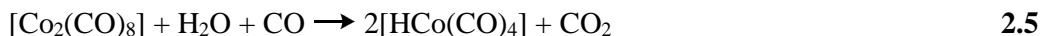
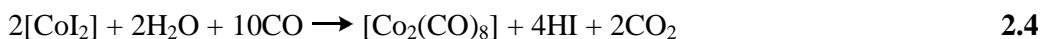
⁹⁰ C. Elschenbroich, A. Salzer, *Organometallics: A Concise Introduction*, 2nd Ed, New York, VCH Publishers, 1992.

As the σ -donor properties of the phosphine decreases, the π -acceptor ability increases. Similarly, when electrons are removed from the metal centre the ability of the metal to participate in back-donation to the anti-bonding CO π^* orbitals is reduced and as a result, the CO bond order increases.

Although many transition metal compounds can be used in carbonylation reactions to produce acetic acid or acetic anhydrides, Rh and Ir are the most active and preferred catalysts. Cobalt is mentioned only for comparison. The three main important industrial processes for the synthesis of acetic acid will be discussed, namely the cobalt BASF process, the rhodium Monsanto process and the iridium Cativa process.

2.7.3.1 Cobalt Catalysed BASF Process

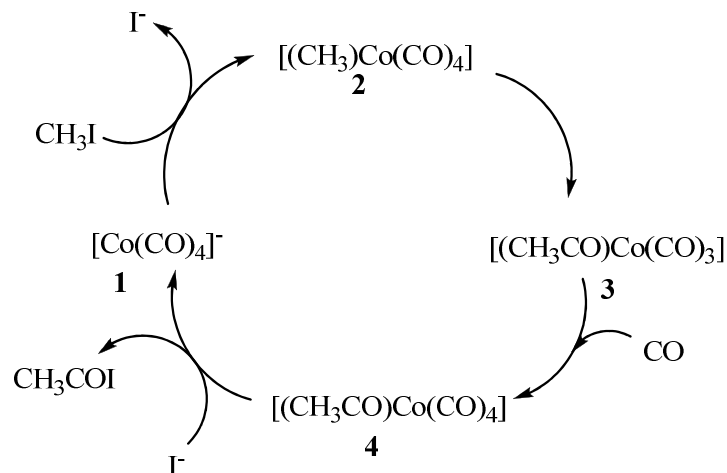
The first process for the carbonylation of methanol was commercialised by BASF in 1960. The process operates at high temperatures (250 °C) and pressures (680 bar) with the use of an iodide promoted cobalt catalyst. Selectivity to acetic acid is about 90% based upon methanol^{91,92} and 70% based on CO. The presence of iodide is required to convert methanol into methyl iodide, since methanol inserts CO into the O-H bond, generating methyl formate, and not into the C-O bond to give acetic acid. Therefore the actual substrate of carbonylation is methyl iodide.⁹³ The starting reagent is $[\text{CoI}_2]$ which is transformed to HI and $[\text{Co}_2(\text{CO})_8]$ and then finally to the activated catalyst $[\text{HCo}(\text{CO})_4]$. Small amounts of H_2 enhance the catalytic activity which is in agreement with the postulation of the hydridic cobalt carbonyl complex being the active species.⁶⁰ The basic catalytic cycle with the cobalt catalyst is illustrated by Scheme 2.4. The tetracarbonyl cobalt anion (Eq. 2.6) is formed from cobalt iodide, by Eqs. 2.4-2.5.



⁹¹ H. Hohenschutz, N. von Kutepow, W. Himmler, *Hydrocarbon Process.*, 1966, **45**, 141.

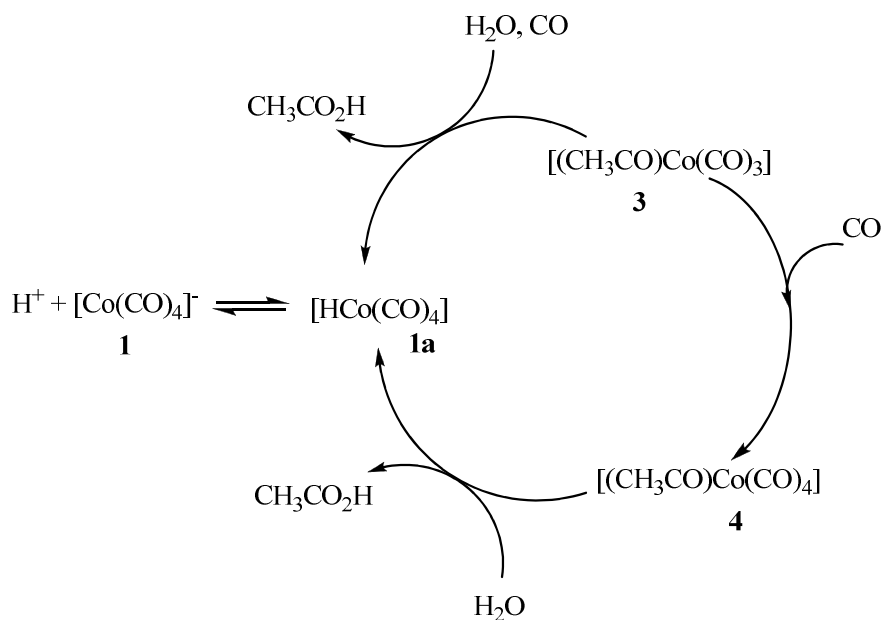
⁹² N. von Kutepow, W. Himmler, H. Hohenschutz, *Chem.-Ing.-Tech.*, 1965, **37**, 383.

⁹³ D. Forster, M. Singleton, *J. Mol. Catal.*, 1982, **17**, 299.



Scheme 2-13: BASF cobalt catalysed reaction of acetic acid formation⁴⁹

The catalytic cycle is initiated by a nucleophilic attack by **1** on CH₃I producing **2** and I⁻. CO insertion into a metal alkyl bond produces the 16-electron species **3**. Another CO group is inserted into **3** providing **4** which then react with I⁻ to eliminate acetyl iodide. Formation of acetic acid and recycling of water occur by reactions that will be discussed for the rhodium cycle. Both **3** and **4** react with water to give acetic acid in Scheme 2-14. The hydrido cobalt carbonyl **1a** produced in these reactions catalyses Fischer-Tropsch-type reactions and the formation of by-products. Eq. 2.5 and 2.6 ensure the equilibrium between **1** and **1a**.



Scheme 2-14: Equilibrium between species [Co(CO)₄]⁻ and [HCo(CO)₄].⁴⁹

The rate of the cobalt catalysed process is strongly dependent on both the CO pressure and MeOH concentration. High temperatures are needed for adequate reaction rates and in turn high CO pressures are necessary to stabilize the catalyst at high temperatures. The selectivity toward acetic acid is 90% based on methanol and 70% based on CO. By-products consist of CO₂ and 4-5% of organic products such as, methane, acetaldehyde, ethanol and ethers. The catalytic cycle is largely influenced by the presence of hydrogen as it decreases selectivity to acetic acid formation and increases the amount of organic by-products formed.⁹⁴

The BASF cobalt catalysed process was replaced by rhodium and iridium complexes that tend to operate at milder reaction conditions with increased selectivities. Below, is a graph comparing rhodium and cobalt in the homogenous carbonylation of methanol illustrating the importance of continuous development of different organometallic catalysts and ligands. The graph compares the required metal concentration (Conc.), pressures, temperatures, as well as the obtained selectivity.⁹⁵

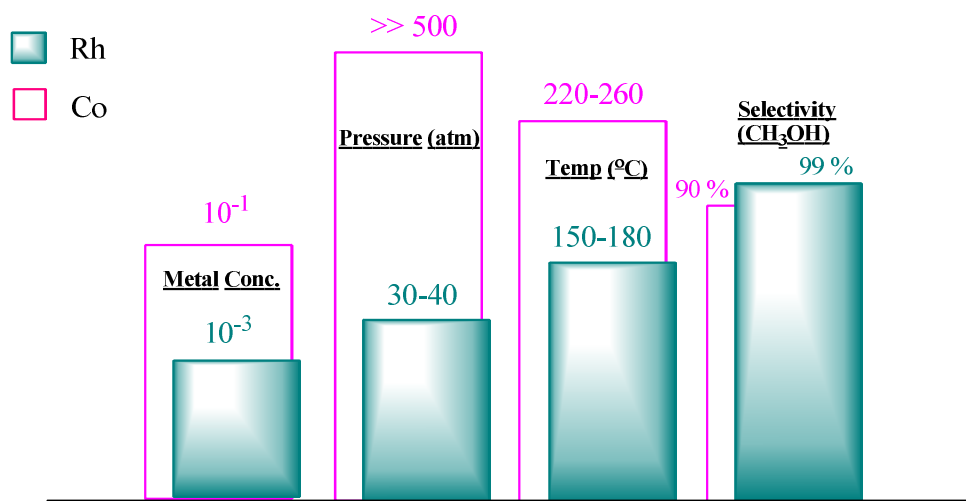


Figure 2-11: Catalytic breakthrough of rhodium vs. cobalt in homogeneous catalysis for the carbonylation of methanol.

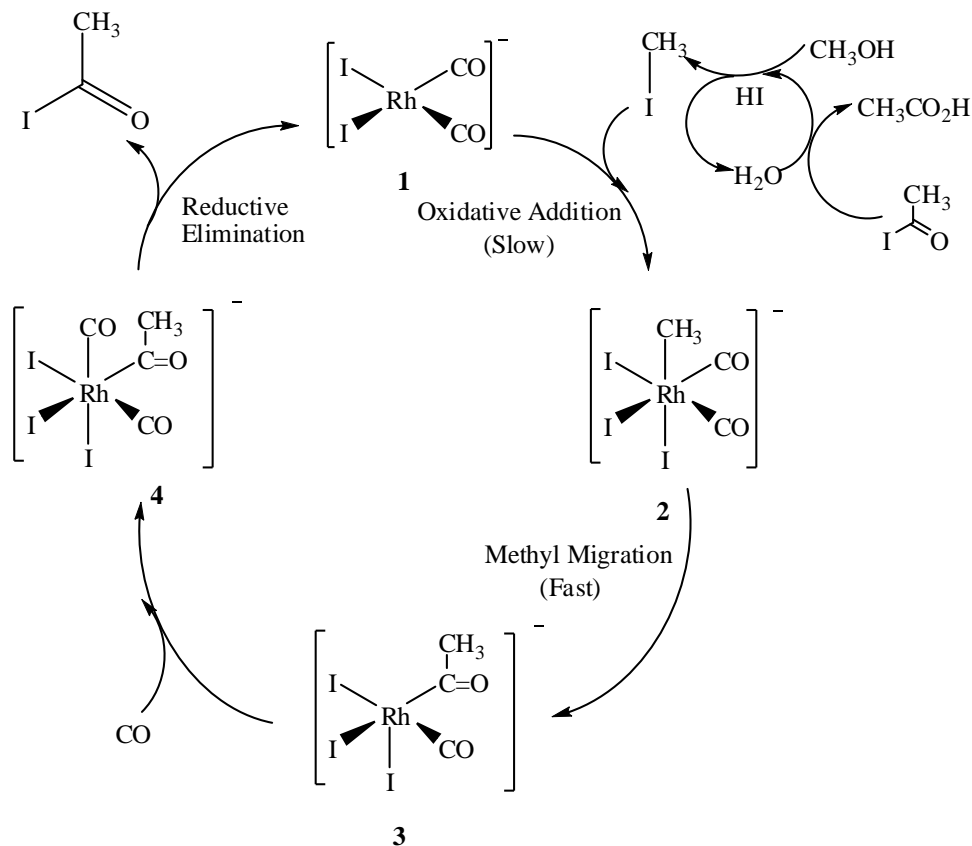
⁹⁴ C. Masters, *Homogeneous Transition-Metal Catalysis*, New York, Chapman & Hall, 1981.

⁹⁵ W.A. Hermann, B. Cornils, *Angew. Chem. Int. Ed. Engl.*, 1997, **36**, 1048.

2.7.3.2 Rhodium Catalysed Monsanto Process

In 1966, Monsanto developed the rhodium-catalysed^{86,96} process for the carbonylation of methanol to produce acetic acid. The process reacts under mild reaction conditions (30-60 bar and 150-200 °C) with exceptional catalyst activity and higher than 99% selectivity. It employs a rhodium/iodide catalyst and has completely replaced the cobalt catalysed process (BASF)⁹³ used in the 1950s.

As shown in the reaction mechanism below (Scheme 2-15), the active catalyst, $[\text{Rh}(\text{CO})_2\text{I}_2]^-$, undergoes oxidative addition, insertion and reductive elimination with the result being the net production of acetic acid from the insertion of carbon monoxide into methanol. The rhodium catalyst is able to fulfill its role because it is capable of changing its coordination number to shuttle between the +1 and +3 oxidation state.



Scheme 2-15: Rhodium Monsanto Process.²³

⁹⁶ F.E. Paulik, J.F. Roth, *J. Chem. Soc., Chem. Commun.*, 1968, 1578.

Kinetics prove the overall reaction rate is first order in both [Rh] and [MeI] and zero order in [MeOH] and CO partial pressure above 2 atm.⁹⁷ The oxidative addition of MeI to (1) forming the hexacoordinated alkyl Rh(III) intermediate, [MeRh(CO)₂I₃]⁻ (2), was found to be the rate-determining step of the cycle. The alkyl Rh(III) intermediate (2) is kinetically unstable and methyl migratory-insertion then occurs rapidly to form the acyl complex, [(MeCO)Rh(CO)I₃]⁻ (3). Insertion of CO converts this complex to the six-coordinated dicarbonyl species, [(MeCO)Rh(CO)₂I₃]⁻ (4). Finally, reductive elimination of acetyl iodide regenerates (1) and the cycle restarts. Acetyl iodide reacts with water to give acetic acid and hydrogen iodide (HI). Both the first step (reaction of methanol with HI to give methyl iodide, Eq. 2.7) and the last (the reaction of acetyl iodide with water to give acetic acid and regenerate HI, Eq. 2.8) are simple organic reactions.



All iodide in the system occurs as methyl iodide and the rate of the catalytic process is independent of the methanol concentration and CO pressure. A large amount of water (14-15 wt%) is an indispensable ingredient for the above two reactions to achieve high catalyst activity and stability. However, a high concentration of water causes a major loss of carbon monoxide due to the water-gas shift reaction:



If the water content is less than 14-15 wt%, the rate-determining step becomes the reductive elimination of the acyl species from the catalyst species (4). Therefore, although the percentage of selectivity in methanol is in the high 90s, the selectivity in carbon monoxide may be as low as 90%. Water and methyl acetate is also generated *in situ* from the reaction of methanol and acetic acid. Not only water, but also HI can cause by-product formation,

⁹⁷ J. Hjortkjaer, V. W. Jenson, *Ind. Eng. Chem., Prod. Res. Dev.* 1976, **15**, 46.



The above two reactions (Eq. 2.10 and Eq. 2.11) involve the oxidation of Rh(I) to Rh(III). Rh(III) iodide precipitates from the reaction medium which results in a loss of active catalyst. It has to be converted back to Rh(I) by water and carbon monoxide.

Companies such as Hoechst have developed a slightly different process in which the water content is low in order to save CO feedstock. In the absence of water the catalyst precipitates. The HI content is lowered when the water concentration is low and therefore the formation of Rh(III) as well as the reduction of Rh(III) to Rh(I) is much slower. The water-gas shift reaction is suppressed by keeping the water content low by adding methyl acetate as part of the methanol source. Stabilisation of the rhodium species and lowering of the HI content can be achieved by the addition of iodide salts (Li, ammonium, phosphonium, etc.). Low catalyst usage and high reaction rates can be achieved at low water concentration by introducing tertiary phosphine oxide additives.⁹⁸

Detailed kinetic, spectroscopic and analytic studies of the rhodium catalysed carbonylation of ROH (R = Me, Et and Pr) has been reported.^{99,100} The reaction rates are first order in both Rh concentration and added hydrogen iodide concentration and independent of CO pressure in all cases. $[\text{Rh}(\text{CO})_2\text{I}_2]^-$ was the only rhodium species observed under catalytic conditions since after the oxidative addition of MeI, all steps are fast.

2.7.3.3 Iridium Catalysed CATIVA™ Process

The iridium-catalysed methanol carbonylation chemistry was first discovered by Paulik and Roth and later defined in more detail by Forster.^{101,102,103,104} The low-water methanol

⁹⁸ N. Hallinan, J. Hinnenkamp, *J. Chem. Ind.*, 2001, **82**, 545.

⁹⁹ T.W. Dekleva, D. Foster, *J. Am. Chem. Soc.*, 1985, **107**, 3565.

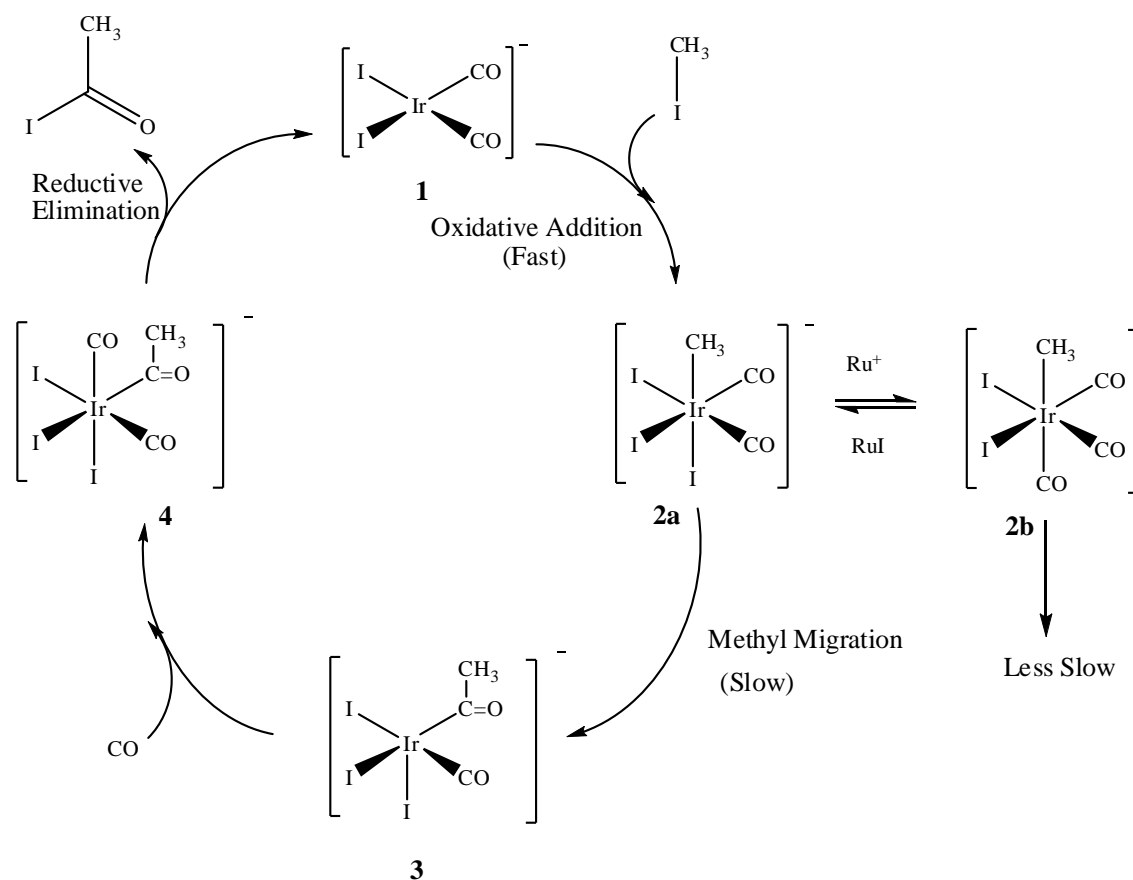
¹⁰⁰ D. Foster, T.W. Dekleva, *J. Chem. Educ.*, 1986, **63**, 204.

¹⁰¹ M.J. Howard, M.D. Jones, M.S. Roberts, S.A. Taylor, *Catal. Today*, 1993, **18**, 325.

¹⁰² G.J. Sunley, D.J. Watson, *Catal. Today*, 2000, **58**, 293.

carbonylation technology, Cativa™, was commercialized in 1996 by BP, ultimately replacing the high-water, rhodium-catalysed Monsanto process which had been used by BP. The iridium catalyst, $[\text{Ir}(\text{CO})_2\text{I}_2]^-$, (or combination of iridium and another metal, usually ruthenium, $[\text{Ru}(\text{CO})_4\text{I}_2]^-$) provides higher reaction rates and selectivity.¹⁰² The catalyst is about 25% faster than the Monsanto rhodium catalyst with exceptional product quality.¹⁰⁴

The mechanism for the Cativa™ process is more complex than that for Monsanto. For the iridium based cycle, neutral and anionic species exist as well as the employment of promoters. As seen in the reaction mechanism below, (Scheme 2-16), the active iridium catalyst species, $[\text{Ir}(\text{CO})_2\text{I}_2]^-$, proceeds through a series of reaction steps similar to the Rh catalyst, however, the iridium cycle operates with different kinetics.



Scheme 2-16: Iridium Cativa™ Process.²³

¹⁰³ D.J. Watson, *Chem. Ind. (Dekker)*, 1998, **75**, 369.

¹⁰⁴ J.H. Jones, *Platinum Met. Rev.*, 2000, **44** (3), 94.

The oxidative addition of MeI to iridium is much faster than that of the corresponding rhodium complexes^{105,106} with the rate-determining step now being the migration of the methyl group to the co-ordinated CO.^{102,107} This is a general trend for third row metals. Migration reactions for platinum complexes are also slower than those for palladium. The metal-to-carbon σ -bonds are stronger, more localized and more covalent than those in second-row metal complexes, hence a stabilisation of the Ir-CH₃ bond. Promoters are added to assist in the removal of iodide to increase the rate-limiting step. Two distinct classes of promoters exist: simple iodide complexes of Zn, Cd, Hg, Ga and In or carbonyl complexes of Re, Ru, Os or W. The promoters abstract iodide from the ionic methyl-iridium species, [MeIr(CO)₂I₃] (**2a**), forming the neutral species, [MeIr(CO)₃I₂] (**2b**), resulting in methyl migration being 800 times faster.

The iridium catalyst is able to operate at low water levels (lower than 8 wt %) leading to fewer by-product formation, improved carbon monoxide efficiency and decreased steam consumption, however a larger amount of catalyst is necessary to achieve an activity comparable to the rhodium catalyst based process. One of the major advantages of the iridium catalyst is its high solubility allowing for greater catalyst concentration, making higher reaction rates probable.⁶⁰ It is robust and stable under a wide range of experimental conditions which is ideal for optimisation of the methanol carbonylation process. The CativaTM process delivers acetic acid with a selectivity in excess of 99% based upon methanol.

¹⁰⁵ P.R. Ellis, J.M. Pearson, A. Haynes, H. Adams, N.A. Bailey, P.M. Maitlis, *Organometallics*, 1994, **13**, 3215.

¹⁰⁶ T.R. Griffin, D.B. Cook, A. Haynes, J.M. Pearson, D. Monti, G.E. Morris, *J. Am. Chem. Soc.*, 1996, **118**, 3029.

¹⁰⁷ T. Ghaffar, J.P.H. Charmant, G.J. Sunley, G.E. Morris, A. Haynes, P.M. Maitlis, *Inorg. Chem. Commun.* 2000, **3**, 11.

3

BASIC THEORY OF SOLID AND SOLUTION STATE CHARACTERISATION

3.1 INTRODUCTION

Characterisation techniques assist in identifying starting materials, possible intermediates and final products of reaction mixtures. Non-destructive methods such as Infrared spectroscopy (IR), Ultraviolet/Visible spectroscopy (UV-vis) and X-ray Diffraction crystallography (XRD) identify the components without destroying the sample during the characterisation process. These techniques also play a major role in determining the mechanism of reactions in chemical kinetic studies. The basic theory of these characterisation techniques will be discussed in this chapter.

3.2 INFRARED SPECTROSCOPY (IR)

Infrared spectroscopy is a valuable tool for organic and inorganic compound characterisation. This method identifies a compound or its functional groups due to the fact that all molecular compounds (except for some homonuclear molecules such as O₂ and H₂) absorb infrared radiation. Each compound has a unique infrared spectrum much like a molecular fingerprint that can be used to determine whether or not a desired product was indeed synthesised. So even though the same type of bond is present in two different compounds they do not give the same spectra since the bonds experience different environments.¹

¹ J. Coates, *Encyclopedia of Analytical Chemistry; Interpretation of Infrared Spectra, A Practical Approach*, 2000, 10815.

An infrared spectrum is obtained by passing infrared radiation through a sample and determining what fraction of radiation is absorbed at a particular energy. Frequency (ν) is the number of wave cycles passing through a point in one second. Wavelength (λ) is the length of one complete wave cycle and the relation between the two can be illustrated as follows:

$$\nu = \frac{c}{\lambda} \text{ or } \lambda = \frac{c}{\nu} \quad 3.1$$

where c = speed of light (3×10^{10}) cm sec⁻¹.

For energy calculations, the following equation can be used:

$$E = h\nu = \frac{hc}{\lambda} \quad 3.2$$

where h = Planck's constant. Energy is thus linear to frequency. Another unit which is widely used in infrared spectroscopy is the wavenumber, $\bar{\nu}$, in cm⁻¹. This is the number of waves in a length of one centimetre and is given by the following relationship:

$$\bar{\nu} = \frac{1}{\lambda} = \frac{\nu}{c} \quad 3.3$$

IR works on the basis of changes in molecular dipoles associated with vibrations and rotations of the atoms of a molecule. A molecule can be looked at as an arrangement of atoms joined by bonds with spring-like properties. Vibrations involve either a change in bond length (stretching) or bond angle (bending). Some bonds stretch in-phase (symmetrical) or out-of-phase (asymmetric stretching). Only molecules that possess an electric dipole moment that changes during the vibration, shows infrared absorption. The number of ways a molecule can vibrate is comparative to the number of atoms and bonds within the molecule. Molecular vibration energy is generated when molecules absorb infrared radiation. IR radiation causes the excitation of vibrational and rotational transitions of covalent bonds, but has too little energy to excite electrons. The energy at which any peak in an absorption spectrum appears corresponds to the frequency of vibration of a certain part of a molecule.²

² K, Nakamoto, *Infrared Spectra of Inorganic and Coordination Compounds*, 2nd Ed., New York: John Wiley & Sons, Inc., 1970.

The carbonyl group stretching frequency characteristically falls in the range from 2360 to 1080 cm^{-1} . However, metal carbonyl (M-CO) complexes² range from 2200 to 1700 cm^{-1} and due to this distinct trait,³ the carbonyl group absorption frequency is often used for complex characterisation.⁴ Due to the difference in electronegativity between the carbon and oxygen atom the carbonyl group is permanently polarized. Any vibrational stretching of this bond will then in fact alter the dipole moment. Carbonyl is a strong π -acceptor ligand that assists in removing electron density from a metal centre, stabilising electron rich low oxidation state species. The carbonyl stretching frequency is thus largely affected by ligands *trans* to the carbonyl group as they compete for electrons. As the electron-donating capability of the ligand decreases, the electron density of the metal also decreases. As electrons are removed from the metal centre the ability of the metal to partake in back-donation to the anti-bonding π^* orbitals of the CO group is reduced and as a result, the $\nu(\text{CO})$ increases. The carbonyl stretching frequency is a useful technique to evaluate what effect different ligands have on the relative electron density on metal centres.

3.3 ULTRAVIOLET-VISIBLE SPECTROSCOPY (UV-VIS)

UV-Vis spectroscopy is primarily used in the quantitative determination of solutions of transition metal ions and highly conjugated organic compounds.⁵ This method is based on the absorption of energy. Ultraviolet and visible light range in wavelengths from 190 to 800 nm. The absorption of electromagnetic radiation causes the transition between electronic energy levels, i.e. electrons residing in the ground state (highest occupied molecular orbital -HOMO) can get promoted to the excited state (lowest unoccupied molecular orbital - LUMO).⁶ Therefore electrons in the HOMO of a sigma bond (σ) can get excited to the empty anti-bonding σ^* -orbital (LUMO) of that bond. This is noted as a $\sigma \rightarrow \sigma^*$ transition. Likewise, electrons from the π -bonding orbital can be promoted to the anti-bonding π^* -orbital. Non-bonding (lone pair electrons) orbitals (n) have their own transitions. The following molecular electronic transitions exist:

³ B. Stuart, *Modern Infrared Spectroscopy*, Editor: D.J. Ando, England: John Wiley & Sons, Inc., 1996.

⁴ E.W. Abel, M.A. Bennet, G. Wilkinson, *J. Chem. Soc.*, 1959, 2323.

⁵ C.N.R. Rao, *Ultra-Violet & Visible Spectroscopy: Chemical Applications*, 2nd Ed., England: Butterworth & Co. (Publishers) Ltd., 1967.

⁶ D.L. Pavia, G.M. Lampman, G.S. Kriz, *Introduction to Spectroscopy*, 3rd Ed., USA: Thomson Learning Inc., 2001.

- $\sigma \rightarrow \sigma^*$
- $\pi \rightarrow \pi^*$
- $n \rightarrow \sigma^*$
- $n \rightarrow \pi^*$

The electromagnetic radiation that is absorbed has energy exactly equal to the energy difference between the excited and ground states. The wavelength at which the molecules absorb energy depends on how tightly its valence electrons are bound to the atom. Electrons are not strongly held in double and triple bonds and are easily excited yielding useful absorption peaks.

3.4 X-RAY DIFFRACTION (XRD)

The geometry of a molecule is a fundamental property to identify as it aids considerably in proposing a mechanism of a reaction. X-ray crystallography is a very powerful identification technique of characterising complexes in the solid state. It is used to determine exactly how the atoms of a compound are arranged in space. This is accomplished when X-ray beams irradiates a crystal sample and is scattered into many directions by each atom in the crystal. These scattered beams create a diffraction pattern which is interpreted mathematically by computer, producing a three-dimensional picture of the electronegativity of electrons within a crystal which in turn determine the mean positions of the atoms. From the diffraction pattern, bonds, angles, disorders and a great deal of other information is also obtained.⁷

X-rays had been discovered in 1805, but it wasn't until 1912 that the diffraction of X-rays by crystals was discovered. The observation of X-ray diffraction by crystals confirmed that X-rays were a form of electromagnetic radiation.⁸ X-ray radiation is used due to the size of the observed species. The size of the object needs to be at least half the wavelength of the light used to see it. X-rays have wavelengths in the range of 0.02 to 100 Å (1 Å = 10⁻¹⁰ metres), which is similar to the size of atoms, making it the ideal electromagnetic radiation to observe crystals. Visible light has a wavelength longer than the distance between

⁷ W. Clegg, *Crystal Structure Determination*, New York: Oxford University Press, Inc., 1998.

⁸ W. Friedrich, P. Knipping, M. von Laue, *Interferenz-Erscheinungen bei Röntgenstrahlen*, 1912, 202.

atoms and is thus unable to penetrate on molecular scale. The smaller wavelengths of X-rays are idyllic for structural analysis on molecular level proving useful also in the medical field for imaging internal structures and organs.

A crystal is a solid compound in which the atoms are periodically arranged in three dimensions making them ideal for XRD since it will show repeated patterns within the entire structure. A lattice of the structure is an array of identical points and is built up from many unit cells. The unit cell is the smallest possible unit that is a representation of the whole crystal as it is repeated in all directions of the crystal axes to produce the complete crystal. A unit cell consists of three edge lengths (a, b, c) and three angles (α , β , γ).⁹ The directions and planes in a crystal lattice are known as Miller indices (hkl). There is a limited number of ways that a set of objects can be arranged in three-dimensional space to result in a crystallographic periodic system. The space group of a crystal describes the symmetry of the unit cell, and can be one of 230 different types. These space group variations are well established and can be found in the International Tables for Crystallography.¹⁰

3.4.1 Bragg's Law

X-rays are diffracted by "lattice planes" within a crystal. All X-rays reflected from a given plane are in phase after reflection. Neighboring plane X-rays travel different path lengths and are out of phase after reflection. Bragg's law is used to correct phase difference¹¹ for diffracted rays by two adjacent planes:

$$n\lambda = 2d_{hkl}\sin\theta \quad 3.4$$

where n represents an integer, λ the wavelength, d_{hkl} the distance between successive parallel crystal planes and θ the angle of incidence and reflection.¹²

⁹ D.W.A. Sharpe, *The Penguin Dictionary of Chemistry*, 3rd Ed., London: Penquin Books Ltd., 2003.

¹⁰ *International Tables for Crystallography*, A, 5th Ed., Kluwer Academic Publishers, 2002.

¹¹ M.F.C. Ladd, R.A. Palmer, *Structure Determination by X-ray Crystallography*, New York: Plenum Press, 1977.

¹² J.M. Buerger, *X-Ray Crystallography*, London: Academic Press, 1971.

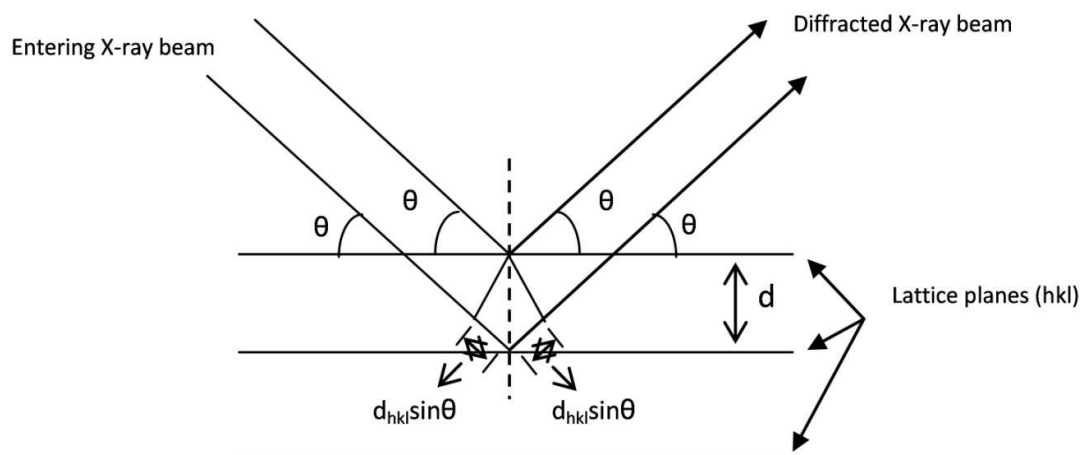


Figure 3-1: Bragg's assembly of X-Ray diffraction.

X-rays are reflected by evenly spaced planes within a crystal structure at the same angle. A part of a X-ray that's not reflected off the upper atomic plane with angle θ , can pass on to a next deeper level into the crystal and reflect at the same angle. All X-rays reflected of a given plane is in phase afterwards. X-rays travel a distance of $2d_{hkl} \sin \theta$ between adjacent planes. The orientation of a set of planes is represented by Miller indices (hkl). The spacing between these lattice planes is represented as d . For application purposes these lattice planes can be thought of as reflecting the X-rays from it, even though this is not exactly true seeing as X-rays are scattered by electrons of atoms. Each hkl value represents a point in the reciprocal space that is created from the set of hkl planes in real space. If the reciprocal lattice, the lattice created by diffracted X-rays, can be indexed, the hkl values can be assigned to each diffraction spot with a specific intensity.

The Laue class is assigned to the crystal from the relation of the intensity weighted reciprocal lattice. By using the systematic extinctions in the reciprocal space the space group can be assigned. The systematic extinctions occur from the specific symmetry in the crystal and are determined from structure factors in a certain space group.¹⁰ If the proper space group can be assigned, the chance of solving the structure is quite high.

3.4.2 Structure Factor

An atom's coordinates in a unit cell is described in terms of Miller index (hkl). Each is a number between 0 and 1 and cell edges are defined by vectors a, b and c. The position of an atom expressed in terms of fractional coordinates is given as:

$$R = hx + ky + lz \quad 3.5$$

The structure factor, F_{hkl} , expresses the overall scattering of all atoms (j) in the unit cell relative to that of a single electron. This is expressed as:¹¹

$$F_{hkl} = \sum_{j=1}^N f_j \exp [i2\pi(hx_j + ky_j + lz_j)] \quad 3.6$$

where f_j is the scattering factor of each individual N atoms and (x_j, y_j, z_j) are the coordinates of each atom in the unit cell. The structure factor's magnitude is dependent on the relative position of the atoms and their scattering factors. The equation represents a wavelet with an amplitude of f_j and phase $\Phi_j = 2\pi(hx_j + ky_j + lz_j)$ which expresses the path length for each scattered wavelet. The structure factor is then simply the resultant of wavelets scattered by the N atoms in the unit cell.¹³ The equation can also be written as:

$$F_{hkl} = \sum_{j=1}^N f_j [\cos 2\pi(hx_j + ky_j + lz_j) + i \sin 2\pi(hx_j + ky_j + lz_j)] \quad 3.7$$

The energy in a cosine wave is proportional to the square of the amplitudes of the wave. In X-ray diffraction the intensity of the scattered wave is used, $I_0(hkl)$, representing an experimentally observed quantity. $I_0(hkl)$ can be used to represent $|F_{hkl}|^2$ which is the ideal intensity. Therefore:

$$I_0(hkl) \propto |F_0(hkl)|^2 \quad 3.8$$

This allows the experimental $I_0(hkl)$ values to be directly related to the structure properties by $|F_{hkl}|$.

¹³ L.V. Azaroff, *Elements of X-ray Crystallography*, New York: McGraw-Hill, Inc., 1968.

The X-ray diffraction pattern created when X-rays are scattered by electrons associated with atoms in a unit cell can be used to determine the crystal structure. Atoms with higher atomic numbers yield greater concentrations of electrons than atoms with lower atomic number. Electron density is a function of position and can be expressed as $p(X, Y, Z)$. Through the relation of electron density and structure factor the following equation is obtained.

$$F_{hkl} = \int p(x, y, z) \exp[i2\pi(hx_n + ky_n + lz_n)] dV \quad 3.9$$

3.4.3 ‘Phase Problem’

Analysis of a crystal structure by X-ray diffraction is fraught by the inability to determine the complete vectorial structure factor. In determining a crystal structure the modulus, $|F(hkl)|$, can be obtained from the intensity data (Eq. 3.8), but the corresponding phase, $\Phi(hkl)$, cannot be directly measured. In order to determine the structure, both amplitude and phase must be known as it cannot be solved directly from the observed intensity data. This incapacity to determine the phase is known as the ‘Phase Problem’ and can be overcome by a number of methods of which two are very common.

3.4.3.1 Direct Method

The direct method resolves the approximate reflection phases from measured X-ray intensities *via* mathematical formulae. The direct method proves most useful for structures consisting only of light atoms. The Patterson function is used with compounds where one atom or a small number of atoms are substantially heavier than the rest.¹¹

3.4.3.2 Patterson Function

The Fourier transform of the squared amplitudes, $|F_0(hkl)|^2$, with all phases set equal to zero gives the Patterson Function.

$$P(u, v, w) = V^{-1} \sum_h \sum_k \sum_l (F_{hkl})^2 \exp [-2\pi i(hu + kv + lw)] \quad \mathbf{3.10}$$

The Patterson Function bears a resemblance to an electron density map with peaks of positive electron density in various positions. The Patterson Function is a map of vectors between pairs of atoms in the structure. For every peak at point (u, v, w), there are two atoms in the structure whose x coordinates differ by u, y coordinates differ by v and z coordinates differ by w. The Patterson peaks reveal where atoms lie relative to each other but not where they lie relative to the unit cell origin. The Patterson peaks are proportional in size of the atoms involved.

3.4.4 Least Square Refinement

The least square refinement is a technique used to compare the calculated diffraction pattern with the observed diffraction pattern to acquire the degree of resemblance between them. The comparison of the calculated structure factor (F_c) to the experimental data (F_o) is described in terms of *residual index* or *R-factor*.¹⁴

$$R = \frac{\sum |F_o| - |F_c|}{\sum |F_o|} \quad \mathbf{3.11}$$

If the value of the R-factor is between 0.02 and 0.07 it indicates a complete and correct crystal structure determination from good quality experimental data.

A more meaningful equation than the basic R-factor employs a new residual factor which is widely used for crystal structure determination. A weighting factor is added for each reflection, w, incorporating information on the relative reliability of different measurements.

$$wR^2 = \frac{\sum w(F_o^2 - F_c^2)^2}{\sum w(F_o^2)^2} \quad \mathbf{3.12}$$

¹⁴ G.H. Stout, L.H. Jensen, *X-ray Structure Determination: A Practical Guide*, London: The Macmillan Company, 1968.

3.5 THEORETICAL ASPECTS OF CHEMICAL KINETICS

3.5.1 INTRODUCTION

Chemical kinetics deals with the quantitative determination of the rates of chemical reactions, factors which influence the rates and the explanation of the rates in terms of the reaction mechanisms of chemical processes. In chemical kinetics the rate of changing concentrations of reactants or products with respect to time is followed. If the effect of various influencing factors on the reaction rate is known, an interpretation of the empirical laws in terms of reaction mechanism can be formulated. Factors that may have an effect on the reaction rate include: concentration, pressure, temperature, effect of catalyst, sensitivity to light and air and solvent. Spectrophotometry is often used for kinetic measurements since all molecules have a unique absorption spectrum. Kinetic study by UV-vis spectroscopy is described by the Beer-Lambert law¹⁵, illustrating the relationship of concentration to absorption.

$$\log_{10} \frac{I_0}{I_{\text{trs}}} = \varepsilon Cl = A \quad 3.13$$

where I_0 = intensity of the incident monochromatic light, I_{trs} = transmitted intensity, ε = extinction coefficient, C = concentration, l = path length through the sample and A the absorbance.

3.5.2 Reaction Rates and Rate Laws

The rate of a reaction can be expressed in terms of any one of the reactants or any one of the products of the reaction. The rate of the reaction is the change in the number of molecules of reactants or products over time.

¹⁵ P.W. Atkins, *Physical Chemistry*, Oxford: Oxford University Press Inc., 1994.

In a general reaction:



the rate can be expressed as,

$$\text{Rate of reaction} = -\frac{d[A]}{dt} = -\frac{d[B]}{dt} = \frac{d[C]}{dt} \quad \mathbf{3.14}$$

where $d[A]$ and $d[B]$ are the changes in concentration of reactant over a period of time, dt , and $d[C]$ is the change in concentration of the product. The reactant is being consumed thus the concentration decreases with time hence the minus sign so the rate will be a positive quantity.

The rate law can be defined as “the experimentally determined dependence of the reaction rate on the reagent concentrations”.¹⁶ In general, the rate law has the following form,

$$\text{Rate} = k[A]^\alpha[B]^\beta \dots \quad \mathbf{3.15}$$

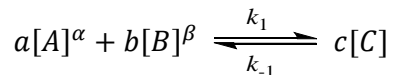
where k is the rate constant, components α and β are determined experimentally and represent the order of the reaction with regards to the concentrations of A and B. The sum of α and β will give the total order of the reaction. The rate constant is independent of A and B concentrations but can be influenced by environmental factors mentioned earlier. The rate constant is unique for every reaction.

In typical catalytic reactions the catalyst concentration remains constant or one reactant is in great excess with respect to the other reactants so that during the reaction run there is a minuscule change in the concentration of the former.¹⁷ In other words, for conditions where $[B] \gg [A]$, the concentration of B will stay constant while the concentration of A varies. These reactions are called *pseudo-n*th order reactions where n is the sum of the exponents of the concentrations that change during the reaction run.

¹⁶ R.B. Jordan, *Reaction Mechanisms of Inorganic and Organometallic Systems*, Oxford: Oxford University Press, Inc., 1991.

¹⁷ J.W. Moore, R.G. Pearson, *Kinetics and Mechanism*, 3rd Ed., New York: John Wiley & Sons, Inc., 1981.

A *pseudo*-first order equilibrium reaction, where $[B] \gg [A]$, can be given as,



$$\text{Rate} = k_{obs}[A]^\alpha - k_{-1}[C] \text{ where } k_{obs} = k[B]^\beta \quad \mathbf{3.16}$$

k_{obs} = the observed rate constant. The rate constant, k , can be determined by varying the concentration of B. The equilibrium constant for an equilibrium reaction is given by,

$$K_{eq} = \frac{k_1}{k_{-1}} \quad \mathbf{3.17}$$

where k_1 = forward reaction and k_{-1} = reverse reaction.

By integration of the initial rate expression from $t=0$ to a random point of time (t), we obtain the equation,

$$\ln \frac{[C]_t}{[C]_0} = -k_{obs}t \text{ or } [C]_t = [C]_0 e^{-k_{obs}t} \quad \mathbf{3.18}$$

$[C]_t$ and $[C]_0$ is the concentration change of the reactant at time = 0 and t respectively. Through the basic principles of the Beer-lambert law, expressing absorbance in terms of concentration, and a bit of mathematical manipulation, the above equation can be given as,

$$A_{obs} = A_\infty - (A_\infty - A_0)e^{-k_{obs}t} \quad \mathbf{3.19}$$

where A_t = absorbance after time t and A_∞ = absorbance at infinite time (when reaction is complete). Absorbance versus time data can be used in a least-squares fit to give k_{obs} for the reaction. The half-life ($t_{1/2}$) for a first order reaction, meaning the time needed for the reactant concentration to decay by 50%, will be:

$$t_{1/2} = \frac{\ln 2}{k_{obs}} = \frac{0.693}{k_{obs}} \quad \mathbf{3.20}$$

3.6 NUCLEAR MAGNETIC RESONANCE (NMR) SPECTROSCOPY

Nuclear magnetic resonance (NMR) spectroscopy is the study of a molecular structure through measurement of the interaction of an oscillating radio-frequency electromagnetic field with a collection of atomic nuclei immersed in a strong external magnetic field. Aside from X-ray crystallography which can determine the complete molecular structure of a compound, NMR spectroscopy is the chemist's most direct tool for identifying the structure of both pure compounds in addition to mixtures. In 1902 the strange behaviour of certain nuclei when subjected to a strong external magnetic field was discovered. Fifty years later the first crude NMR spectrometer was constructed and in following years NMR has completely revolutionized the study of chemistry and biochemistry.

Hydrogen is found in almost all organic compounds and is composed of a single proton and single electron. For NMR purposes, the key feature of the hydrogen nucleus is its angular momentum properties, resembling those of a classical spinning particle. The spinning hydrogen nucleus is positively charged therefore generating a small magnetic field and the resulting spin-magnet possesses a magnetic moment (μ) proportional to the spin. The magnitude of the magnetic moment produced by the spinning nucleus varies for each atom according to the equation:

$$\mu = \frac{\gamma h}{2\pi} \quad 3.21$$

where h = Planck's constant and γ = gyromagnetic or magnetogyric ratio. This is similar to a charge moving in a circle creating a magnetic field (Figure 3-2). The magnetic moment (μ) has both magnitude and direction as defined by its axis of spin. NMR exploits the magnetic properties of nuclei to provide valuable information on the molecular structure of compounds.

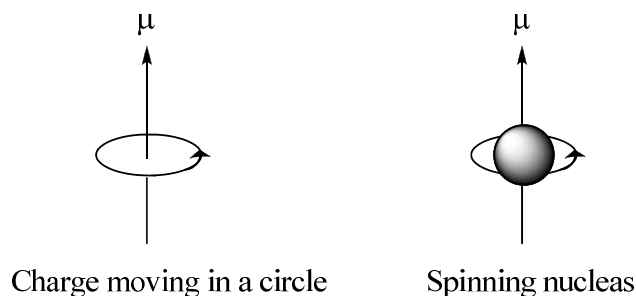


Figure 3-2: Similarities between a charge moving in a circle and a spinning nucleus.

When the atomic number (the number of protons) and the atomic mass (the sum of the protons and neutrons) of an atom is equal, the nucleus has no magnetic properties and has a nuclear spin (I) of zero. These atoms are invisible to NMR, e.g. carbon (^{12}C) and oxygen (^{16}O). When either the atomic number or atomic mass is odd, or if they are both odd, the nucleus has magnetic properties and is understood to be spinning. Spinning nuclei have a nuclear spin of $\frac{1}{2}$ or more (in increments of $\frac{1}{2}$). The nuclei with $I = \frac{1}{2}$ is the most easily examined by NMR spectroscopy e.g. ^1H , ^{31}P and ^{13}C . In order to study nuclear magnetic properties, the nuclei must be subjected to a strong external magnetic field, B_0 . In the absence of the external magnetic field the energy of all the nuclei of the same isotope is equal. The energies of the nuclei are affected when the B_0 field is turned on along a designated axis (z). Magnetic moments have a tendency to align in the $B_0(+z)$ direction over the opposite direction ($-z$). The B_0 force causes the magnetic moment to move in a circular fashion about the $+z$ and $-z$ directions, a motion called precession (Figure 3.3). Nuclei with spin = $\frac{1}{2}$ only has two possible magnetic orientations ($+z$, $-z$) of spin and each is given a nuclear spin quantum number (m) therefore $m = \pm \frac{1}{2}$ due to each B_0 direction.

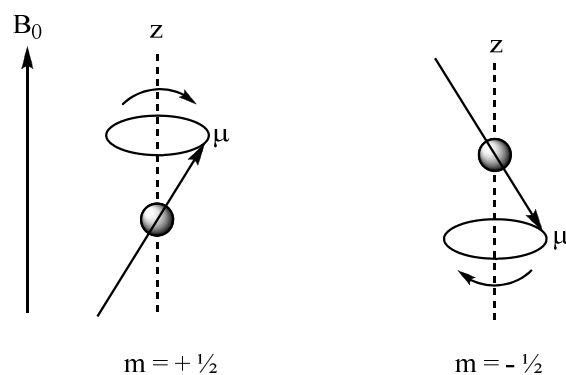


Figure 3-3: Axis of rotation precessing around the magnetic field (B_0).

The frequency of this precession is called the Larmor frequency and is identical to the transition frequency which is given by:

$$E = -\mu B \cos\theta \quad 3.22$$

Complex nuclei have more than two spin states and the total number of possible spin states (multiplicity)¹⁸ is determined by:

$$\text{Multiplicity} = 2I + 1 \quad 3.23$$

The $m = +\frac{1}{2}$ spin state has a slightly lower energy than $m = -\frac{1}{2}$. The tendency of a nucleus to spin in the +z direction in the presence of an external magnetic field is due to the fact that as the B_0 field increases, the difference in energy between the two spin states increases and the frequency of radiation needed to excite the nuclei in the lower level depends on the energy difference between the levels.⁶

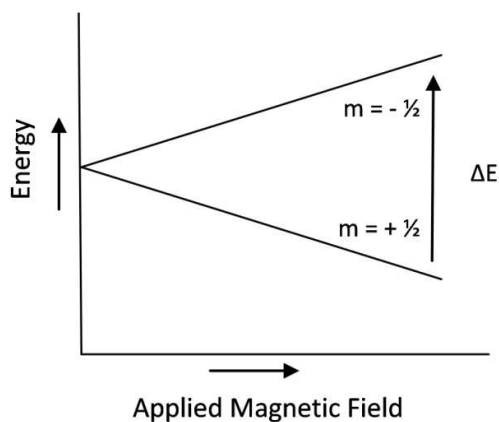


Figure 3-4: Energy difference between spin states as a function of applied magnetic field.

The electron density surrounding the nucleus also has charge, motion and hence a magnetic moment. The magnetic field generated by the electrons alters the applied magnetic field B_0 around the nucleus. The actual field that is present at a given nucleus is dependent on the nature of the surrounding electrons. This electron variation of the B_0 field is termed

¹⁸ P.J. Hore, *Nuclear Magnetic Resonance*, New York: Oxford University Press, Inc., 1995.

shielding. The presence of electron-withdrawing groups in a molecule reduces the electron density around a proton and is termed deshielding causing a higher resonance frequency. Shielding is the exact opposite causing a lower resonance frequency in molecules with electron-donating groups. If two protons in a molecule exist in two distinct magnetic environments, each with spin = $\frac{1}{2}$, ($m = +\frac{1}{2}$ and $m = -\frac{1}{2}$), the form of the resonance is altered and split into two peaks. The distance between two peaks for the resonance of one nucleus split by another is called the coupling constant (J) and is measured in hertz (Hz). It is a measure of how strongly the nuclear spins influence each other. The influence of neighbouring spins on the multiplicity of peaks follow the 'n+1' rule where n = the number of equivalent protons in neighbouring atoms plus 1. Equivalent nuclei don't interact with each other; they only cause splitting of the neighbouring protons.

4

SYNTHESES OF IRIDIUM(I) COMPOUNDS

4.1 INTRODUCTION

The synthesis and characterisation of a range of Ir(I) phosphine complexes are discussed in this chapter. Complex characterisation was performed by using various techniques, including NMR, IR and X-ray crystallography. A search on the Cambridge Structural Database¹ (CSD) showed no examples of *bis*-phosphine, O,O'-bidentate donor ligand iridium(I) complexes.

A well-known hydroformylation precatalyst system is [Rh(acac)(CO)₂]/PPh₃ with the ultimate active catalyst species being [RhH(CO)(PPh₃)₃].^{2,3} In this study, iridium systems are used as model complexes^{4,5} to explore the interaction between [Ir(acac)(CO)₂] and four tertiary phosphine ligands, stepwise manipulating the substituents from triphenylphosphine to tricyclohexylphosphine (Figure 4-1) in order to gather information regarding the kinetics and coordination intermediates during model hydroformylation reactions.

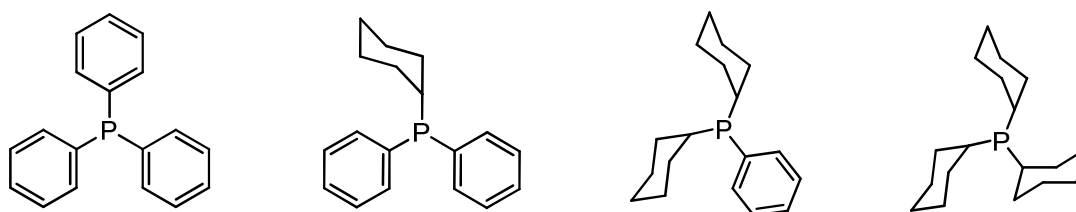


Figure 4-1: Structures of the four tertiary phosphine ligands: triphenylphosphine (PPh₃), cyclohexyldiphenylphosphine (PPh₂Cy), dicyclohexylphenylphosphine (PPhCy₂) and tricyclohexylphosphine (PCy₃).

¹ Cambridge Structural Database (CSD), Version 5.30, May 2009 update, F.H. Allen, *Acta Cryst.*, 2002, **B58**, 380.

² F. Bonati, G. Wilkinson, *J. Chem. Soc.*, 1964, 3156.

³ A.M. Trzeciak, J.J. Ziołkowski, *Inorg. Chim. Acta*, 1985, **96**, 15.

⁴ R. Eisenberg, D.J. Fox, S.B. Duckett, C. Flaschenriem, W.W. Brennessel, J. Schneider, A. Gunay, *Inorg. Chem.*, 2006, **45**, 7197.

⁵ R. Whyman, *J. Organomet. Chem.*, 1975, **94**, 303.

4.2 CHEMICALS AND APPARATUS

All reagents used for the synthesis and characterization were of analytical grade and were purchased from Sigma-Aldrich, South Africa, unless otherwise stated. Reagents were used as received, without further purification. $\text{H}_2\text{IrCl}_6 \cdot 6\text{H}_2\text{O}$ was commercially available from Next Chimica. All organic solvents were purified and dried according to literature.⁶

All the infrared spectra of the complexes were recorded on a Bruker Tensor 27 Standard System spectrophotometer with a laser range of $4000 - 370 \text{ cm}^{-1}$, coupled to a computer. Solid samples were analyzed either as KBr pellets or *via* ATR infrared spectrophotometry. Liquid samples were analyzed in dry organic solvents in a NaCl liquid cell. All data was recorded at room temperature.

All ^1H and ^{31}P NMR spectra were obtained on a Bruker AXS 600 MHz nuclear magnetic resonance spectrometer at 600.28 and 242.99 MHz, respectively in C_6D_6 or C_7D_8 . Chemical shifts of ^1H NMR spectra are reported relative to tetramethylsilane using the C_6D_6 (7.16 ppm) peak. ^{31}P NMR spectra were referenced externally to 85 % H_3PO_4 (0.0 ppm).

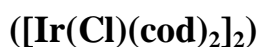
4.3 SYNTHETIC PROCEDURES

The *trans*- $[\text{Ir}(\text{acac})(\text{CO})(\text{PR}_3)_2]$ ($\text{PR}_3 = \text{PPh}_3, \text{PPh}_2\text{Cy}, \text{PPhCy}_2, \text{PCy}_3$) complexes were all synthesised under Schlenk conditions due to the air- and moisture sensitive nature of iridium(I). Crystals, suitable for X-ray crystallography, were obtained from crystallisation from a combination of MeOH, toluene and acetone at $-21.0 \text{ }^\circ\text{C}$.

⁶ D.D. Perrin, W.L.F. Armarego, *Purification of Laboratory Chemicals*, 3rd Ed., Pergamon Press, 1988.

4.3.1 Syntheses of Starting Compounds

4.3.1.1 Synthesis of di- μ -chlorido-bis(1,5-cyclooctadiene)diiridium(I)



Hydrated iridic acid, $\text{H}_2[\text{IrCl}_6] \cdot x\text{H}_2\text{O}$, (500 mg, 1.228 mmol) and hydroquinone (407 mg, 3.697 mmol) were heated under reflux for 1 h with a mixture of ethanol and water (2:1, 30 cm^3). The ethanol/water mixture was deoxygenated by bubbling N_2 through the solvent mixture for half an hour prior to use. *cis*-cycloocta-1,5-diene (cod) (0.605 cm^3 , 4.933 mmol) was then added to the reaction mixture and refluxed for a further 5 hours. The mixture was concentrated to *ca.* 15 cm^3 resulting in the formation of an orange-red solid. The mixture was cooled to room temperature and water (3 cm^3) was added to the solution. The precipitate was filtered and washed with cold methanol (3 x 5 cm^3) to remove traces of unreacted cod and dried overnight in a vacuum desiccator over P_2O_5 .

Yield: 288.7 mg, 70 %

^1H NMR C_6D_6 (7.16): δ 4.2 (s, 4H, =CH, cod), 1.9 (s, 4H, CH_2 , cod), 1.2 (m, 4H, CH_2 , cod)

IR (KBr) ν (cm^{-1}): = 1471, 1446 (C=C, cod)

4.3.1.2 Synthesis of (acetylacetonato)(1,5-cyclooctadiene)iridium(I)



$[\text{Ir}(\text{Cl})(\text{cod})_2]_2$ (100 mg, 0.149 mmol) was dissolved in minimum amount dimethylformamide (DMF) (± 3 cm^3). Acetylacetone (acacH) (32 μl , 0.313 mmol) was added and the reaction mixture was stirred for 20 min. The product was precipitated with ice as a yellow solid and filtered. The product was dried in a vacuum desiccator over P_2O_5 .

Yield: 72.1 mg, 61 %

^1H NMR in C_6D_6 (7.16): δ 4.3 (s, 4H, =CH, cod), 2.2 (m, 4H, CH_2 , cod), 1.5 (m, 4H, CH_2 , cod), 5.1 (s, 1H, C-H, acac), 1.7 (s, 6H, CH_3 , acac)

IR (KBr) ν (cm^{-1}): 1382, 1353 (C=C, cod); 1565, 1528 (C-O (Ar) (Aromatic)), acac)

4.3.1.3 Synthesis of (acetylacetonato)(dicarbonyl)iridium(I) ([Ir(acac)(CO)₂])

[Ir(acac)(cod)] (50 mg, 0.125 mmol) was dissolved in hexane and CO was bubbled through the solution for several hours at a constant temperature of 25.0 °C under an argon atmosphere. A golden-brown precipitate formed and the solvent was removed under vacuum.

Yield: 32.1 mg, 74 %

¹H NMR in C₆D₆ (7.16): δ 5.0 (s, 1H, C-H, acac), 1.5 (s, 6H, CH₃, acac)

IR (ATR) ν (cm⁻¹): 2045, 1984 (C≡O); 1559, 1529 (C-O (Ar), acac)

IR (MeOH) ν (cm⁻¹): 2072, 1996 (C≡O)

4.3.2 Syntheses of *trans*-[Ir(acac)(CO)(PR₃)₂] Compounds

4.3.2.1 Synthesis of *trans*-[Ir(acac)(CO)(PPh₃)₂]

[Ir(acac)(CO)₂] (60 mg, 0.173 mmol) and 1.1 eq PPh₃ (50.1 mg, 0.191 mmol) were dissolved in MeOH (± 5 cm³) and the reaction mixture was stirred at 40.0 °C for 15 min. During this time precipitation of the yellow product started to occur. Most of the solvent was evaporated under vacuum causing further precipitation followed by filtration of the product.

Yield: 81.5 mg, 56 %

¹H NMR in C₆D₆ (7.16): δ 5.2 (s, 1H, C-H, acac), 1.8 (s, 3H, CH₃, acac), 1.3 (s, 3H, CH₃, acac)

³¹P NMR in C₇D₈: δ 18.4

IR (ATR) ν (cm⁻¹): 1942 (C≡O); 1560, 1521 (C-O (Ar), acac)

4.3.2.2 Synthesis of *trans*-[Ir(acac)(CO)(PPh₂Cy)₂]

[Ir(acac)(CO)₂] (60 mg, 0.173 mmol) and 2.1 eq PPh₂Cy (97.4 mg, 0.362 mmol) were dissolved in acetone ($\pm 5 \text{ cm}^3$) and the reaction mixture was stirred at 40.0 °C for 20 min. The solution was concentrated to *ca.* 2 cm³ and addition of hexane caused the precipitation of a yellow solid. The product was filtered and dried in vacuo.

Yield: 74.3 mg, 50 %

¹H NMR in C₆D₆ (7.16): δ 5.6 (s, 1H, C-H, acac), 2.5 (s, 3H, CH₃, acac), 1.9 (s, 3H, CH₃, acac)

³¹P NMR in C₇D₈: δ 33.5

IR (ATR) ν (cm⁻¹): 1952 (C≡O); 1631, 1518 (C-O (Ar), acac)

4.3.2.3 Synthesis of *trans*-[Ir(acac)(CO)(PPhCy₂)₂]

[Ir(acac)(CO)₂] (60 mg, 0.173 mmol) and 2.1 eq PPhCy₂ (99.7 mg, 0.363 mmol) were dissolved in toluene ($\pm 5 \text{ cm}^3$) and the reaction mixture was stirred at 80.0 °C for 30 min. All solvents were evaporated and addition of MeOH and hexane caused the formation of two layers: a brown top layer and yellow bottom layer. The yellow layer was extracted and removal of solvents yielded a yellow solid.

Yield: 79.5 mg, 53 %

¹H NMR in C₆D₆ (7.16): δ 5.9 (s, 1H, C-H, acac), 2.7 (s, 3H, CH₃, acac), 2.5 (s, 3H, CH₃, acac)

³¹P NMR in C₇D₈: δ 34.0

IR (ATR) ν (cm⁻¹): 1954 (C≡O); 1606, 1496 (C-O (Ar), acac)

4.3.2.4 Synthesis of *trans*-[Ir(acac)(CO)(PCy₃)₂]

[Ir(acac)(CO)₂] (60 mg, 0.173 mmol) and 2.1 eq PCy₃ (101.4 mg, 0.361 mmol) were dissolved in toluene ($\pm 5 \text{ cm}^3$) and the reaction mixture was stirred at 80.0 °C for 30 min. After all solvents were evaporated, hexane was added causing the precipitation of a yellow solid. The products was filtered and dried in vacuo.

Yield: 90.1 mg, 60 %

¹H NMR in C₆D₆ (7.16): δ 5.9 (s, 1H, C-H, acac), 2.8 (s, 3H, CH₃, acac), 2.3 (s, 3H, CH₃, acac)

³¹P NMR in C₇D₈: δ 33.2

IR (ATR) ν (cm⁻¹): 1934 (C≡O); 1630, 1517 (C-O (Ar), acac)

4.4 DISCUSSION

The *trans*-[Ir(acac)(CO)(PR₃)₂] (PR₃ = PPh₃, PPh₂Cy, PPhCy₂, PCy₃) compounds were successfully synthesized and characterized with IR, ¹H NMR and ³¹P NMR. Very little literature information was found for pentacoordinated complexes of the type [M(acac)(CO)(PR₃)₂] and none regarding iridium as metal centre.¹ The particular solvent used during syntheses was of great importance since chlorinated solvents yielded Vaska-type compounds and many other resulted in the decomposition of the products to an oil. MeOH and toluene were the most suitable solvents for the syntheses of the particular complexes. Different temperatures were used due to solubility differences in each solvent and to ensure the completion of the reaction.

Only the *bis*-phosphine complexes were formed even when a less than 1:1 ratio ligand:Ir was utilized during synthesis. It is well known that ligands such as CO has the ability to stabilise five-coordinate intermediate^{7,8} complexes through π -back donation of the excess electron density. Some difficulties were however encountered with the attempted preparation of *trans*-[Ir(acac)(CO)(PPh₃)₂]. Only PPh₃ of the four ligands investigated showed selectivity

⁷ J.P. Fackler, W.C. Seidel, J.A. Fetchin, *J. Am. Chem. Soc.*, 1968, **90**, 2708.

⁸ R.G. Pearson, D.A. Sweigert, *Inorg. Chem.*, 1970, **9**, 1167.

for its intended molar ratio coordination to the metal centre. The extent of coordination for the other three ligands could not be controlled.

Upon addition of 1 eq of PPh_3 to $[\text{Ir}(\text{acac})(\text{CO})_2]$ one carbonyl ligand is substituted, giving $[\text{Ir}(\text{acac})(\text{CO})(\text{PPh}_3)]$, followed by the addition of a second phosphine ligand forming the five-coordinated compound, *trans*- $[\text{Ir}(\text{acac})(\text{CO})(\text{PPh}_3)_2]$ (**A**). This is evident from ^1H NMR and infrared spectra, Figure 4-2 **A** and Figure 4-3, respectively indicating the presence of the acac^- ligand and exhibiting a $\text{PPh}_3:\text{acac}^-$ integral ratio of 2:1 in the ^1H NMR spectrum thus confirming the *bis*-phosphine complex.

On the other hand when 2 eq of the phosphine ligand is added to $[\text{Ir}(\text{acac})(\text{CO})_2]$, product (**B**) is formed with ^1H NMR (Figure 4-2 **B**) and infrared spectra (Figure 4-3) showing the absence of the acac^- ligand and together with a significant shift in ^{31}P NMR from δ 18.4 to 15.3 ppm for products **A** and **B**, respectively (Figure 4-4) it is evident that two different complexes are formed dependent on ligand concentration. The broad peak at *ca.* 8.43 ppm in the ^{31}P NMR spectrum (Figure 4-4) might be representative of fast exchange between the coordinated and free PPh_3 . The different products isolated for PPh_3 as ligand yielded valuable information as to the mechanism and chemical behaviour of [(acetylacetonato)(dicarbonyl)iridium(I)] coordination reactions.

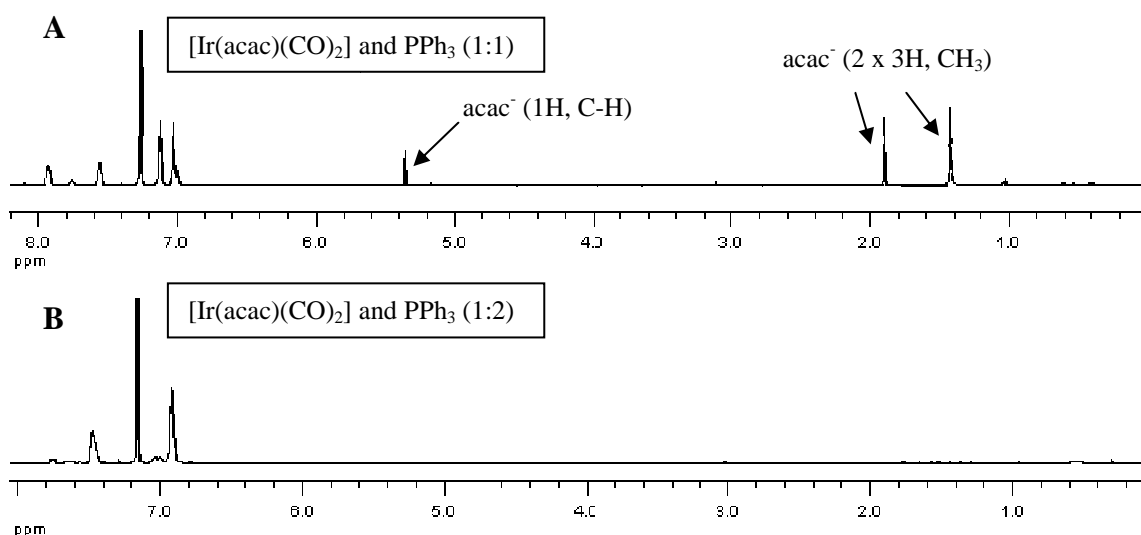


Figure 4-2: ^1H NMR spectra of the products formed when reacting $[\text{Ir}(\text{acac})(\text{CO})_2]$ with PPh_3 in 1:1 (**A**) and 1:2 (**B**) ratios (indicated in parenthesis after heading), obtained in C_6D_6 .

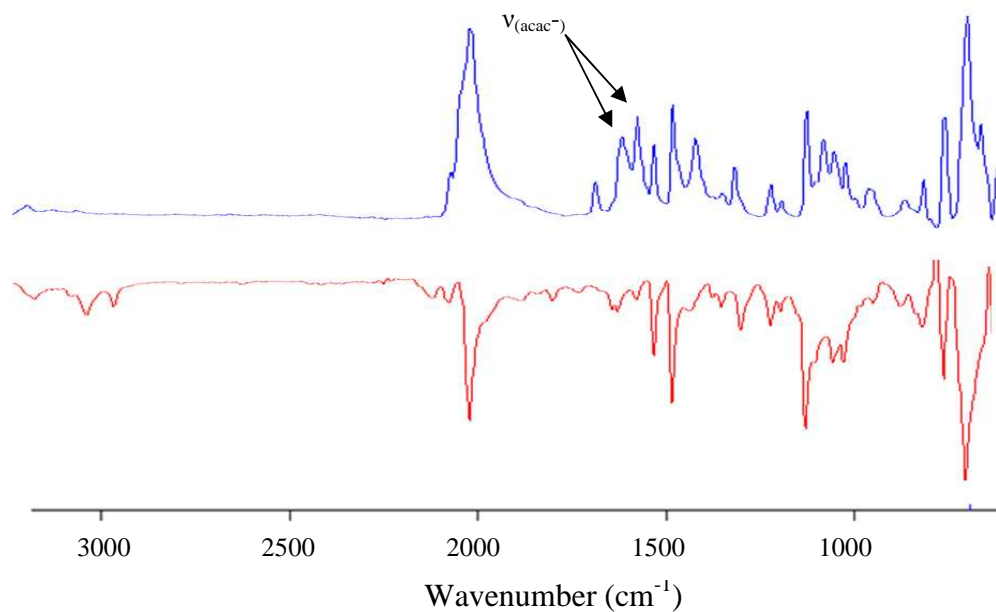


Figure 4-3: Stacked inversion ATR Infrared spectra of products A (blue) and B (red) indicating the absence of the acac⁻ ligand in product B.

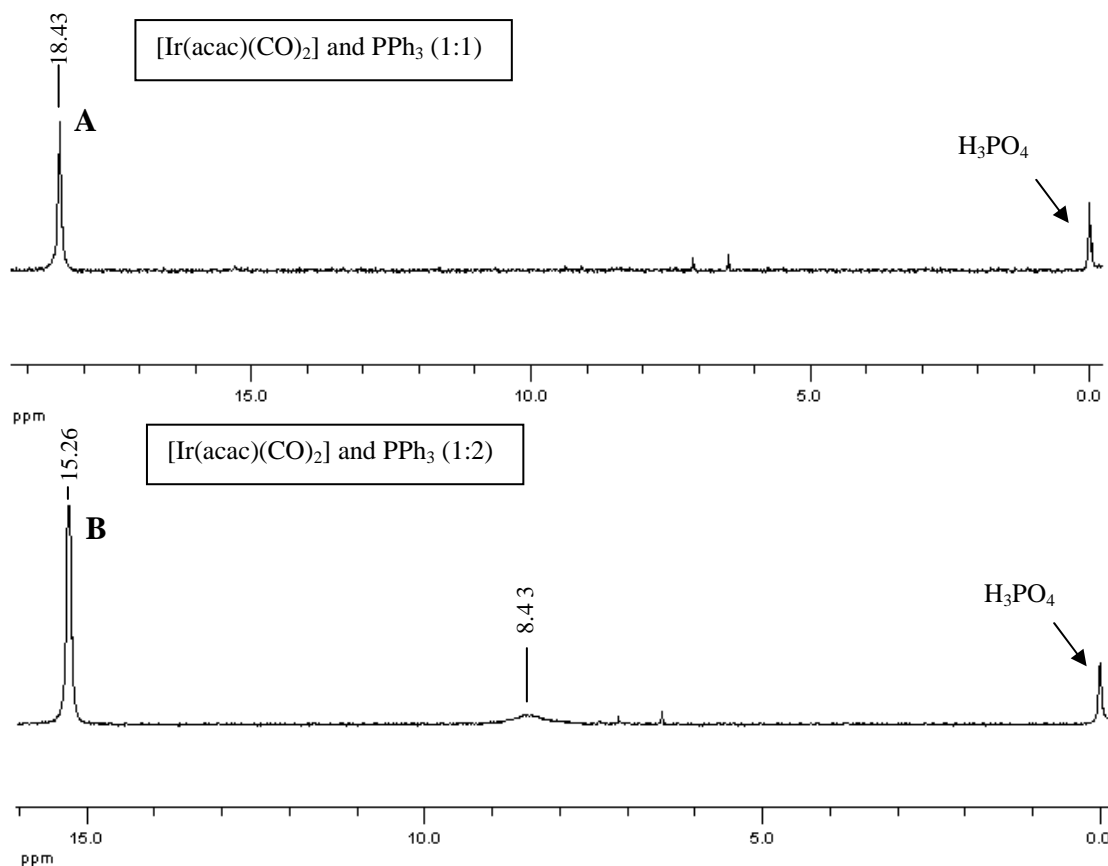


Figure 4-4: ³¹P NMR spectra indicating peak shift of the different products formed when reacting [Ir(acac)(CO)₂] with PPh₃ in 1:1 (A) and 1:2 (B) ratios (indicated in parenthesis after heading), obtained in C₇D₈.

In the series of phosphine ligands (PPh₃, PPh₂Cy, PPhCy₂, PCy₃) a phenyl ring is systematically substituted by a more bulky cyclohexyl ring, increasing the electron density on the metal centre and manipulating the steric effects on the iridium complexes. The steric and electronic properties of the *trans*-[Ir(acac)(CO)(PR₃)₂] complexes are therefore gradually varied with the systematic change of ligands from PPh₃ to PCy₃. It can be seen in Table 4-1 that the carbonyl stretching frequency, $\nu_{(\text{CO})}$, decreases as the phenyl rings are systematically substituted by a cyclohexyl ring. As the electron density on the metal centre increases, the back donation of electrons from the metal to the π^* -orbital of the C atom increases thus strengthening the Ir-C bond and weakening the C \equiv O bond resulting in a lower CO bond order. It is therefore clear from Table 4-1 that the electron-donating ability of *trans*-[Ir(acac)(CO)(PR₃)₂] complexes increase from PPh₃ to PCy₃. A similar trend is observed in the IR data (Table 4-1) for the Vaska-type compounds, *trans*-[RhCl(CO)(PR₃)₂], showing an increasing $\nu_{(\text{CO})}$ as the σ -donor ability of the phosphine decreases and the π -acceptor power increases.^{9,10}

Table 4-1: IR data for *trans*-[Ir(acac)(CO)(PR₃)₂] and *trans*-[RhCl(CO)(PR₃)₂] complexes.

PR ₃	<i>trans</i> -[Ir(acac)(CO)(PR ₃) ₂] ^a	<i>trans</i> -[RhCl(CO)(PR ₃) ₂] ^b
	$\nu_{(\text{CO})}$ (cm ⁻¹) (MeOH)	$\nu_{(\text{CO})}$ (cm ⁻¹) (Toluene)
PPh ₃	2007	1979
PPh ₂ Cy	1992	1966
PPhCy ₂	1957	1964
PCy ₃	1923	1943

^a This MSc Study; ^b Ref [11]

In general, the $\nu_{(\text{CO})}$ frequencies in *trans*-[RhCl(CO)(PR₃)₂] complexes decrease with an increase in σ/π -donor properties of the P-ligand in the order PPh₃ > PPh₂Cy > PPhCy₂ > PCy₃ concluding that infrared is a powerful tool in investigated the electron-donating ability of a ligand.

⁹ W. Strohmeier, T. Onada, *Z. Naturforsch. Teil. B*, 1968, **23**, 1377.

¹⁰ L. Vaska and J. Peone, *Chem. Commun.*, 1971, 418.

¹¹ A. Roodt, S. Otto, G. Steyl, *Coord. Chem. Rev.*, 2003, **245**, 121.

An interesting observation from this study is the change in carbonyl stretching frequencies in the case of *trans*-[Ir(acac)(CO)(PPh₃)₂] and *trans*-[Ir(acac)(CO)(PPh₂Cy)₂] from solid state ATR to MeOH solution being 65 cm⁻¹ and 40 cm⁻¹ respectively (ν_{CO} cm⁻¹: PPh₃: 1942 (ATR), 2007 (MeOH); PPh₂Cy: 1952 (ATR), 1992 (MeOH)). This can be due to packing effects in the solid state which induces a bent mode of the Ir-C≡O moiety. A similar trend in shifting carbonyl frequencies was noticed for the structure of *trans*-[RhCO(PPh₃)₂Cl], determined in different studies, *i.e.*, that of Roodt *et al.*¹² and Rheingold *et al.*¹³ The ν_{CO} of 1965 cm⁻¹, obtained by Roodt (as was also found by Dunbar *et al.*¹⁴), differs with 18 cm⁻¹ from that obtained by Rheingold, 1983 cm⁻¹, due to the bent mode of the Rh-C≡O moiety. The Rh-C-O angle for the study with $\nu_{\text{CO}} = 1965$ cm⁻¹ is *ca.* 165-170 ° compared to 177 ° for $\nu_{\text{CO}} = 1983$ cm⁻¹. It is anticipated that a bent mode for the Rh-C≡O moiety results in a less effective d- π^* overlap with a consequent increase in C-O bond strength.

In another case, the change in ν_{CO} for [Rh(cacsm)(CO)(PPh₃)₂]¹⁵ (cacsm = [(methyl 2-(cyclohexylamino)-1-cyclopentene-1-dithiocarboxylate)]) in a KBr-pellet to CHCl₃ solution was 50 cm⁻¹, confirming substantial solvent interaction (ν_{CO} cm⁻¹: 1944 (KBr), 1994 (CHCl₃)). An interesting fact is that this complex crystallized from solution as an adduct with an acetone solvent molecule that could indicate that co-packing might influence the carbonyl stretching frequency.

Two new crystallographic structural determinations were successfully completed and ultimately yielded information as to the final mechanism and chemical behaviour of these iridium(I) systems. The crystallographic structural determination of *trans*-[Ir(acac- κ O)(CO)(PPhCy₂)₂] (synthesis in Section 4.3.2.3) and *trans*-[Ir(acac- κ^2 O,O)(CO)(PCy₃)₂] (synthesis in Section 4.3.2.4) are discussed in detail in Chapter 5 while the kinetic study for the reaction between [Ir(acac)(CO)₂] and PPh₃ is discussed in Chapter 6.

¹² A. Roodt, G. Kemp, W. Purcell, *Rhodium Express*, 1995, **12**, 21.

¹³ A.L. Rheingold, S.J. Geib, *Acta Cryst. Sect. C*, 1987, **43**, 784.

¹⁴ K.R. Dunbar, S.C. Haefner, *Inorg. Chem.*, 1992, **31**, 3676.

¹⁵ G.J.J. Steyn, A. Roodt, I. Poletaeva, Y.S. Varshavsky, *J. Organomet. Chem.*, 1997, **536-537**, 197.

5

CRYSTAL STRUCTURE DETERMINATION OF COMPLEXES

5.1 INTRODUCTION

Literature revealed no reports of four- or five-coordinated Ir(I) complexes containing two phosphine ligands and a β -diketone donor ligand.¹ This Chapter deals with two new crystal structures in which the O,O'-bidentate ligand displays surprising behaviour by either binding to Ir(I) as a β -diketonato chelate ring or by demonstrating a non-chelating trait and binding only through one carbonyl oxygen of the acac⁻ ligand. All comparisons between crystal structures will therefore be done with the rhodium analogue complexes. The complexes *trans*-[Ir(acac- κ O)(CO)(PPhCy₂)₂] (**1**) and *trans*-[Ir(acac- κ^2 O,O)(CO)(PCy₃)₂] (**2**) were characterized by means of X-ray crystallography and are described below.

5.2 EXPERIMENTAL

The X-ray reflection data was collected on a Bruker X8 ApexII 4K diffractometer,² equipped with graphite monochromated MoK α radiation ($\lambda = 0.71073 \text{ \AA}$) with ω - and ϕ -scans at 100K. After a completed collection, the first 50 frames were repeated to check for decomposition, which was not observed. The frames were integrated using a narrow-frame integration algorithm and reduced with the Bruker SAINT-Plus and XPREP software packages, respectively.³ Data was corrected for absorption effects by using the multi-scan technique SADABS.⁴ The structures were solved by the direct method package SIR975 and refined

¹ Cambridge Structural Database (CSD), Version 5.30, May 2009 update, F.H. Allen, *Acta Cryst.*, 2002, **B58**, 380.

² Bruker, *APEX2*, (Version 1.0-27), Bruker AXS Inc., Madison, Wisconsin, USA, 2005.

³ Bruker, *SAINTE-Plus*, Version 7.12 (including XPREP), Bruker AXS Inc., Madison, Wisconsin, USA, 2004.

⁴ Bruker, *SADABS*, Version 2004/1, Bruker AXS Inc., Madison, Wisconsin, USA, 1998.

⁵ A. Altomare, M.C. Burla, M. Camalli, G.L. Cascarano, C. Giacovazzo, A. Guagliardi, A.G.G. Moliterni, G. Polidori, R. Spagna; *J. Appl. Cryst.*, 1999, **32**, 115.

using WinGX⁶ software, incorporating SHELXL⁷. All graphical representations of the crystal structures were done with DIAMOND⁸. All structures are shown with thermal ellipsoids drawn at 50% probability level unless specified otherwise. All non-hydrogen atoms were refined anisotropically. Methyl, methane and aromatic H atoms were placed in geometrically idealized positions (C-H = 0.95-0.98 Å) and constrained to ride on their parent atoms ($U_{\text{iso}}(\text{H}) = 1.5U_{\text{eq}}(\text{C})$ and $1.2U_{\text{eq}}(\text{C})$).

⁶ L.J. Farrugia, *J. Appl. Cryst.*, 1999, **32**, 837.

⁷ G.M. Sheldrick, *SHELXL97*, Program for the refinement of crystal structures, University of Göttingen, Germany, 1997.

⁸ K. Brandenburg, H. Putz, *DIAMOND*, Release 3.0c, Crystal Impact GbR, Bonn, Germany, 2005.

CHAPTER 5

Table 5-1: Crystallographic and refinement details for *trans*-[Ir(acac-κO)(CO)(PPhCy₂)₂] and *trans*-[Ir(acac-κ²O,O)(CO)(PPhCy₃)₂].

Compound	[Ir(acac-κO)(CO)(PPhCy ₂) ₂]	[Ir(acac-κ ² O,O)(CO)(PPhCy ₃) ₂]
Empirical formula	C ₄₄ H _{65.50} Ir O _{5.50} P ₂	C ₄₃ H ₇₃ IrO ₃ P ₂
Formula weight (g mol ⁻¹)	936.60	892.15
Temperature (K)	100(2)	100(2)
Wavelength (Å)	0.71073	0.71069
Crystal system	Monoclinic	Monoclinic
Space group	C2/c	C2/c
Unit cell dimensions:		
<i>a</i> , <i>b</i> , <i>c</i> (Å)	21.8586(6), 21.6370(6), 18.7589(4)	23.306(5), 9.978(5), 20.784(5)
<i>α</i> , <i>β</i> , <i>γ</i> (°)	90.0, 104.488(2), 90.0	90.0, 114.590(5), 90.0
Volume (Å ³)	8590(0)	4395(3)
<i>Z</i>	8	4
Density (calculated) (g cm ⁻³)	1.448	1.348
Absorption coefficient (mm ⁻¹)	3.23	3.15
F(000)	3844	1848
Crystal Colour	yellow	yellow
Crystal Morphology	Cuboid	Cuboid
Crystal size (mm ³)	0.39 x 0.36 x 0.30	0.23 × 0.20 × 0.10
Theta range (°)	1.35 to 28.34	2.83 to 28.22
Index ranges	-29<= <i>h</i> <=29, -28<= <i>k</i> <=28, -25<= <i>l</i> <=24	-31<= <i>h</i> <=31, -13<= <i>k</i> <=13, -27<= <i>l</i> <=27
Reflections collected	74944	37248
Independent reflections	10693	5457
R _{int}	0.0468	0.0560
Completeness to theta (°, %)	28.34, 99.7	28.35, 99.5
Max. and min. transmission	0.4444 and 0.3659	0.7439 and 0.5315
Refinement method	Full-matrix least-squares on F ²	Full-matrix least-squares on F ²
Data / restraints / parameters	10693 / 22 / 474	5457 / 8 / 154
Goodness-of-fit on F ²	1.278	1.079
Final R indices [I>2σ(I)]	R1 = 0.0312, wR2 = 0.0910	R1 = 0.0654, wR2 = 0.1777
R indices (all data)	R1 = 0.0453, wR2 = 0.1225	R1 = 0.0722, wR2 = 0.1848
Largest diff. peak and hole (e.Å ⁻³)	3.813 and -1.829	4.660 and -6.720

5.3 CRYSTAL STRUCTURE DETERMINATION OF

trans-[Ir(acac-κO)(CO)(PPhCy₂)₂]

Trans-[Ir(acac-κO)(CO)(PPhCy₂)₂] (**1**) was synthesized according to the procedure described in Section 4.2.2.3. Yellow crystals suitable for X-ray diffraction were obtained. The complex crystallized in the monoclinic space group, *C2/c*, with eight molecules in the unit cell. The molecular structure of (**1**) with numbering scheme of the complex is presented in Figure 5-1. Positional parameters and all bond distances and angles are given in the supplementary data (Appendix I).

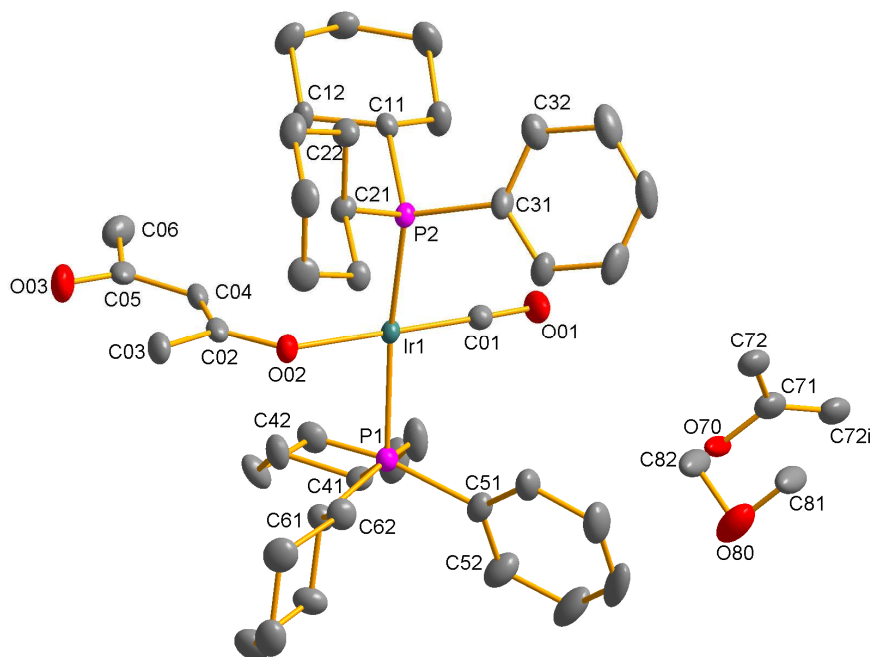


Figure 5-1: DIAMOND representation of *trans*-[Ir(acac-κO)(CO)(PPhCy₂)₂] showing the atom numbering scheme. For the phenyl/cyclohexyl rings, the first digit refers to the ring number, while the second digit refers to the carbon atom in the ring. Hydrogen atoms are omitted for clarity, 50 % probability displacement ellipsoids. Symmetry transformations used to generate equivalent atoms: 1-x, y, 3/2-z.

The complex exhibited a non-chelating acac⁻ ligand, linked to Ir(I) only through O02. The central Ir atom has a slightly distorted square-planar four-coordination and shows a *trans* bis-dicyclohexylphenylphosphine (PPhCy₂) orientation, the O02 carbonyl oxygen of the acac⁻ ligand and C01 of the linear carbonyl ligand.

CHAPTER 5

Complex **1** crystallized with one acetone- and methanol solvate molecule, each found in a 1:1 ratio to the iridium complex and forming part of the main molecular unit cell. The C71 and O70 atoms of the acetone solvate are situated on special positions, generating atom C72i across a two-fold rotation axis. The methanol solvate molecule displays a 50 % disorder on the C-atoms (C81 and C82). Selected bond lengths and angles are summarized in Table 5-2.

Table 5-2: Selected bond distances (Å) and angles (°) with estimated standard deviations in parentheses.

Selected bond lengths (Å)			
Ir1-C01	1.807(5)	C02-C03	1.515(6)
Ir1-O02	2.071(3)	C02-C04	1.374(7)
Ir1-P1	2.333(1)	C04-C05	1.427(6)
Ir1-P2	2.329(1)	C05-O03	1.248(6)
P1-C41	1.841(4)	C05-C06	1.509(7)
P1-C51	1.830(5)	C11-C12	1.530(6)
P1-C61	1.857(5)	C11-C16	1.529(6)
P2-C11	1.839(4)	C21-C22	1.514(6)
P2-C21	1.850(4)	C21-C26	1.528(6)
P2-C31	1.829(5)	C31-C32	1.393(7)
O01-C01	1.161(6)	C31-C36	1.401(6)
O02-C02	1.296(5)		

Selected bond angles (°)			
C01-Ir1-P1	90.9(2)	C51-P1-C41	104.4(2)
C01-Ir1-P2	90.5(2)	C51-P1-C61	103.6(2)
O02-Ir1-P1	89.08(9)	C41-P1-C61	105.9(2)
O02-Ir1-P2	89.62(9)	C51-P1-Ir1	112.4(2)
O01-C01-Ir1	178.4(4)	C41-P1-Ir1	117.5(2)
C01-Ir1-O02	179.7(2)	C61-P1-Ir1	111.8(2)
C02-O02-Ir1	131.1(3)	O02-C02-C04	123.6(4)
P2-Ir1-P1	167.94(4)	O02-C02-C03	113.3(4)
C31-P2-Ir1	111.8(2)	C04-C02-C03	123.0(4)
C11-P2-Ir1	119.1(1)	C02-C04-C05	127.2(4)
C21-P2-Ir1	111.9(2)	O03-C05-C04	124.6(5)
C31-P2-C11	104.2(2)	O03-C05-C06	119.1(4)
C31-P2-C21	103.3(2)	C04-C05-C06	116.2(4)
C11-P2-C21	105.2(2)		

A plane through P1, O02, P2 and Ir1 illustrates the distorted square planar geometry around the Ir centre (Figure 5-2), with important distances from the plane listed in Table 5-3. The phosphine ligands are bent away from the plane in a boat-like position with a P1-Ir1-P2 angle of $167.94(4)^\circ$ and P1, P2 plane distances of $0.234(1) \text{ \AA}$. The carbonyl ligand is bent slightly above the plane with C01 and O01 distances of $0.026(5) \text{ \AA}$ and $0.015(4) \text{ \AA}$, respectively. The carbonyl ligand has an almost horizontal geometry with a O02-Ir1-C01 angle of $179.7(2)^\circ$ and O01-C01-Ir1 angle of $178.4(4)^\circ$. The O02 atom of the acac⁻ ligand deviates with a distance of $-0.058(3) \text{ \AA}$ from the plane and can be considered linear with a O02-Ir1-C01 bond angle of $179.7(2)^\circ$. The acac⁻ ligand with torsion angle C03-C02-C05-O03 has a value of $-2.467(2)^\circ$ indicating that the bidentate ligand is slightly twisted with C02 and O3 atoms slightly below the plane and C03 and C05 atoms slightly elevated above the horizontal plane.

Table 5-3: Selected distances between specific atoms and the horizontal plane through P1, C01, P2, O02 and Ir(1).

Atom	Distance (Å)
Ir1	-0.0086(1)
C01	0.026(5)
O01	0.015(4)
O02	-0.058(3)
P1	0.234(1)
P2	0.234(1)

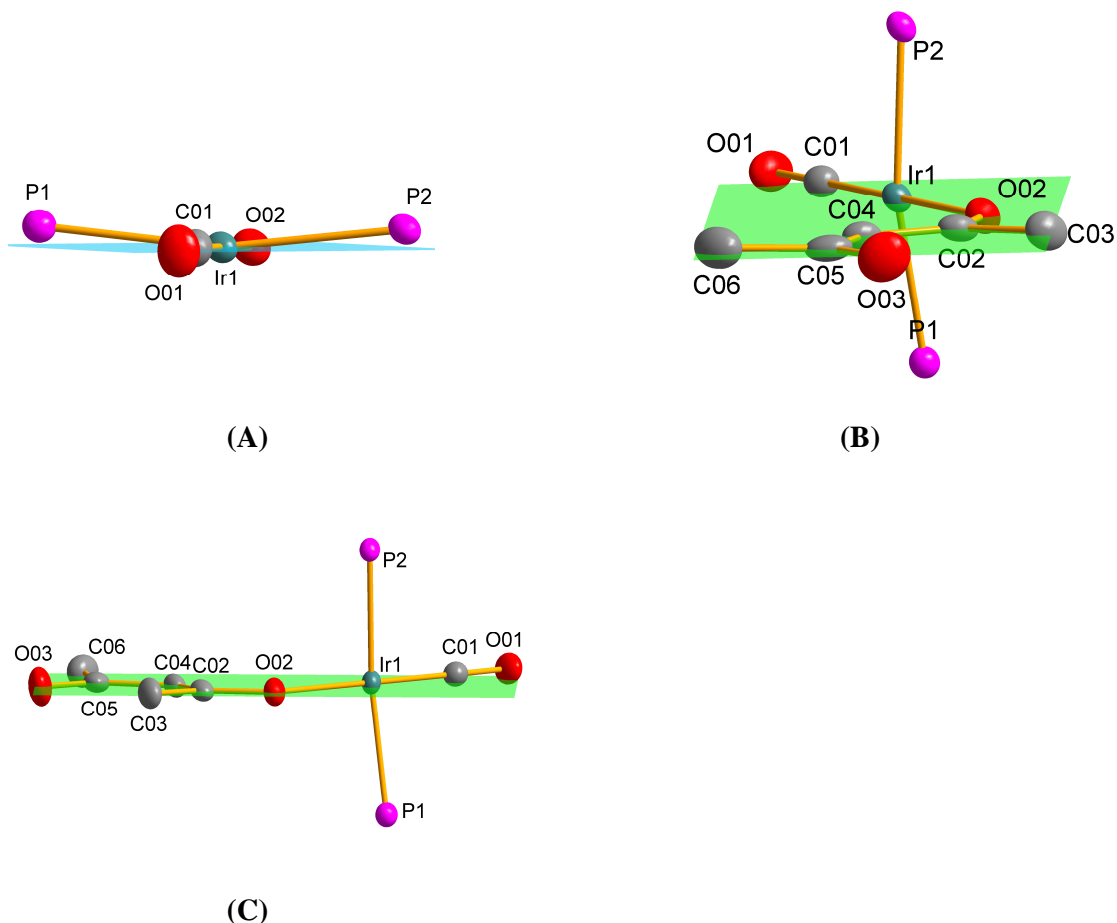


Figure 5-2: Partial structure of $trans\text{-}[\text{Ir}(\text{acac}\text{-}\kappa\text{O})(\text{CO})(\text{PPhCy}_2)_2]$. (A) – Side view of ligands bonded to Ir(I) metal centre. (B) – Front and (C) - Side view of non-chelating acac⁻ ligand with respect to Plane 2. Displacement ellipsoids drawn at the 50% probability level.

The phenyl rings of the phosphine ligands are planar, within experimental error. The average C-C bond distances of 1.385 Å and 1.387 Å for C3 and C5 phenyl rings respectively, along with 120 ° angles are within expected range of phenyl rings.⁹ The cyclohexyl rings C1, C2, C4 and C6 indicate no ring distortion and all have average C-C bond lengths which agree with the expected value of 1.540 ± 0.015 Å.¹⁰ The bulky phosphine ligands are in a *trans* arrangement which minimizes intramolecular steric interactions. The O02-Ir1-P1 and C01-Ir1-P2 bite angles are of similar magnitude, 89.08(9) ° and 90.5(2) ° respectively. Bite angles of O02-Ir1-P2 and C01-Ir1-P1 are also comparable, 89.62(9) ° and 90.9(2) °, respectively indicating the little steric effect of the PPhCy₂ ligands.

⁹ G.J. Lamprecht, J.G. Leipoldt, C.P. van Biljon, *Inorg. Chim. Acta*, 1984, **88**, 55.

¹⁰ J. March, *Advanced Organic Chemistry: Reactions, Mechanisms and Structures*, 4th Ed., New York: John Wiley & Sons, Inc., 1992.

An enolate-type delocalization resonance is found in the acac^- bidentate ligand. The coordinated C02-O02 has a distance of 1.296(5) Å and intermediate-bond-order backbone C-C bond [C02-C04 and C04-C05] distances are 1.374(7) Å and 1.427(6) Å respectively. The carbon atoms in the acac^- backbone thus have longer bonds than expected for an average C=C bond (1.32 Å),¹⁰ but shorter than a single C-C bond of 1.53 Å. The C05-O03 value for the uncoordinated end, however, is much shorter: 1.248(6) Å and similar to the value of 1.23 Å for a ketonic C=O bond (International Table for X-ray crystallography, 1962).¹¹ The C02-O02 and C05-O03 bonds are *trans* with respect to the C02-C04 bond, which differs from chelated acac^- complexes where both C-O oxygens have a *cis* configuration within the distorted square-planar configuration around the metal centre. The triple bond character of the carbonyl functionality has a longer distance (C01-O01 = 1.161(6) Å) than the expected value of 1.13 Å which indicates π back-donation from an electron rich Ir metal centre which will then shorten the Ir1-C01 bond distance.

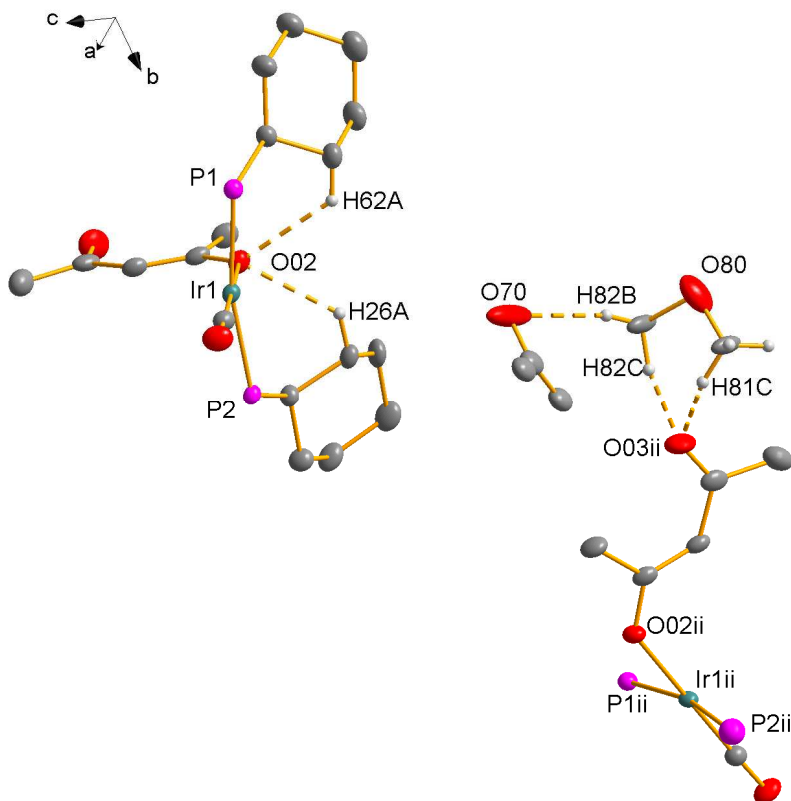


Figure 5-3: Inter- and intramolecular hydrogen bond interactions for *trans*-[Ir(acac- κ O)(CO)(PPhCy₂)₂] complexes. Only applicable hydrogen atoms with relevance to hydrogen bond interactions are indicated. Displacement ellipsoids drawn at the 50% probability level.

¹¹ *International Tables of X-ray Crystallography*, Vol. III, Dordrecht: Kluwer Academic Publishers, 1962.

Inter- and intramolecular hydrogen bonding is indicated in Figure 5-3. Intramolecular bonding exists between O02 and H62A with donor-acceptor (D-A) bond distance of 3.154(6) Å and between O02 and H26A, D-A = 3.124(6) Å. An intramolecular interaction also takes place between O70 and H82B with D-A = 3.44(1) Å. Intermolecular bonding occurs between O03ii and H81C of the Ir1i molecule (D-A = 2.71(1) Å) and between O03ii and H82C of the Ir1i molecule (D-A = 2.74(1) Å). A complete list of hydrogen bonds is given in Table 5-4.

Table 5-4: Hydrogen bonds for *trans*-[Ir(acac-κO)(CO)(PPhCy₂)₂] [Å and °].

D-H...A	d(D-H)	d(H...A)	d(D...A)	<(DHA)
C26-H26A...O02	0.99	2.4	3.124(6)	129
C62-H62A...O02	0.99	2.46	3.154(6)	126.3
C81-H81C...O03ii	0.98	1.78	2.71(1)	157.5
C82-H82B...O70	0.98	2.47	3.44(1)	169.5
C82-H82C...O03ii	0.98	1.78	2.74(1)	165.9

Symmetry transformations used to generate equivalent atoms:

(ii) $-x+3/2, y+1/2, -z+3/2$

Molecular packing within the unit cell (Figure 5-4) shows a “head to head” arrangement of *trans*-[Ir(acac-κO)(CO)(PPhCy₂)₂] complexes along the c-axis. No π-stacking was observed.

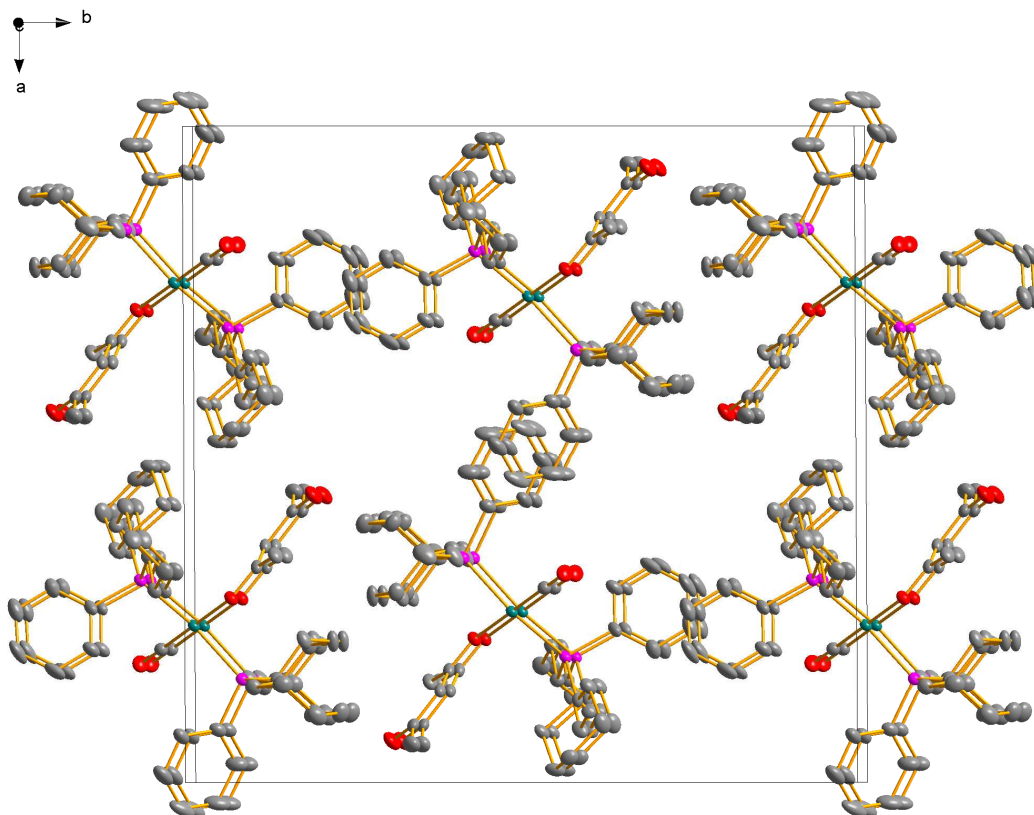


Figure 5-4: Complexes of *trans*-[Ir(acac- κ O)(CO)(PPhCy₂)₂] displaying a sheet-like “head to head” crystal packing along the c-axis. Hydrogen atoms and solvent molecules omitted for clarity, 50 % probability displacement ellipsoids.

5.4 CRYSTAL STRUCTURE DETERMINATION OF

trans-[Ir(acac- κ^2 O,O)(CO)(PCy₃)₂]

Trans-[Ir(acac- κ^2 O,O)(CO)(PCy₃)₂] (**2**) was synthesized according to procedure described in Section 4.2.2.4. Yellow crystals suitable for X-ray diffraction were obtained. The complex crystallized in the monoclinic space group, *C2/c*, with four molecules in the unit cell. The molecular structure with numbering scheme of the complex is represented in Figure 5-5. Atoms generated through the two-fold rotation axis are represented by atom ending with “i”. Positional parameters and all bond distances and angles are given in the supplementary data (Appendix I).

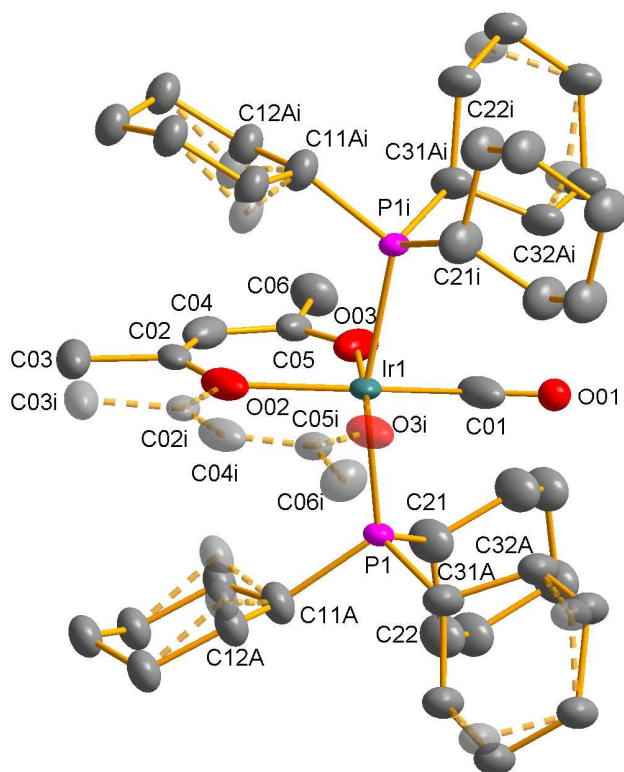


Figure 5-5: DIAMOND representation of *trans*-[Ir(acac- κ^2 O,O)(CO)(PCy₃)₂] showing the atom numbering scheme. For the cyclohexyl rings, the first digit refers to the ring number, while the second digit refers to the carbon atom in the ring. Hydrogen atoms are omitted for clarity, 50 % probability displacement ellipsoids. Symmetry transformations used to generate equivalent atoms: -x, y, 1/2-z.

The complex displays a five-coordinate trigonal bipyramidal coordination with significant distortion in the trigonal plane [O03-Ir1-C01 angle of 90.9(3) °] towards square-pyramidal geometry in the solid state. The Ir(I) metal centre is bonded to a β -diketone chelate ring, *trans* positioned tricyclohexylphosphine (PCy₃) ligands and a carbonyl group. Distances and angles within the six chair-shaped cyclohexane groups are normal.¹⁰

There is a two-fold rotation axis along the Ir-CO bond. The structure displays a disorder on the cyclohexyl rings C1 and C3 in a 50:50 % ratio. The chelated acac⁻ ligand is disordered with O02 atom positioned on the rotation axis displaying 50 % displacement of all atoms that form part of the bidentate ligand (O03, C05, C06, C04, C02 and C03).

Although acetylacetonate is a symmetrical ligand, the Ir1-O03 and Ir1-O02 (virtually *trans* to the CO ligand) distances are 2.09(2) Å and 2.126(9) Å respectively. Furthermore, a significant difference in O03-C05 and O02-C02 distances (1.23(2) Å and 1.48(2) Å) together

CHAPTER 5

with noteworthy discrepancies in the distances of the three carbon atoms in the acac⁻ backbone (C02-C04, C04-C05 = 1.33(3) Å, 1.43(2) Å) indicate that the asymmetric distortion is quite considerable. The O02-Ir1-O03 bite angle is 89.1(3) °.

The O02-Ir1-P1 and C01-Ir1-P1 bite angles are 97.88(4) ° and 82.12(4) °, respectively that could indicate some extend of steric demand or electronic interactions between the β-diketone- and PCy₃ ligands. The carbonyl group in this crystal structure was refined constrained to fixed positions and can therefore not supply accurate information about π back-donation from the electron rich Ir(I) metal centre.

Table 5-5: Selected bond lengths and angles for *trans*-[Ir(acac-κ²O,O)(CO)(PCy₃)₂].

Selected bond lengths (Å)			
Ir1-C01	1.76(1)	C02-C04	1.33(3)
Ir1-O03	2.09(2)	C02-C03	1.55(3)
Ir1-O02	2.126(9)	C04-C05	1.43(2)
Ir1-P1	2.331(2)	C05-C06	1.52(2)
P1-C11A	1.852(8)	C11A-C12A	1.45(2)
P1-C21	1.859(9)	C11A-C16A	1.46(2)
P1-C31A	1.851(8)	C21-C22	1.54(1)
O02-C02	1.48(2)	C21-C26	1.52(1)
O03-C05	1.23(2)	C31A-C32A	1.52(1)
O01-C01	1.10(2)	C31A-C36A	1.54(1)

Selected bond angles (°)			
C01-Ir1-O03	91.0(3)	C31A-P1-Ir1	109.6(3)
O03-Ir1-O03i	178.1(7)	C11A-P1-Ir1	119.6(3)
C01-Ir1-O02	180.0(0)	C21-P1-Ir1	112.2(3)
O03-Ir1-O02	89.0(3)	C04-C02-O02	129(1)
C01-Ir1-P1	82.11(4)	C04-C02-C03	121(2)
O03-Ir1-P1	89.8(4)	O02-C02-C03	111(1)
O02-Ir1-P1	97.89(4)	O03-C05-C04	120(2)
P1-Ir1-P1i	164.23(8)	O03-C05-C06	119(2)
O01-C01-Ir1	180.0(0)	C04-C05-C06	121(2)
C02-O02-Ir1	118.1(7)	C04-C02-O02	129(1)
C05-O03-Ir1	134.1(13)	C02-C04-C05	129.6(2)

A plane was constructed through atoms O03, O03i, P1 and P1i to indicate the distorted trigonal bipyramidal geometry around the Ir(I) centre (Figure 5-6 A and B). Important distances between selected atoms and the plane are given in Table 5-6. Ir1 lies $-0.3124(5)$ Å from the plane with Ir1-P bond lengths of $2.331(2)$ Å. The phosphine ligands are bent from the plane in an upside-down boat position with a P1 plane distance of $0.007(2)$ Å and P1-Ir1-P1i angle of $164.23(8)$ °. The O03 and O03i atoms of the acac⁻ ligand deviates with a distance of $-0.35(1)$ Å from the plane and can be considered linear with a O03-Ir1-O03i bond angle of $178.1(7)$ °.

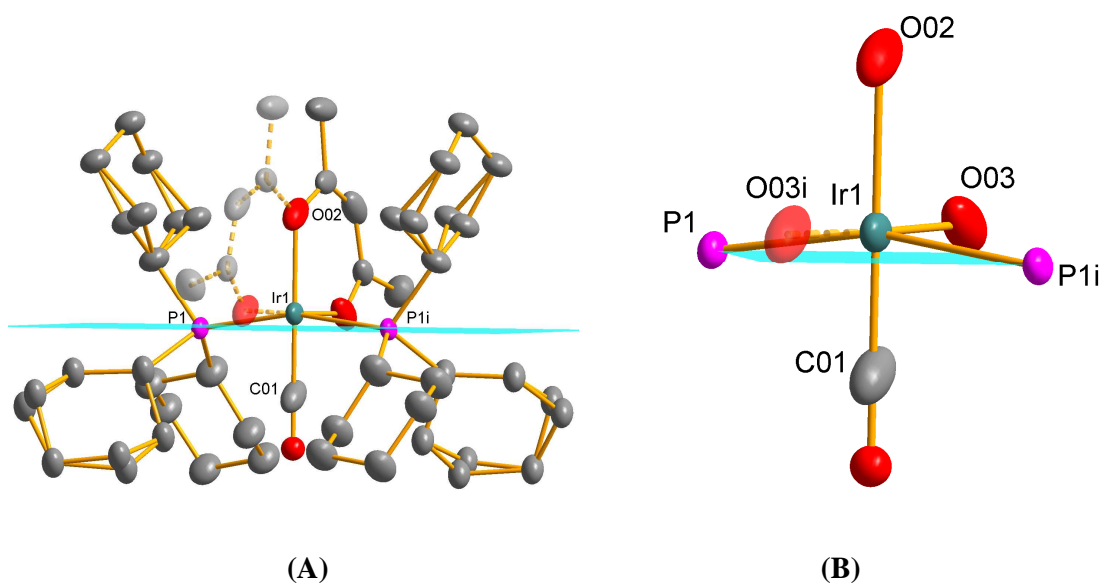


Figure 5-6: Partial structure of *trans*-[Ir(acac- κ^2 O,O)(CO)(PCy₃)₂]. (A) – Position of acac⁻ and phosphine ligands with regards to Plane 1. (B) – Side view of ligands bonded to the Ir(I) centre with respect to the horizontal plane. Displacement ellipsoids drawn at the 50% probability level.

Table 5-6: Selected distances between specific atoms and the horizontal plane through atoms O(03), O(03i), P(1), P(1i).

Atom	Distance (Å)
Ir1	$-0.3124(5)$
O03	$-0.35(1)$
P1	$0.007(2)$

A second plane was constructed through atoms O01, C01, O02 and O03 illustrated by Figure 5-7 **A** and **B**. The proton (H04) bonded to the central atom in the acac⁻ ring (C04) indicates the greatest deviation with a distance of 0.0226(1) Å from the plane; all other atoms are considered in line with the plane within standard deviation. The carbonyl ligand shows no deviation from the plane and has a linear geometry with a O02-Ir1-C01 angle of 180.0(0) ° and O01-C01-Ir1 angle of 180.0(0) °.

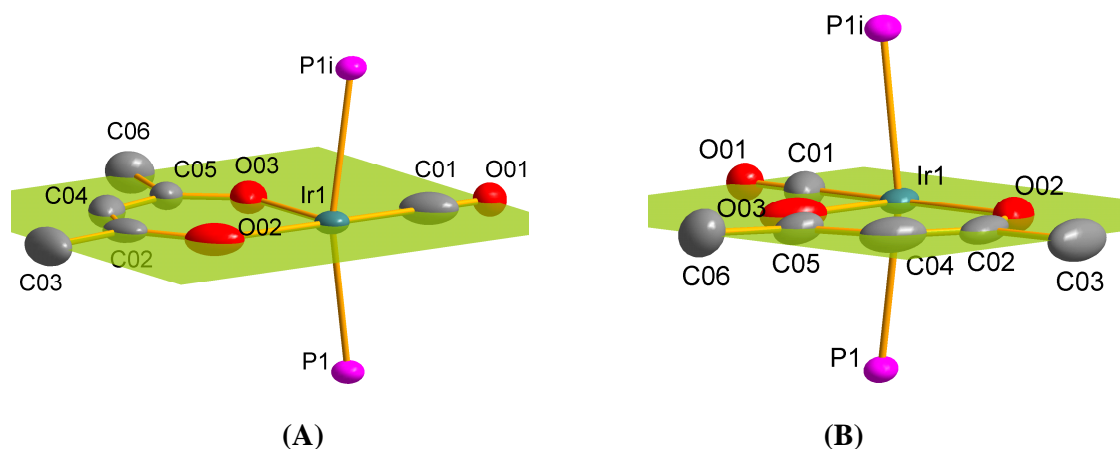


Figure 5-7: (A) – Side- and (B) front view of bidentate ligand with regards to Plane 2. Displacement ellipsoids drawn at the 50% probability level.

Table 5-7: Selected distances between specific atoms and the horizontal plane through atoms O01, C01, O02, O03.

Atom	Distance (Å)
C04	0.02(2)
H04	0.0226(1)
C02	0.02(2)
C03	0.04(2)
H04	0.0226(1)
C02	0.02(2)
C05	0.02(2)
C06	-0.02(2)

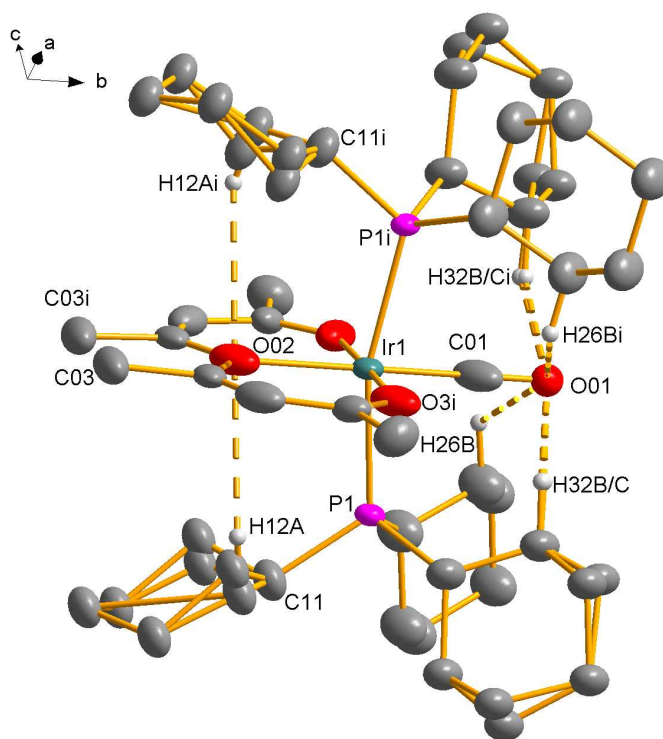


Figure 5-8: Intramolecular hydrogen bond interactions for *trans*-[Ir(acac- κ^2 O,O)(CO)(PCy₃)₂] complexes as viewed along the *c*-axis. Only applicable hydrogen atoms with relevance to hydrogen bond interactions are shown. Displacement ellipsoids drawn at the 50% probability level.

Intramolecular hydrogen bonding is indicated in Figure 5-8. Intramolecular bonding exists between O02 and H12A with donor-acceptor (D-A) bond distance of 3.63(2) Å and between O01 and H26B, D-A = 2.864(9) Å. Also, between O01 and H32B/C with D-A = 2.770(8) Å. A complete list of hydrogen bond interactions is given in Table 5-8.

Table 5-8: Hydrogen bonds for *trans*-[Ir(acac- κ^2 O,O)(CO)(PCy₃)₂] [Å and °].

D-H...A	d(D-H)	d(H...A)	d(D...A)	<(DHA)
C12A-H12A...O02	0.99	2.85	3.63(2)	136
C26-H26B...O01	0.99	2.26	2.864(9)	118
C32A-H32B...O01	0.99	1.92	2.770(8)	142
C32A-H32C...O01	0.99	1.92	2.770(8)	142

A “head to tail” crystal packing of the $trans$ -[Ir(acac- κ^2 O,O)(CO)(PCy₃)₂] complexes can be seen along the c -axis (Figure 5-9) with no π -stacking within the unit cell.

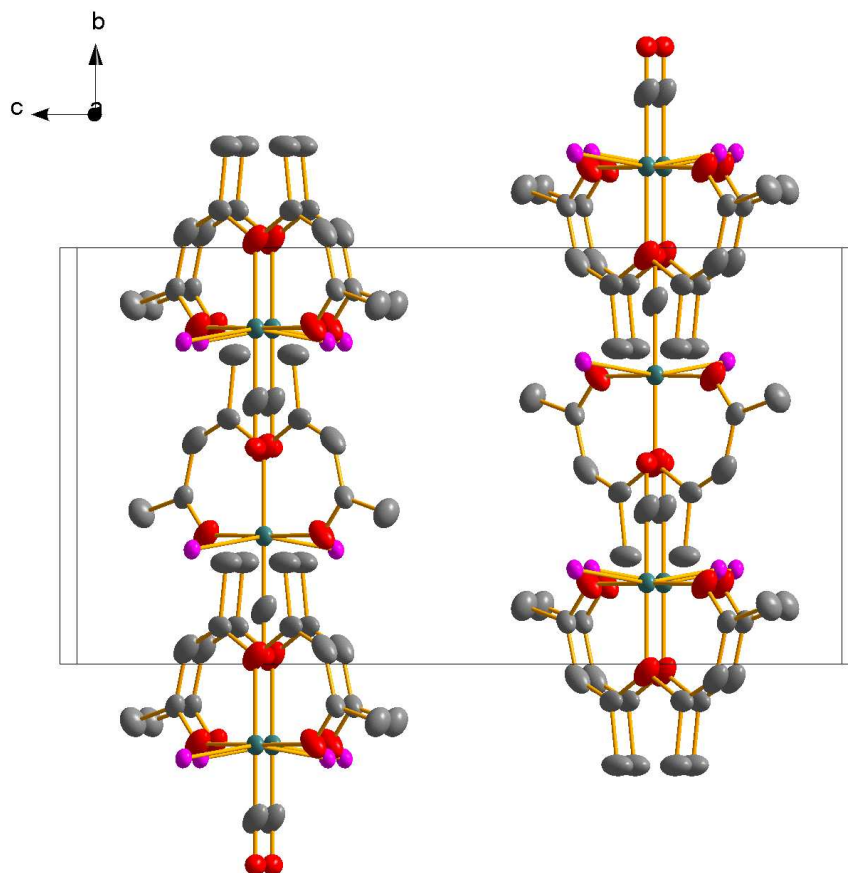


Figure 5-9: $trans$ -[Ir(acac- κ^2 O,O)(CO)(PCy₃)₂] complexes showing a “head to tail” crystal packing. Hydrogen atoms and cyclohexyl rings are omitted for clarity, 50 % probability displacement ellipsoids.

In order to quantitatively confirm the structure of $trans$ -[Ir(acac- κ^2 O,O)(CO)(PCy₃)₂], additional refinement in the triclinic $P\bar{1}$ spacegroup was performed. The asymmetric unit cell consists of two independent molecules resembling the results found when refined in the monoclinic spacegroup.

As illustrated in Figure 5-10, atoms O1 (molecule 1) and O4 (molecule 2) can be considered the same as atom O02 found in Figure 5-5. The carbonyl carbon is $trans$ to these oxygen atoms in all cases. The chelated bidentate ligand of molecule 1 is representative of the acac⁻ ligand generated through the two-fold rotation axis consisting of O02, C02i, C03i, C04i,

C05i, C06i and O3i as found in the monoclinic spacegroup (Figure 5-5). The acac^- ligand of molecule 2 represents the acac^- ligand consisting of O02, C02, C03, C04, C05, C06, O03.

Conflicting refinement data of crystallographic structures did not yield distinct theoretical placement probability for carbonyl oxygens.

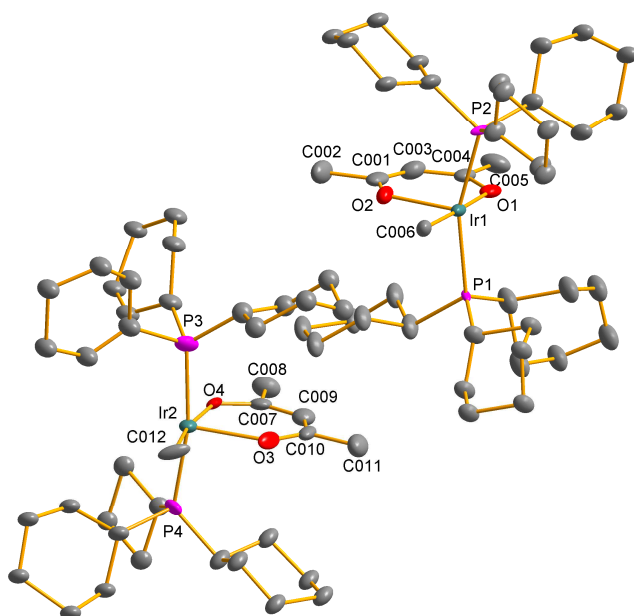


Figure 5-10: DIAMOND representation of $\text{trans-}[\text{Ir}(\text{acac-}\kappa^2\text{O,O})(\text{CO})(\text{PCy}_3)_2]$, as refined in the triclinic $P\bar{1}$ spacegroup, showing the atom numbering scheme. Hydrogen atoms are omitted for clarity, 50 % probability displacement ellipsoids.

Even though the dry product can fairly easily be reproduced, yielding crystalline products showed to be a challenge. Technical issues prevented the replication of the crystalline product for analysis. It was found that crystals were stable in solution for only two days therefore constricting the data collection to specific availability of hardware. The completion of this project could not be delayed any further therefore it was ultimately decided that the existing data was sufficient evidence for proof of structural characterisation for $\text{trans-}[\text{Ir}(\text{acac-}\kappa^2\text{O,O})(\text{CO})(\text{PCy}_3)_2]$. The re-determination of this structure will however be done as part of a future project.

5.5 DISCUSSION

Due to a lack of pentacoordinated *bis*-phosphine Ir(I) structures found in literature¹ all comparisons between crystal structures are done with rhodium analogue structures.

For rhodium complexes it is known that moderately basic and not very bulky phosphines such as PPh₃ or PEt₃ substitutes only one carbonyl ligand of [Rh(acac)(CO)₂]¹² to form [Rh(acac)(CO)(PPh₃)].¹³ The formation of [Rh(acac)(CO)(PPh₃)₂]¹⁴ is achieved by substitution of the chlorido ligand of *trans*-[Rh(Cl)(CO)(PPh₃)₂] by sodium 2,4-pentanedionate. The addition of highly basic tertiary phosphines to [Rh(acac)(CO)₂] causes the substitution of one carbonyl ligand with acac⁻ linked to Rh only through one Rh-O bond thus forming *trans*-[Rh(acac-κO)(CO)(PR₃)₂] which has a square-planar structure compared to the trigonal bipyramidal geometry of a chelated *trans*-[Rh(acac-κ²O,O)(CO)(PR₃)₂] complex. “Ordinary” phosphines such as PPh₃ or PEt₃ and very bulky phosphines like P(*t*-Bu)₃ do not coordinate two phosphine molecules to [Rh(acac)(CO)₂].

Table 5-9 presents a comparative summary of the crystal structures in this study, *trans*-[Ir(acac-κO)(CO)(PPhCy₂)₂] (**1**) and *trans*-[Ir(acac-κ²O,O)(CO)(PCy₃)₂] (**2**), with five-coordinated *bis*-phosphine compounds with a non-chelated acac⁻ ligand, *trans*-[Rh(acac-κO)(CO)(PCy₃)₂]¹⁵ (**3**) and *trans*-[Rh(acac-κO)(CO)(PPrⁱ)₂]¹⁶ (**4**), in addition to *mono*-phosphine complexes with a chelated β-diketone ring, [Rh(acac)(CO)(PPhCy₂)]¹⁷ (**5**) and [Rh(acac)(CO)(PCy₃)]¹⁸ (**6**), as found in literature.

¹² F. Huq, A.C. Skapski, *J. Cryst. Mol. Struct.*, 1974, **4**, 411.

¹³ J.G. Leipoldt, S.S. Basson, L.D.C. Bok, T.I.A. Gerber, *Inorg. Chim. Acta*, 1978, **26**, L35.

¹⁴ K. Joseph, S.A. Pardhy, S.K. Pandit, S. Gopinathan, C. Gopinathan, *Inorg. Chim. Acta*, 1984, **84**, 149.

¹⁵ G.B. Ansell, S. Leta, A.A. Oswald, E.J. Mozeleski, *Acta Cryst.*, 1986, **C42**, 1516.

¹⁶ S. Yoshida, Y. Ohgomori, Y. Watanabe, K. Honda, M. Goto, M. Kurahashi, *J. Chem. Soc. Dalton Trans.*, 1988, 895.

¹⁷ A. Brink, A. Roodt, H.G. Visser, *Acta Cryst.*, 2007, **E63**, m48.

¹⁸ A.M. Trzeciak, B. Borak, Z. Ciunik, J.J. Ziołkowski, M.F.C. Guedes da Silva, A.J.L. Pombeiro, *Eur. J. Inorg. Chem.*, 2004, 1411.

CHAPTER 5

Table 5-9: Comparison of selected crystallographic data of *trans*-[Ir(acac-κO)(CO)(PPhCy₂)₂] (1), *trans*-[Ir(acac-κ²O,O)(CO)(PCy₃)₂] (2), *trans*-[Rh(acac-κO)(CO)(PCy₃)₂] (3), *trans*-[Rh(acac-κO)(CO)(PPrⁱ)₂] (4) and [Rh(acac)(CO)(PPhCy₂)] (5).

Complex	(1) ^a	(2) ^a	(3) ^b	(4) ^c	(5) ^d
Crystal system	Monoclinic	Monoclinic	Triclinic	Monoclinic	Monoclinic
Space group	<i>C2/c</i>	<i>C2/c</i>	<i>P1</i>	<i>P2₁/n</i>	<i>P2₁/n</i>
<i>a, b, c</i> (Å)	21.8586(6), 21.6370(6), 18.7589(4)	23.306(5), 9.978(5), 20.784(5)	10.499(2), 11.968(2), 19.469(4)	12.759(4), 24.19(1), 9.433(4)	10.076(5), 12.990(5), 17.973(5)
<i>α, β, γ</i> (°)	90.0, 104.488(2), 90.0	90.0, 114.590(5), 90.0	71.13(1), 71.11(1), 67.29(1)	90.0, 90.88(4), 90.0	90.0, 90.576(5), 90.0
Volume (Å ³)	8590.0(4)	4395(3)	2069.3(3)	2991(2)	2347(2)
Z	8	4	2	4	4
Density (g cm ⁻³) (calculated)	1.488	1.348	1.269	1.26	1.427
Cone Angle: P1, P2 (°)	151.72, 160.00	158.4, 158.4	-	-	-
Bond Distances (Å)					
M-O02	2.071(3)	2.126(9)	2.052(5)	2.056(6)	2.078(2)
M-O03	-	2.09(2)	-	-	2.041(2)
M-C01	1.807(5)	1.76(1)	1.7869(7)	1.78(1)	1.797(3)
C01-O01	1.161(6)	1.10(2)	1.14(1)	1.15(2)	1.152(3)
M-P1	2.333(1)	2.331(2)	2.348(2)	2.359(2)	2.2424(9)
M-P2	2.329(1)	2.331(2)	2.361(2)	2.355(2)	-
O02-C02	1.296(5)	1.48(2)	1.291(9)	1.29(1)	1.273(3)
C02-C03	1.515(6)	1.55(3)	1.46(1)	1.49(2)	1.504(3)
C02-C04	1.374(7)	1.33(3)	1.38(1)	1.37(1)	1.396(3)
C04-C05	1.427(6)	1.43(2)	1.42(1)	1.43(1)	1.384(3)
C05-O03	1.248(6)	1.23(2)	1.24(1)	1.24(1)	1.279(3)
C05-C06	1.509(7)	1.52(2)	1.50(2)	1.52(2)	1.509(3)
Bond Angles (°)					
P1-M-C01	90.9(2)	82.11(4)	88.15	88.5(4)	89.34(7)
P2- M-C01	90.5(2)	-	91.1(3)	89.0(4)	-
P1-M-O02	89.08(9)	97.89(4)	93.2(2)	94.4(2)	175.32(5)
P2-M-O02	89.62(9)	-	87.5(2)	90.4(2)	-
O02-M-C01	179.7(2)	180.0(0)	172.8(1)	172.6(4)	177.06(8)
M-C01-O01	178.4(4)	180.0(0)	177.2(8)	177.9(1)	179.9(2)
M-O02-C02	131.1(3)	118.1(7)	136.0(6)	134.7(6)	126.3(2)
P1-M-P2	167.94(4)	164.23(8)	178.9(1)	176.9(1)	-

^a This MSc Study; ^b Ref [15]; ^c Ref [16]; ^d Ref[17]

The Tolman cone angle (θ_T) is the most widely used method for determining ligand steric behaviour at a metal centre as described by Tolman (1977).¹⁹ The steric demand of the phosphine ligands, in this study, was quantified by the effective Tolman cone angle (θ_E), using the actual Ir-P bond distance and a van der Waals radius of 1.2 Å for hydrogen. In solution, the ligand substituents orientation might differ, resulting in a variation in cone angle size. The effective cone angles, (θ_E), indicate an increasing steric demand of the phosphine ligands from PPh₃ to PCy₃. The orientation of the phenyl- and cyclohexylrings of the *bis*-PPhCy₂ ligands in complex **(1)**, with respect to the diketone and carbonyl ligands, are equal therefore the difference in θ_E between the P1 and P2 dicyclohexylphenyl phosphine ligands (151.72 ° and 160.0 °, respectively) of the *trans*-[Ir(acac-κO)(CO)(PPhCy₂)₂] **(1)** complex may be as a result of crystal packing.

The M-O02 distance for **(1)**, 2.071(3) Å, compares to 2.078(2) Å and 2.041(2) Å for **(5)** and 2.088(1) Å and 2.046(1) Å for [Rh(acac)(CO)(PCy₃)]¹⁸ **(6)** where both carbonyl oxygens have a chelated *cis* configuration within the distorted square-planar configuration around the Rh atom. It is also in good comparison with non-chelated complexes **(3)** and **(4)** (2.052(5) Å and 2.056(6) Å respectively). The coordinated C02-O02 with a distance of 1.296(5) Å and intermediate-bond-order backbone C-C bond [C02-C04 and C04-C05] distances of 1.374(7) Å and 1.427(6) Å, respectively are similar to the corresponding values of 1.291(9) Å, 1.38(1) Å, 1.42(1) Å found in [Rh(acac-κO)(CO)(PCy₃)₂] **(3)**, 1.29(1) Å, 1.37(1) Å and 1.43(1) Å found in [Rh(acac-κO)(CO)(PPrⁱ₃)₂] **(4)** and 1.273(3) Å, 1.396(3) Å and 1.384(3) Å found in [Rh(acac)(CO)(PPhCy₂)] **(5)**. The slightly longer M-O distances of **(2)**, 2.126(9) Å and 2.09(2) Å, is due to the asymmetric distortion of the chelated acac⁻ ligand where in the case of [Rh(acac)(CO)(PCy₃)]¹⁸ **(6)** these bonds were near identical (2.088(1) Å and 2.046(1) Å).

The M-P distances in complexes **(1)**-**(4)** are similar and compare well with corresponding bond distances in four-coordinate Vaska-type analogues, [Rh(CO)(Cl)(PPh₃)₂] and [Rh(CO)Cl{P(*p*-tol)₃}₂]²⁰, displaying values of 2.322(1) Å and 2.333(2) Å respectively. These values also correspond with M-P bond lengths in five-coordinate *trans*-[Rh(CO)(tropBr₃)PPh₃]₂] complexes of 2.337(2) Å.²⁰ This implies that the donor atom (P) is

¹⁹ C.A. Tolman, *Chem. Rev.*, 1977, **77**, 313.

²⁰ A. Roodt, S. Otto, G. Steyl, *Coordination Chemistry Reviews*, 2003, **245**, 121.

the prime determinate factor regarding the M-P bond, and that the M-P bond variation is fairly insensitive toward substituents on the P-atom as well as the ligand on the metal centre *trans* to the carbonyl moiety.

The carbonyl (C≡O) bond length generally increases as the σ -donating ability of the phosphine ligands increases. From the crystallographic data it can be seen by increasing C01-O01 bond length from Complexes (3) to (2) as well as increasing $\nu_{(\text{CO})}$ given in Chapter 4 (Table 4-1).

Complexes (1) and (2) show distorted square planar geometries with P1-M-P2 angles of 167.94(4) ° and 164.23(8) ° respectively. The other complexes show near linear geometry with respect to P1-M-P2 angles. Compounds (1) and (2) can be considered linear with regards to O02-M-C01 and M-C01-O01 angles with Complex (4) showing the biggest deviation with O02-M-C01 angle of 172.6(4) °.

The applicability of complexes of Rh(I), Ir(I), Pd(II), Pt(II) and other d^8 metal ions as synthetic catalysts in chemistry is significant and thus research into the mechanistic details of these reactions are extremely important. Substitution reactions usually form part of such catalytic cycles. Pathways for square-planar substitution reactions involve the nucleophilic attack of the ligand on the metal centre of the complex and then proceeding *via* a five-coordinate transition state or intermediate, with the complex assuming a regular trigonal bipyramidal structure.²¹ Ultimately an understanding of the formation of these four- and five-coordinated iridium species, with alternating chelated and non-chelated β -diketone ligands in addition to various influencing phosphorus ligands, will contribute to solving mechanistic pathways of reactions involved in hydroformylation processes. Some aspects will be addressed in Chapter 6, where the kinetics of the reaction between [Ir(acac)(CO)₂] and phosphorus ligands will be discussed.

²¹ R.J. Cross, J. Chem. Soc. Rev., 1985, 197.

6

KINETICS OF RAPID SUBSTITUTION OF CO BY TERTIARY PHOSPHINE LIGANDS

6.1 INTRODUCTION

Kinetic investigations produce insight into the mechanism by which chemical alterations occur. The well-known catalytic system for hydroformylation, hydrogenation and isomerisation of olefins is based on rhodium, where $[\text{Rh}(\text{acac})(\text{CO})_2]$ in the presence of tertiary phosphines or phosphites (PR_3) ($\text{PR}_3 = \text{PPh}_3, \text{P}(\text{OPh})_3$) is used as catalyst precursor.^{1,2,3,4,5} In the case of hydroformylation, the starting material, $[\text{Rh}(\text{acac})(\text{CO})_2]$ in the first step involves the substitution of a CO group by PR_3 , yielding $[\text{Rh}(\text{acac})(\text{CO})(\text{PR}_3)]$,^{5,6} which is eventually converted into the catalytically active hydrido complex, $[\text{HRh}(\text{CO})(\text{PR}_3)_3]$.^{6,7} Weaker π -acceptors only produce the monosubstituted products even when used in large excess^{4,6,7} while strong π -acceptor ligands such as $\text{PR}_3 = \text{P}(\text{OPh})_3$ or $\text{P}(\text{NC}_4\text{H}_4)_3$ generate the di-substituted $[\text{Rh}(\text{acac})(\text{PR}_3)_2]$ complex. Iridium compounds are often used as model complexes since Ir(I) and Ir(III) complexes with similar ligand sets to those proposed in rhodium chemistry tend to behave in the same way. Very little information concerning the intimate mechanism of these systems exist that could reveal valuable information leading to the designing and optimising of new catalyst species. This study deals with a kinetic investigation of the reaction between $[\text{Ir}(\text{acac})(\text{CO})_2]$ and PPh_3 to examine the mechanism that could in turn deliver insight into such procedures as hydroformylation.

¹ B. Moasser, W.L. Gladfelter, D.C. Roe, *Organometallics*, 1995, **14**, 3832.

² A. van Rooy, E.N. Orji, P.G.J. Kramer, P.W.N.M. van Leeuwen, *Organometallics*, 1995, **14**, 34.

³ H. Yamashita, B.L. Roan, T. Sakakura, M. Tanaka, *J. Mol. Catal.*, 1993, **81**, 255.

⁴ A.M. Trzeciak, T. Głowiak, R. Grzybek, J.J. Ziołkowski, *J. Chem. Soc., Dalton Trans.*, 1997, 1831.

⁵ A.M. Trzeciak, E. Wolszczak, J.J. Ziołkowski, *New J. Chem.*, 1996, **20**, 365.

⁶ F. Bonati, G. Wilkinson, *J. Chem. Soc.*, 1964, 3156.

⁷ A.M. Trzeciak, J.J. Ziołkowski, *Inorg. Chim. Acta*, 1985, **96**, 15.

6.2 GENERAL CONSIDERATIONS

All reagents and chemicals were of analytical grade. All organic solvents were dried and distilled prior to use. Kinetic measurements were performed on a Varian Cary 50 Conc UV-Visible Spectrophotometer (slower reactions), equipped with a Julabo F12-mV temperature cell regulator (accurate within 0.1 °C) in a 1.000 ± 0.001 cm quartz cuvette cell. Faster reactions were performed on a Hi-Tech SF-61DX2 Stopped-flow instrument equipped with a low temperature CryoStopped-Flow system that can facilitate temperatures as low as -80.0 °C. This low temperature option uses methanol as thermostating agent and provides temperature control (± 0.2 °C) of the sample flow lines and observation cell. The dead time of the mixing unit is estimated to be less than 2.0 ms. The Stopped-flow instrument is a multiple wavelength apparatus in the Diode-Array mode in which the initial reactions were collected in order to find the appropriate wavelength of considerable absorbance change. After this specific wavelength was selected, the Stopped-flow system was changed to the more sensitive Photo-Multiplier setup so that the whole kinetic study could be performed. The Hi-Tech Stopped-flow instrument is Microsoft Windows operated with Kinet Asyst Stopped-Flow Kinetic Studio software for the acquisition and analysis of kinetic data. All the kinetic runs were performed under *pseudo* first-order conditions in which the ligand concentration is at least ten times the total concentration of the iridium complexes. The Scientist Micromath, Version 2.01⁸ program was used to fit the data to selected functions. The solid lines in the figures represent computer least squares fits of data, while experimental values are represented as individual points, denoted by selected symbols.

6.3 CALCULATIONS

Complex kinetics often includes several consecutive reactions occurring in the same time frame. The equations for evaluating the absorbance change *vs* time are discussed below.

A general one-step reaction, where k_1 represents the forward reaction and k_{-1} represents the reverse reaction, can be illustrated as:

⁸ MicroMath Scientist for Windows, Version 2.01, Copyright © 1986 – 1995, MicroMath, Inc.



Under *pseudo* first-order conditions where $[L] \gg [M]$, the *pseudo* first-order rate constant is given by

$$k_{obs} = k_1[L] + k_{-1} \quad \mathbf{6.2}$$

A plot of k_{obs} vs $[L]$ yields a straight line with intercept, k_{-1} , and slope, k_1 . The *pseudo* first-order rate constant for such a substitution reaction may be obtained from fitting experimental data obtained as a function of time to Eq. 6.3 (Paragraph 3.5.2).

$$A_{obs} = A_{\infty} - (A_{\infty} - A_0)e^{-k_{obs}t} \quad \mathbf{6.3}$$

Similarly, in the case of a two-step consecutive reaction, with two *pseudo* first-order rate constants (k_{obs1} and k_{obs2} respectively) and provided that $[L] \gg [M]$, the rate constants for both steps can be obtained from least-squares fits using Eq. 6.4.

$$A_{obs} = (A_0 - B_0)e^{(-k_{obs1}.t)} + (B_0 - B_I)e^{(-k_{obs2}.t)} + B_I \quad \mathbf{6.4}$$

For Eqs. 6.3 and 6.4 the variables are defined as:

A_{obs} represents the observed absorbance as found in kinetic data, A_0 the initial absorbance at the start of the experiment, A_{∞} the infinite final product absorbance as found in kinetic data, B_0 the theoretical/calculated initial absorbance of the 2nd product, B_I the infinite final product absorbance as found in kinetic data, t the time (s) and k_{obs} the observed rate constant for a one-step *pseudo* first-order reaction where k_{obs1} represents k_{obs} for the first reaction of a two-step *pseudo* first-order reaction and k_{obs2} for the second reaction of a two-step *pseudo* first-order reaction.

Mechanistic aspects for these reactions were determined by the activation parameters ΔH^\ddagger (activation enthalpy) and ΔS^\ddagger (entropy of activation). The logarithmic form of the Eyring equation in Eq. 6.5 was used to obtain these activation parameter values.

$$\ln \frac{k}{T} = \ln \frac{k_B}{h} - \frac{\Delta H^\ddagger}{RT} + \frac{\Delta S^\ddagger}{R} \quad 6.5$$

In Eq. 6.5 a graph of $\ln \frac{k}{T}$ vs. $\frac{1}{T}$ will give slope, $(-\frac{\Delta H^\ddagger}{T})$ and intercept, $(\ln \frac{k_B}{h} + \frac{\Delta S^\ddagger}{R})$. k_B is representative of the Boltzmann constant and h is Planck's constant.

6.4 RESULTS AND DISCUSSION

6.4.1 Experimental Procedures

Stability tests of the reagent solutions were the first examinations performed in the kinetic study. The solutions were scanned for a longer period of time than the studied reactions occur, to establish that the reagents themselves do not undergo changes such as decomposition, polymerisation or coordination while in solution since these additional reactions would significantly complicate the nature of the kinetics. Solutions of $[\text{Ir}(\text{acac})(\text{CO})_2]$ and PPh_3 in methanol were observed for ± 3 days signifying no noteworthy decomposition or interaction between the solvent and starting reagents (Figure 6-1).

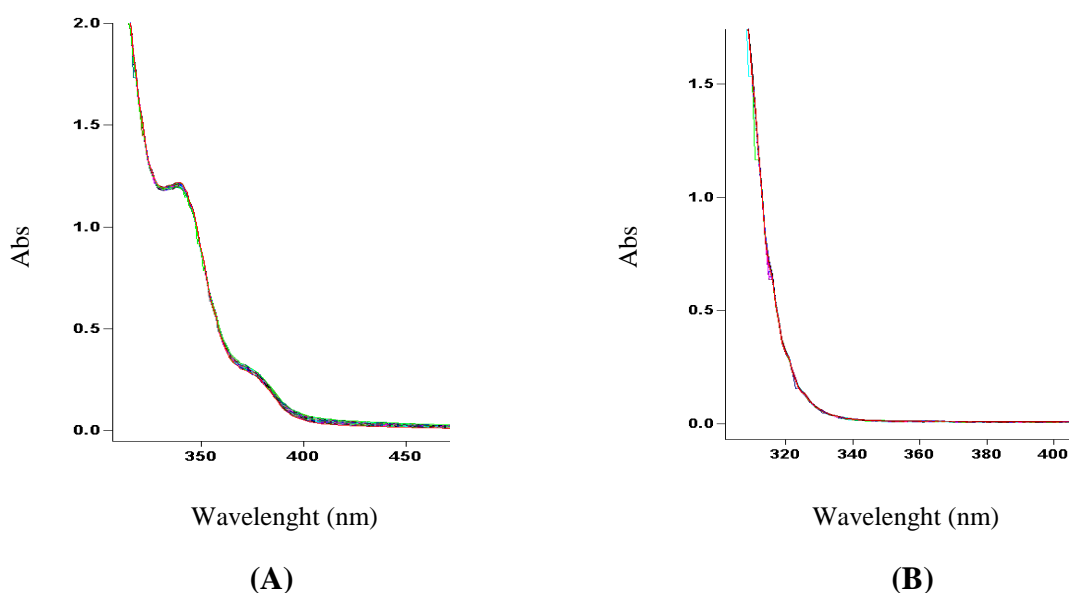


Figure 6-1: UV-vis spectral scans of a solvent stability test over three days at 25.0 °C in MeOH of (A) $[\text{Ir}(\text{acac})(\text{CO})_2] = 0.5 \text{ mM}$ and (B) $[\text{PPh}_3] = 5.0 \text{ mM}$.

All the reactions were performed under *pseudo* first-order conditions with the entering ligand in excess of at least 10 times that of the metal complex. The different ligand concentrations were prepared from a stock solution of 20.0 mM PPh_3 with dilutions ranging from 1.0 mM to 10.0 mM. Even though the stability of the solutions was confirmed for more than 24 hours, fresh solutions were prepared for each set of kinetic experiments.

Typical results obtained from a kinetic run evaluated *via* Stopped-flow spectroscopy, illustrating the change in absorbance *vs* time is shown in Figure 6-2.

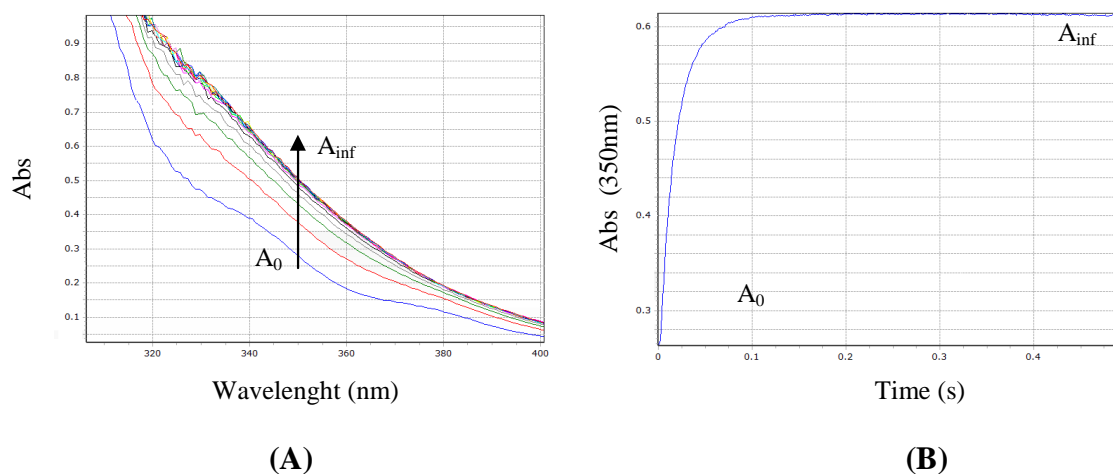


Figure 6-2: Typical Diode-array scan result of CO substitution in $[\text{Ir}(\text{acac})(\text{CO})_2]$ with PPh_3 . (A) Wavelength scans over time ($\Delta t = 0.5 \text{ s}$); (B) Absorbance *vs.* time trace at $\lambda = 350 \text{ nm}$. $[\text{Ir}] = 0.1 \text{ mM}$, $[\text{PPh}_3] = 1.0 \text{ mM}$, MeOH, $-20.0 \text{ }^\circ\text{C}$.

The data obtained from the kinetic experiments were fitted to mathematical models given in Eq. 6.3 and Eq. 6.4 representing a one-step *pseudo* first-order (Figure 6-3 **A**) and two-step *pseudo* first-order (Figure 6-3 **B**) reaction respectively. From Figure 6-3 and all the other data sets it is clear that the data fit the second model better, indicating that a two-step *pseudo* first-order reaction is taking place.

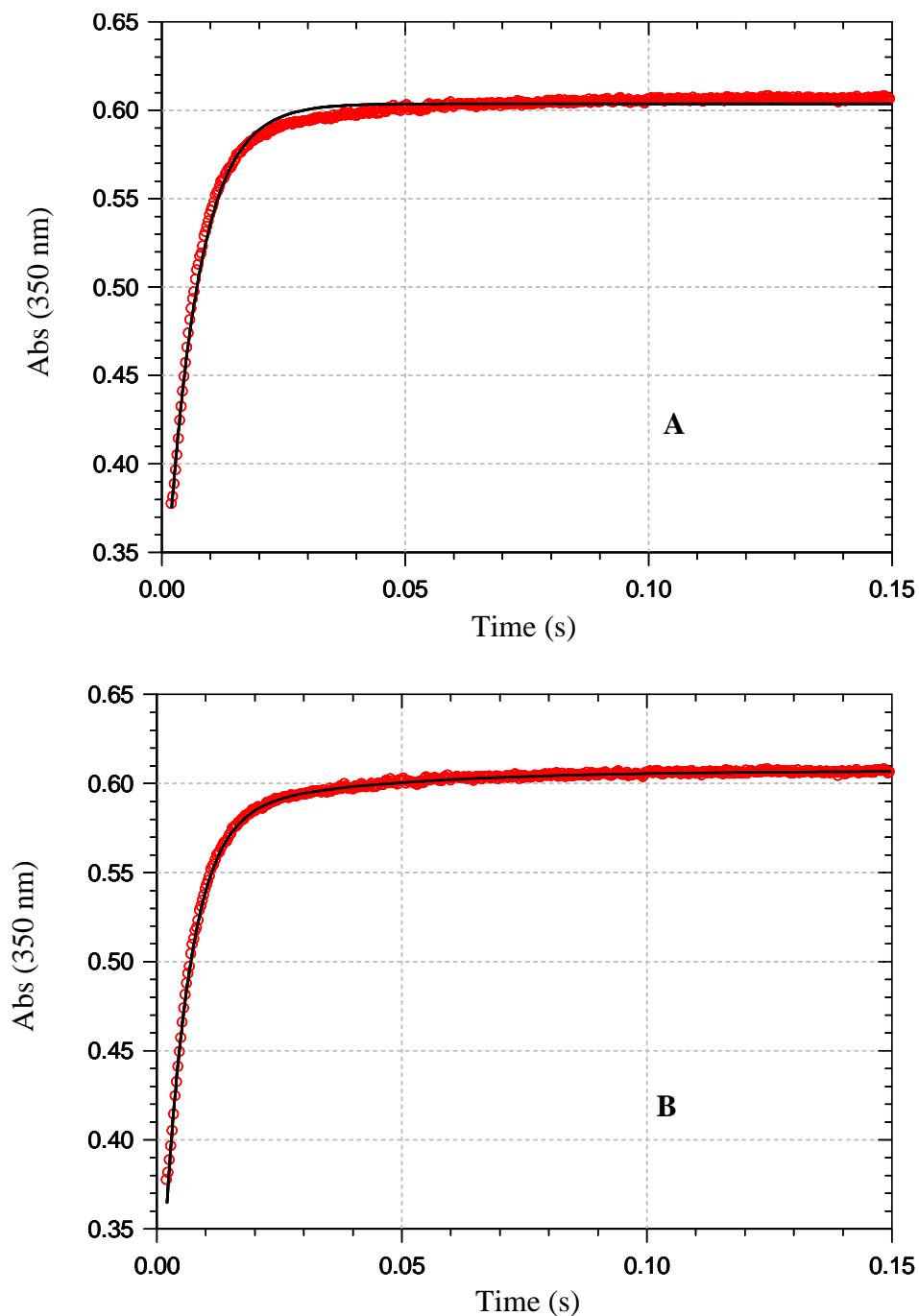


Figure 6-3: Photo-Multiplier data fitted for a (A) one-step and (B) two-step reaction using Eqs. 6.1 and 6.2 for (A) and (B) respectively. $[\text{Ir}(\text{acac})(\text{CO})_2] = 0.1 \text{ mM}$ + $\text{PPh}_3 = 2.5 \text{ mM}$, MeOH, $-20.0 \text{ }^\circ\text{C}$.

Due to the rapid rates of the reactions and thus the need for extremely low temperatures, methanol was best suited as solvent due to its low freezing point of $-97.5\text{ }^{\circ}\text{C}$.⁹ The pressure of the drive syringe plunger mechanism of the Stopped-flow machine was held for 1 second, allowing the reaction to run to completion before pressure release to ensure correct data collection for the extremely fast reactions.

Independently, kinetic runs were also performed with each starting material, $[\text{Ir}(\text{acac})(\text{CO})_2]$ and PPh_3 , against methanol as solvent within the fast time frame at which the studied reactions occur, indicating no reaction thus ruling out the possibility of mistaking an equipment artefact or solvent mixing as a kinetic reaction. The phosphine ligand also shows no absorption at 350 nm (Figure 6-1 **B**) implying that the absorbance change followed at 350 nm is an accurate representation of the kinetic reaction between $[\text{Ir}(\text{acac})(\text{CO})_2]$ and PPh_3 only.

A small ligand concentration range of 1.0 to 5.0 mM was used due to a loss of initial kinetic data points for the first reaction at high PPh_3 concentrations (Figure 6-4) caused by the rapid nature of the reaction. With increasing ligand concentrations from $[\text{PPh}_3] = 1.0\text{ mM}$ (Figure 6-4 **A**) to $[\text{PPh}_3] = 8.0\text{ mM}$ (Figure 6-4 **B**) the initial absorbance values are 0.28 and 0.55 respectively. This indicates that the rate of the first reaction exceeds the dead-time of the Stopped-flow machine (Figure 6-4 **B**) with reaction half-life values lower than 2 ms causing the loss of initial data points making an accurate calculation of the observed rate constants for the reactions at high ligand concentrations impossible.

⁹ D.R. Lide, *Handbook of Chemistry and Physics*, Boca Raton, FL: CRC Press, 2005.

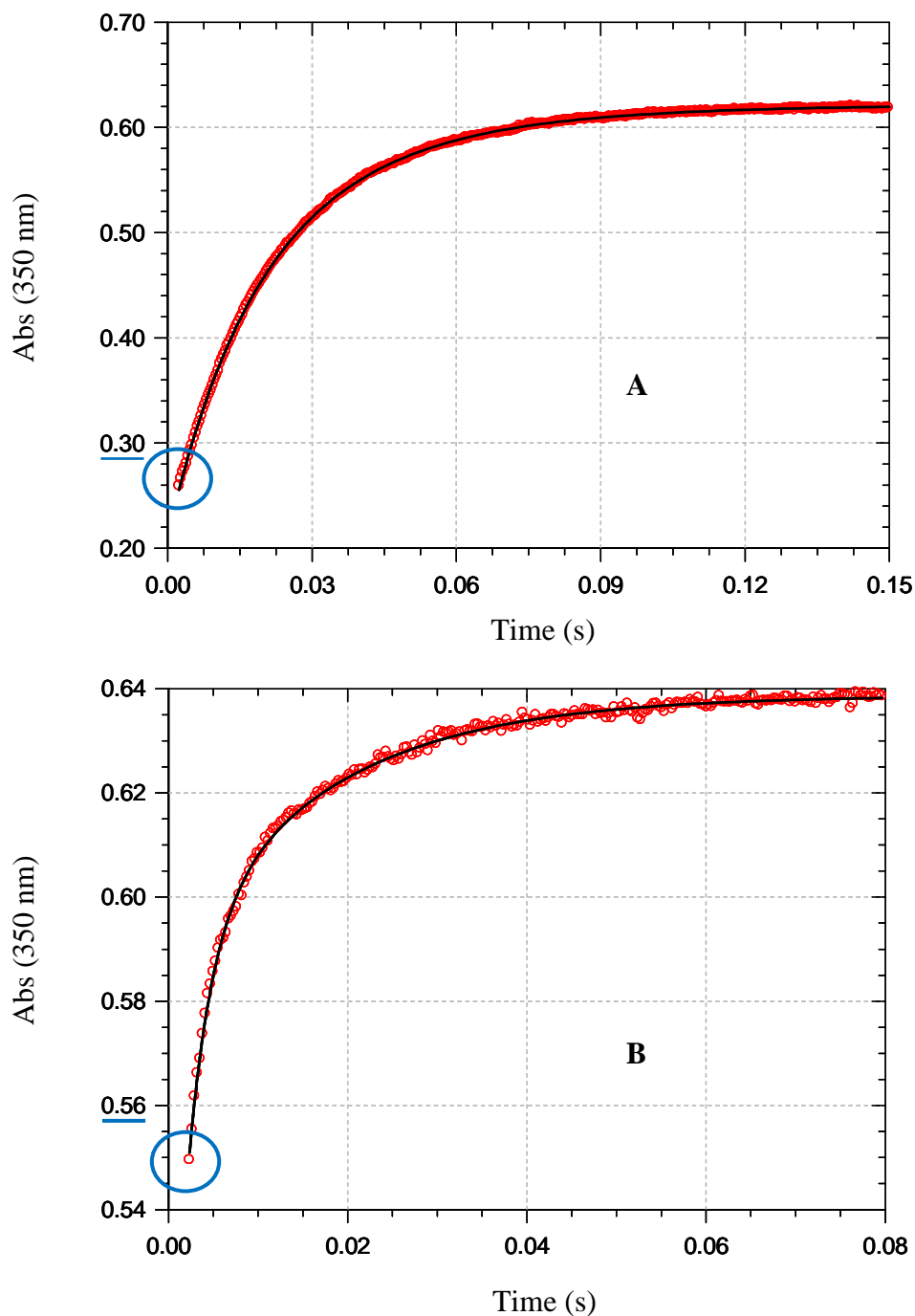


Figure 6-4: Photo-Multiplier data fitted for a two-step reaction illustrating the loss in initial data points for the first reaction with increasing PPh_3 concentrations from (A) – $[PPh_3] = 1.0 \text{ mM}$ to (B) – $[PPh_3] = 8.0 \text{ mM}$. $[Ir] = 0.1 \text{ mM}$, MeOH, $-30.0 \text{ }^\circ\text{C}$.

Crystallographic data discussed in Chapter 5 indicates that these systems form the *bis*-phosphine complexes in which the $acac^-$ ligand either binds as a β -diketone chelate ring or by binding to the metal centre only through one oxygen atom. ^1H NMR confirms the formation of $[Ir(acac)(CO)(PPh_3)_2]$ (Figure 4-2 A) while upon utilizing higher phosphine concentrations ^1H NMR indicates that the $acac^-$ ligand is no longer coordinated to the metal

centre (Figure 4-2 **B**). From the above preliminary kinetic observations and information gathered from Chapter 5, the proposed mechanism is explained in detail in the rest of this chapter.

6.4.2 Preliminary Analysis of Rate Data Obtained via Stopped-Flow Techniques

All data was fit to Eq. 6.4. The observed rate constants (k_{obs} : k_{obs1} – first reaction, k_{obs2} – second reaction) for the two consecutive reactions were taken experimentally as an average over four runs for various concentrations of the entering ligand (Table 6-1). Individual observed rate constants are reported in Appendix II.

Table 6-1: Comparison of the observed rate constants for two consecutive steps for the reaction kinetics between $[\text{Ir}(\text{acac})(\text{CO})_2]$ and PPh_3 at different temperatures, k_{obs1} represents the 1st reaction and k_{obs2} the second. $[\text{Ir}] = 0.1 \text{ mM}$, MeOH .

Observed rate constants, (k_{obs}) for two consecutive steps (s^{-1})								
Ligand (10^3) [PPh_3] (M)	-10.0 °C		-20.0 °C		-30.0 °C		-40.0 °C	
	k_{obs1}	k_{obs2}	k_{obs1}	k_{obs2}	k_{obs1}	k_{obs2}	k_{obs1}	k_{obs2}
1.0	92(1)	-	65.7(7)	16.4(8)	58(3)	29(3)	44(3)	19(3)
1.5	137(4)	-	108(2)	24(5)	85.5(6)	34(1)	71(3)	21(5)
2.0	184(4)	-	141(2)	29(7)	122(3)	30(7)	114(3)	29(3)
2.5	232(7)	-	198(4)	34(3)	174(5)	45(6)	147(3)	29(3)
3.0	279(8)	-	246(6)	42(7)	209(8)	45(11)	188(3)	33(2)
5.0	-	-	-	-	332(15)	65(5)	293(7)	35.0(6)

The reaction at -10.0 °C produced non-reproducible results for the rate constant k_{obs2} even after repeating the reaction several times and was therefore omitted from the kinetic study. Early indications therefore seem to suggest a small formation constant for the second step. The relationships between the different *pseudo* first-order rate constants (k_{obs1} and k_{obs2}) and $[\text{PPh}_3]$ are discussed separately.

For the **first reaction** good linear first-order plots passing through the origin were obtained. The effect of the concentration of the entering ligand and temperature dependence are illustrated in Figure 6-5.

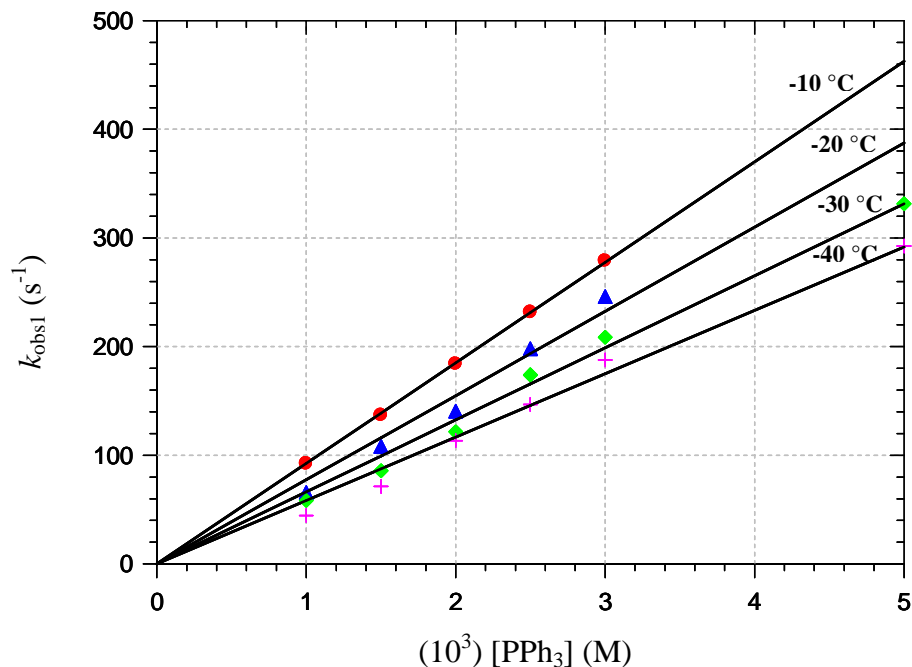
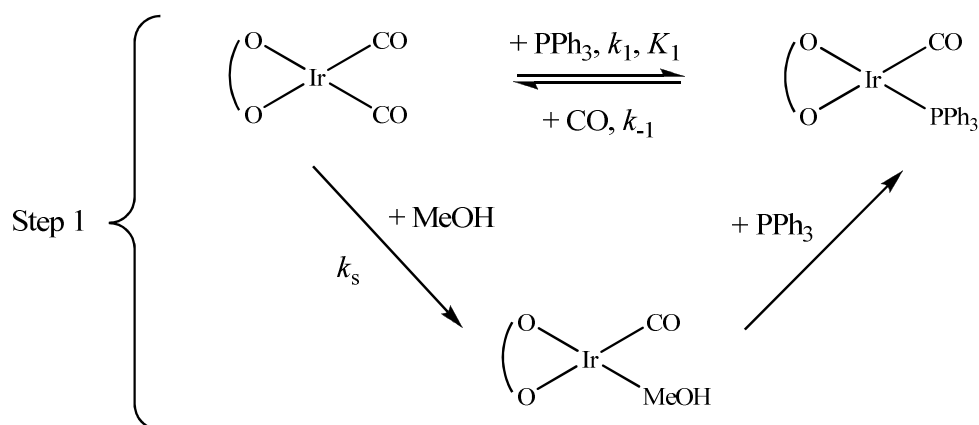


Figure 6-5: Plot of k_{obs1} vs $[\text{PPh}_3]$ for the reaction between $[\text{Ir}(\text{acac})(\text{CO})_2]$ and PPh_3 at different temperatures, $[\text{Ir}] = 0.1 \text{ mM}$, $\lambda = 350 \text{ nm}$, MeOH .

This points to a simple first-order reaction and the general reaction for the 1st step can be best described by the following scheme:



Scheme 6.1: The proposed reaction for data obtained from Stopped-flow spectroscopy for the 1st step of CO substitution in $[\text{Ir}(\text{acac})(\text{CO})_2]$ with PPh_3 .

The rate law for the first reaction of the two-step process found monitored by Stopped-flow spectroscopy is represented by Eq. 6.6:

$$\text{Rate} = \{k_s + k_1[\text{L}]\}[\text{Ir}(\text{acac})(\text{CO})_2] - k_{-1}[\text{Ir}(\text{acac})(\text{CO})(\text{PPh}_3)][\text{CO}] \quad \mathbf{6.6}$$

where k_s represents the solvent pathway, k_1 and k_{-1} represents the forward- and reverse reactions, respectively and [L] the entering ligand i.e. PPh_3 . A graph of k_{obs} vs $[\text{PPh}_3]$ was linear in all cases passing through the origin (implying $k_s = 0$ in terms of the general rate law for square planar substitution reactions where $\text{rate} = (k_s + k_1[\text{L}])(\text{substrate})$). The observed zero intercept is to be expected, since the displacement of a bidentate ligand by solvent molecules, here methanol, would be much more difficult than that of the displacement of a monodentate ligand.^{10,11,12} Eq. 6.6 is therefore simplified to Eq 6.7.

$$\text{Rate} = k_1[\text{Ir}(\text{acac})(\text{CO})_2][\text{L}] \quad \mathbf{6.7}$$

Under *pseudo* first-order conditions where $[\text{L}] \gg [\text{Ir}]$, the rate constant can be determined by Eq 6.8.

$$k_{\text{obs1}} = k_1[\text{L}] \quad \mathbf{6.8}$$

where k_{obs1} represents the observed rate constant.

The values of the second-order rate constants for the reaction of $[\text{Ir}(\text{acac})(\text{CO})_2]$ with the entering ligand (PPh_3) were obtained from the slope of the linear plots of k_{obs1} vs [L] and are listed in Table 6-2.

¹⁰ F. Basolo, R. Pearson, *Mechanism of Inorganic Reactions*, 2nd Ed., New York: John Wiley & Sons Inc., 1965.

¹¹ J.G. Leipoldt, S.S. Basson, G.J. van Zyl and G.J.J. Steyn, *J. Organomet. Chem.*, 1991, **418**, 241.

¹² J.C. Swarts, W.C. du Plessis, T.G. Vosloo, *Inorg. Chim. Acta*, 2002, **331**, 188.

Table 6-2: Summary of the second-order rate constants for the first reaction followed by Stopped-flow spectroscopy for the reaction between [Ir(acac)(CO)₂] and PPh₃, [Ir] = 0.1 mM, [PPh₃] = 1.0 mM – 5.0 mM, λ = 350 nm, MeOH.

	-10.0 °C	-20.0 °C	-30.0 °C	-40.0 °C	$\Delta H_{k_1}^\ddagger$ (kJ mol ⁻¹)	$\Delta S_{k_1}^\ddagger$ (J K ⁻¹ mol ⁻¹)	%TΔS [‡]
$(10^{-3}) k_1$ (M ⁻¹ s ⁻¹)	92.5(3)	77(3)	66(1)	58(2)	5.8(6)	-127(2)	85%

A temperature dependence study of the reaction was also conducted for determination of the activation parameters. The activation parameters of the first reaction between [Ir(acac)(CO)₂] and PPh₃ were determined by fitting the data to Eq. 6.5 (see Figure 6-6). The standard enthalpy change of activation ($\Delta H_{k_1}^\ddagger$) was calculated as 5.8(6) kJ mol⁻¹ and the standard entropy change of activation ($\Delta S_{k_1}^\ddagger$) was calculated as -127(2) J K⁻¹ mol⁻¹.

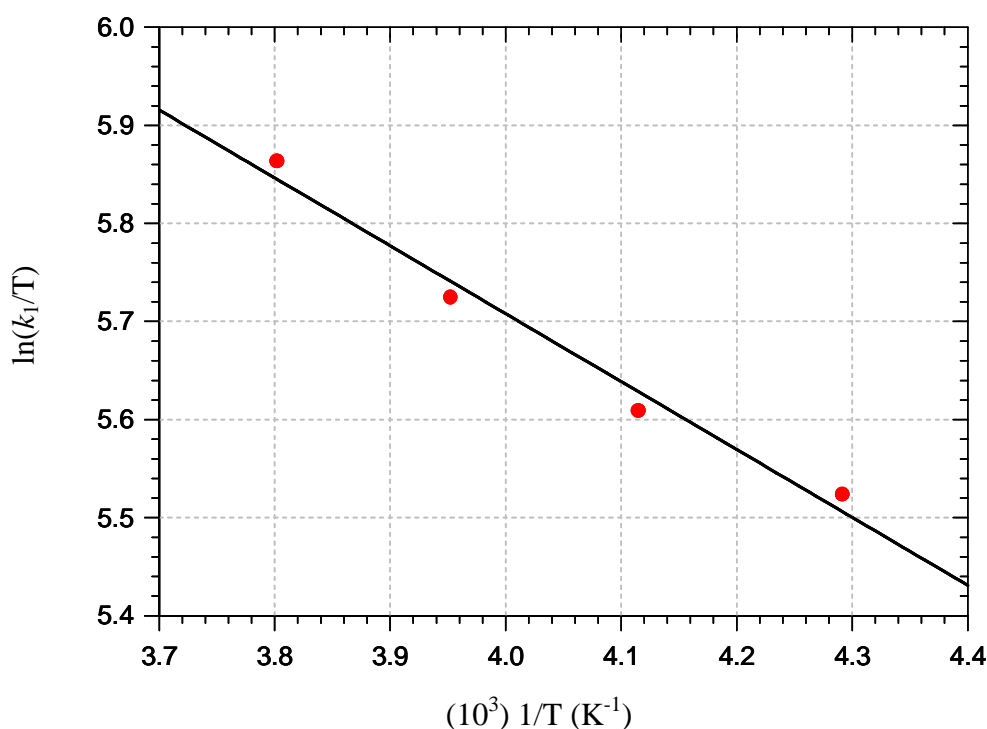


Figure 6-6: Eyring Plot of $\ln(k_1/T)$ vs $1/T$ for the reaction between [Ir(acac)(CO)₂] and PPh₃ for a temperature range of -40 °C to -10 °C.

Data obtained for the **second step** gives a nonlinear relationship between $k_{\text{obs}2}$ and ligand concentration, indicating probable limiting kinetics (Figure 6-7).

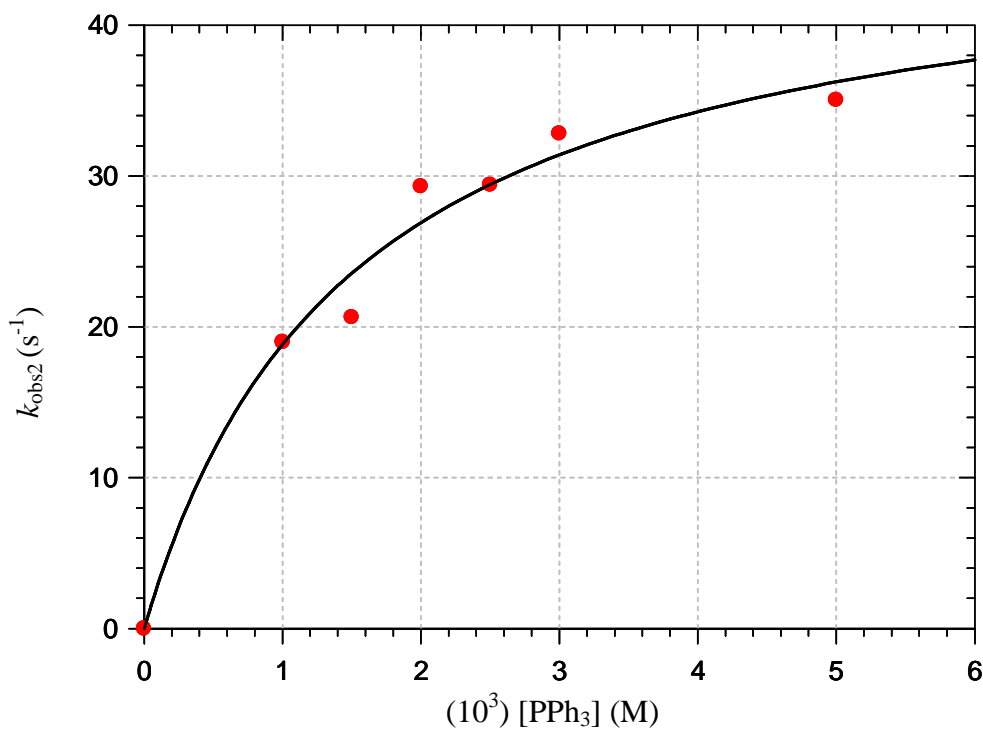
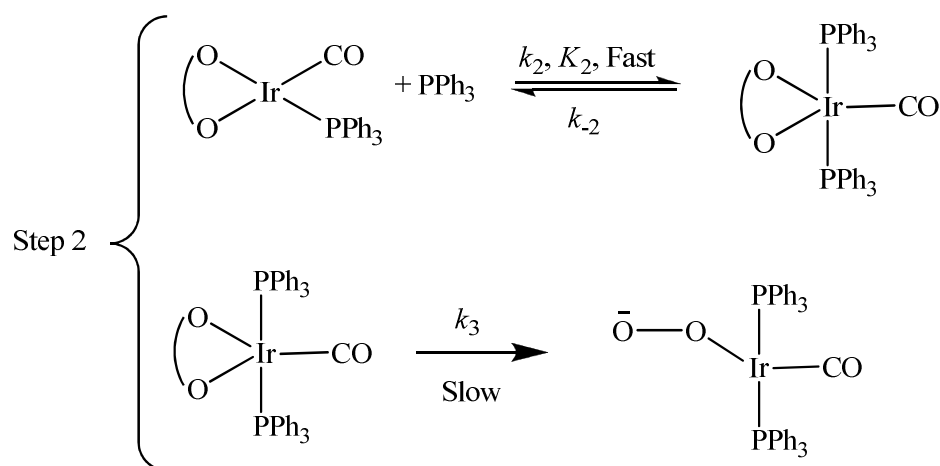


Figure 6-7: Plot of $k_{\text{obs}2}$ versus PPh_3 concentration for the second Stopped-flow reaction (Data from Table 6-1) at -40.0°C in MeOH, $[\text{Ir}] = 0.1 \text{ mM}$.

The typical rate equation which predicts the relationship between $k_{\text{obs}2}$ and $[\text{L}]$ as illustrated in Figure 6-7 is given by Eq.6.9 (see Appendix II for the full derivation).

$$k_{\text{obs}2} = \frac{k_3 \frac{k_2}{k_{-2}} [\text{L}]}{1 + \frac{k_2}{k_{-2}} [\text{L}]} = \frac{k_3 K_2 [\text{L}]}{1 + K_2 [\text{L}]} \quad \mathbf{6.9}$$

This suggests a rapid pre-equilibrium, ligand dependent, first step followed by a slower, ligand independent, second step and is illustrated by Scheme 6-2.



Scheme 6.2: The proposed reaction for data obtained from Stopped-flow spectroscopy for the 2nd step for the reaction kinetics between $[\text{Ir}(\text{acac})(\text{CO})_2]$ and PPh_3 .

Table 6-3: Summary of the second-order rate constants for the second reaction followed by Stopped-flow spectroscopy for the reaction between $[\text{Ir}(\text{acac})(\text{CO})_2]$ and PPh_3 , $[\text{Ir}] = 0.1 \text{ mM}$, $[\text{PPh}_3] = 1.0 \text{ mM} - 5.0 \text{ mM}$, $\lambda = 350 \text{ nm}$, MeOH .

	-20.0 °C	-30.0 °C	-40.0 °C	$\Delta H_{k_3}^\ddagger$ (kJ mol ⁻¹)	$\Delta S_{k_3}^\ddagger$ (J K ⁻¹ mol ⁻¹)
$(10^{-2}) K_2 (\text{M}^{-1})$	1(3)	4(1)	7(2)		
$(10^{-1}) k_3 (\text{M}^{-1}\text{s}^{-1})$	18(5)	10(1)	4.7(4)	30.8(3)	-79(1)

A temperature dependence study for determination of the activation parameters of the second reaction was done by fitting the data to Eq. 6.5 (Figure 6-8). The standard enthalpy change of activation $\Delta H_{k_3}^\ddagger$ was calculated as 30.8(3) kJ mol⁻¹ and the standard entropy change of activation $\Delta S_{k_3}^\ddagger$ was calculated as -79(1) J K⁻¹ mol⁻¹.

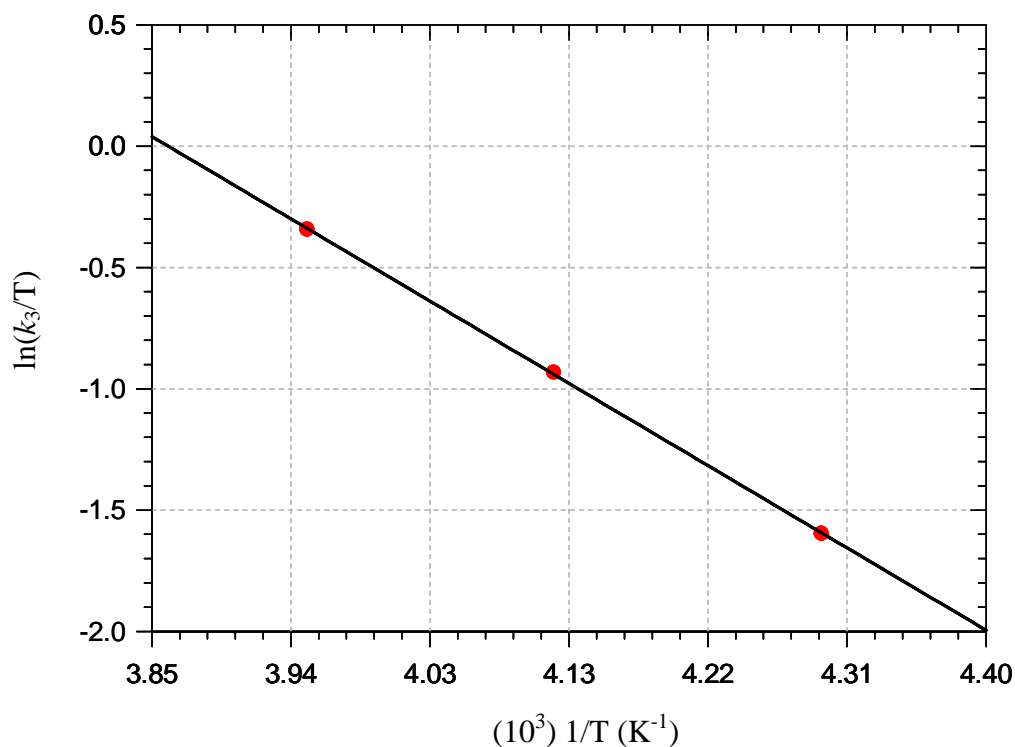
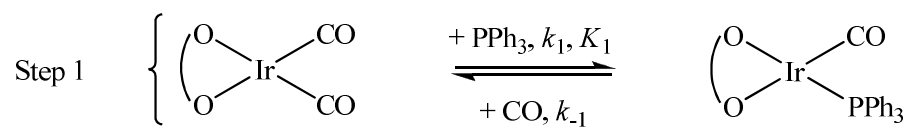
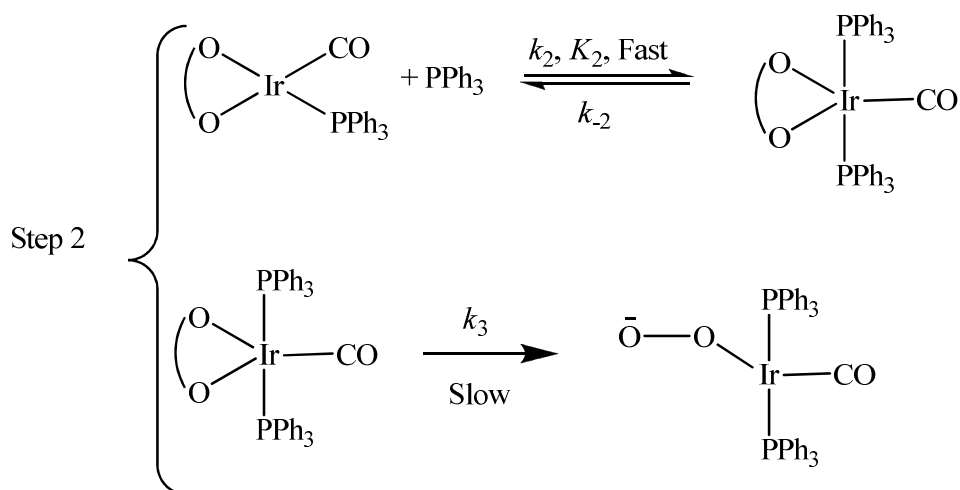


Figure 6-8: Eyring Plot of $\ln(k_3/T)$ vs $1/T$ for the second reaction between $[\text{Ir}(\text{acac})(\text{CO})_2]$ and PPh_3 for a temperature range of $-40.0\text{ }^\circ\text{C}$ to $-20.0\text{ }^\circ\text{C}$.

6.5 OVERALL REACTION MECHANISM

Based on the preliminary results reported above, a minimum of two reactions are observed and the overall kinetic behaviour during the kinetic runs are suggested as in Scheme 6.3:





Scheme 6.3: The two proposed reactions for data obtained from Stopped-flow spectroscopy for the reaction between $[\text{Ir}(\text{acac})(\text{CO})_2]$ and PPh_3 .

6.6 CONCLUSION

These results and as proposed in Scheme 6.3, indicate that the **first reaction step** (Step 1 of Scheme 6.3) is dependent on PPh_3 concentration. This is assumed to be the substitution reaction of one carbonyl ligand of the square-planar d^8 $[\text{Ir}(\text{acac})(\text{CO})_2]$ complex with PPh_3 to form $[\text{Ir}(\text{acac})(\text{CO})(\text{PPh}_3)]$. The large negative entropy value ($\Delta S_{k_1}^\ddagger = -127(2) \text{ J K}^{-1} \text{ mol}^{-1}$) suggests an associative mode of activation as expected for square planar substitution reactions. In general, the rates of the reactions at different temperatures as indicated by the slopes of the k_{obs} vs $[\text{PPh}_3]$ data (see Figure 6-5) do not increase by much for every 10°C temperature adjustment. This is indicative of a higher $T\Delta S^\ddagger$ contribution ($\pm 85\%$ in this case) to the Gibbs Free energy relationship and is similar to that what was found elsewhere^{13,14} for substitution reactions on Pt(II) olefin substrates. The activation enthalpy however further underlines the low energy barrier associated with this first reaction, which is also manifested in the rates observed; at the very limit of even 3rd generation Stopped-flow equipment at low temperatures. It is seen from Figure 6-5 that the straight lines obtained for the fits of k_{obs} vs $[\text{PPh}_3]$ pass through zero which possibly indicates a large equilibrium constant, $K_1 \gg 1$, and points towards favourability toward the forward reaction.

¹³ S. Otto, A. Roodt, *J. Organomet. Chem.*, 2006, **691**, 4626.

¹⁴ M.R. Plutino, S. Otto, A. Roodt, L.I. Elding, *Inorg. Chem.*, 1999, 1233.

Table 6-4: The rate constants and activation parameters for the reaction of [Ir(acac)(CO)₂] and PPh₃ at different temperatures.

	-10.0 °C	-20.0 °C	-30.0 °C	-40.0 °C	ΔH^\ddagger (kJ mol ⁻¹)	ΔS^\ddagger (J K ⁻¹ mol ⁻¹)	% T ΔS^\ddagger
(10 ⁻³) k_1 (M ⁻¹ s ⁻¹)	92.5(3)	77(3)	66(1)	58(2)	5.8(6)	-127(2)	85%
(10 ⁻²) K_2 (M ⁻¹)	-	1(3)	4(1)	7(2)	-	-	-
(10 ⁻¹) k_3 (M ⁻¹ s ⁻¹)	-	18(5)	10(1)	4.7(4)	30.8(3)	-79(1)	40%

The kinetic data for the **second reaction** (Step 2 of Scheme 6.3) did not yield a linear relationship. The resultant fits to Eq. 6.9 seem to support limiting kinetics instead in which a five-coordinated *bis*-PPh₃ complex is formed which proceeds in the rate determining step to undergo ring-opening (confirmed by the X-ray structure Figure 5-1) to form an acac-κO bonded square planar complex. The value of K_2 seems to be small and potentially means that the formation of a five coordinated species is not favorable as supported by the fact that there are only a few examples of five coordinated *bis*-phosphine complexes.^{15,16,17} The high negative value obtained for $\Delta S_{k_3}^\ddagger = -79(1) \text{ J K}^{-1} \text{ mol}^{-1}$ cannot be explained at the moment, but indicates an associative type mechanism. This does not detract from the fact that the proposed reaction scheme is a good representation of the observed data.

The crystallographic and synthetic data as presented in Chapters 4 and 5 provide much information and support for the proposed mechanism. It was shown in Chapter 4 with IR and NMR experiments that (i) acac⁻ is still part of the final complex formed at lower PPh₃ concentrations during synthesis, even at 40 °C; (ii) at higher PPh₃ concentrations it was observed that the acac⁻ ligand is no longer part of the coordination sphere at the higher temperatures. However, at the very low PPh₃ concentrations and the low temperatures at which the kinetic study was performed, the existence of the acac-κO bonded complex is assumed. The X-ray diffraction data lends further support to the proposed mechanism since two different Ir-acac *bis*-phosphine complexes were isolated and characterised in which the acac⁻ ligand binds to Ir(I) either as a β-diketonato chelate ring or only through one carbonyl oxygen of the acac⁻ ligand.

¹⁵ G.B. Ansell, S. Leta, A.A. Oswald, E.J. Mozeleski, *Acta Cryst.*, 1986, **C42**, 1516.

¹⁶ S. Yoshida, Y. Ohgomori, Y. Watanabe, K. Honda, M. Goto, M. Kurahashi, *J. Chem. Soc. Dalton Trans.*, 1988, 895.

¹⁷ A. Roodt, S. Otto, G. Steyl, *Coord. Chem. Rev.*, 2003, **245**, 121.

It is to be expected that the reactivity of these complexes would be very sensitive to the steric and electronic effect of the entering ligand. Further investigation is needed to establish what characteristics of the ligands influence the behaviour of the β -diketone ligand.

Mechanistic studies like these are important when optimizing a catalyst for large industrial processes like hydroformylation. Although the iridium(I) dicarbonyl species showed very different chemical behaviour for substitution reactions than the rhodium analogues,^{5,6} the iridium species may be proven important for the study of transition intermediates of rhodium catalysts.

This study provided insight in the bonding mode of the acac^- ligand in the presence of lower tertiary phosphine concentrations. More over it illustrates the stepwise dissociation of the acac^- , which is often present in $[\text{M}(\text{acac})(\text{CO})_2]$ ($\text{M} = \text{Rh}(\text{I}), \text{Ir}(\text{I})$) complexes frequently utilized as catalyst precursors in hydroformylation and related reactions.

7

EVALUATION OF STUDY

7.1 INTRODUCTION

This chapter includes a summary of the results obtained and scientific relevance of this M.Sc. study, as well as some future research possibilities.

7.2 SCIENTIFIC RELEVANCE AND RESULTS OBTAINED

This study was aimed at investigating model iridium carbonyl complexes used as possible homogeneous catalyst precursors and studying basic reactions which usually occur in processes such as olefin hydroformylation.

Four complexes were successfully synthesized of which two new crystal structures, *trans*-[Ir(acac- κ O)(CO)(PPhCy₂)₂] and *trans*-[Ir(acac- κ^2 O,O)(CO)(PCy₃)₂], have been characterized with single crystal X-ray diffraction and other spectroscopic techniques. The major difference between these complexes is the way in which the acac⁻ ligand coordinates to the metal centre. The acac⁻ ligand binds either as a chelated ring or undergoes ring-opening and is linked to the metal only through one oxygen atom. The co-crystallizing solvent molecules, in the case of *trans*-[Ir(acac- κ O)(CO)(PPhCy₂)₂], do not restrict or interfere with any significant physical properties of the solvated metal complex (see Chapter 5). The products showed different sensitivity towards air and moisture, nevertheless all decomposing in open air within a time frame of a few hours to a day at most. These complexes serve to understand five-coordinated intermediates that form during hydroformylation when incorporating metal carbonyl complexes as precursor catalyst in the presence of phosphine ligands.

The kinetic study to establish the mechanism of the square-planar carbonyl substitution by PR₃ (PR₃ = PPh₃, PPh₂Cy, PPhCy₂, PCy₃) in β -diketonatodicarbonyliridium(I) complexes

revealed that two reactions occur in methanol as solvent. The first reaction involves the substitution of only one carbonyl group to form the monocarbonyl product, $[\text{Ir}(\text{acac})(\text{CO})(\text{PPh}_3)]$, and the second reaction entails two steps of which the first is the addition of a second phosphine ligand forming the *bis*-phosphine complex, *trans*- $[\text{Ir}(\text{acac})(\text{CO})(\text{PPh}_3)_2]$, followed by the rate-determining ring-opening of the acac^- ligand in the second step. This information can be used in the future to manipulate the catalytic reaction conditions to optimize the hydroformylation process by controlling the formation of products with highest reactivity.

7.3 FUTURE RESEARCH

Based on the results obtained from this study, further investigations, to expand on the current available knowledge of the coordination modes and kinetic behaviour of these iridium(I) systems, include:

- Further investigations in the coordination of these systems using a wider range of entering ligands of the form PR_3 (PR_3 = tertiary phosphine/arsine/stibine). Isolation of single crystals thereof for crystallographic investigations confirming complex formation and various isomers.
- Modification of the β -diketonato ligand through various substituents on the ring to enhance electron donating and withdrawing effects.
- The re-synthesis of analogous rhodium *bis*-phosphine complexes as found in literature for better comparisons.
- An extended kinetic investigation studying the substitution- and oxidative addition reactions of these systems. Examining solvent influences by conducting the reactions in solvents of different donicities, polarities, dielectric constants and nucleophilicities.
- The advancement of kinetic study techniques for identifying intermediate phase products.

- Comparing the reaction kinetics with Rh-analogous complexes.
- Theoretical computational calculations would assist in understanding the kinetic and coordination behaviour.
- Evaluate the catalytic activity of these systems in olefin hydroformylation reactions.

APPENDIXES

APPENDIX I

SUPPLEMENTARY DATA TO THE CRYSTAL STRUCTURES

1 Crystal Data for [Ir(acac-*O*)(CO)(PPhCy₂)₂]

Table 1-1. Atomic coordinates ($\times 10^4$) and equivalent isotropic displacement parameters ($\text{\AA}^2 \times 10^3$) for [Ir(acac-*O*)(CO)(PPhCy₂)₂]. $U(\text{eq})$ is defined as one third of the trace of the orthogonalized U^{ij} tensor.

	x	y	z	U(eq)
C(01)	7037(2)	5352(2)	9972(3)	22(1)
C(02)	8281(2)	3911(2)	8960(3)	22(1)
C(03)	8458(2)	3621(2)	8304(3)	28(1)
C(04)	8599(2)	3789(2)	9676(3)	22(1)
C(05)	9129(2)	3389(2)	9923(3)	28(1)
C(06)	9418(2)	3376(3)	10742(3)	38(1)
C(11)	8752(2)	5838(2)	10064(2)	18(1)
C(12)	9231(2)	5310(2)	10250(3)	23(1)
C(13)	9805(2)	5512(3)	10853(2)	29(1)
C(14)	9618(2)	5736(2)	11541(2)	27(1)
C(15)	9102(3)	6226(3)	11362(3)	33(1)
C(16)	8533(2)	6013(2)	10751(3)	28(1)
C(21)	8433(2)	5514(2)	8498(2)	21(1)
C(22)	8916(2)	5987(2)	8401(3)	26(1)
C(23)	9195(2)	5841(2)	7757(3)	30(1)
C(24)	8697(2)	5722(3)	7057(3)	33(1)
C(25)	8215(3)	5256(2)	7151(3)	30(1)
C(26)	7926(2)	5418(2)	7782(2)	22(1)
C(31)	7667(2)	6385(2)	9053(3)	24(1)
C(32)	7966(3)	6957(2)	9198(3)	31(1)
C(33)	7631(3)	7501(3)	8982(3)	42(1)
C(34)	6997(3)	7461(3)	8583(3)	42(1)
C(35)	6707(3)	6913(3)	8429(3)	40(1)
C(36)	7035(2)	6373(2)	8646(3)	28(1)

APPENDIX I

C(41)	6594(2)	3642(2)	10104(2)	20(1)
C(42)	7180(2)	3231(2)	10298(3)	26(1)
C(43)	7158(3)	2812(2)	10946(3)	30(1)
C(44)	7097(2)	3175(2)	11617(3)	28(1)
C(45)	6533(3)	3607(3)	11423(3)	42(1)
C(46)	6561(3)	4030(3)	10782(3)	36(1)
C(51)	5802(2)	4502(2)	9092(3)	26(1)
C(52)	5286(2)	4228(3)	9281(3)	38(1)
C(53)	4694(3)	4513(4)	9078(3)	47(2)
C(54)	4607(3)	5033(3)	8647(3)	47(2)
C(55)	5113(3)	5311(3)	8466(3)	44(2)
C(56)	5706(3)	5041(2)	8673(3)	32(1)
C(61)	6539(2)	3605(2)	8516(2)	23(1)
C(62)	6458(2)	3950(2)	7790(2)	28(1)
C(63)	6501(3)	3504(3)	7173(3)	35(1)
C(64)	6013(3)	2994(3)	7082(3)	38(1)
C(65)	6062(3)	2652(3)	7802(3)	37(1)
C(66)	6052(2)	3085(2)	8446(3)	30(1)
C(71)	5000	7317(6)	7500	79(3)
C(72)	5362(7)	7575(8)	7069(9)	79(3)
O(01)	6818(2)	5664(2)	10346(2)	31(1)
O(02)	7808(1)	4289(1)	8777(2)	22(1)
O(03)	9367(2)	3066(2)	9511(2)	41(1)
O(70)	5000	6759(5)	7500	185(8)
P(2)	8081(1)	5650(1)	9285(1)	17(1)
P(1)	6582(1)	4138(1)	9303(1)	18(1)
Ir(1)	7395(1)	4858(1)	9413(1)	16(1)
C(81)	4419(6)	7669(5)	5103(9)	47(2)
O(80A)	4416(4)	7060(6)	5178(5)	370(7)
C(82)	5012(5)	7007(5)	5691(8)	47(2)
O(80B)	4416(4)	7060(6)	5178(5)	370(7)

APPENDIX I

Table 1-2. Bond lengths [Å] and angles [°] for [Ir(acac-O)(CO)(PPhCy₂)₂].

Bond	Distance (Å)	Bond Angle	Angle (°)
C(01)-O(01)	1.161(6)	C(15)-C(16)-H(16A)	109.7
C(01)-Ir(1)	1.807(5)	C(11)-C(16)-H(16B)	109.7
C(02)-O(02)	1.296(5)	C(15)-C(16)-H(16B)	109.7
C(02)-C(04)	1.374(7)	H(16A)-C(16)-H(16B)	108.2
C(02)-C(03)	1.515(6)	C(22)-C(21)-C(26)	111.1(4)
C(03)-H(03A)	0.98	C(22)-C(21)-P(2)	115.4(3)
C(03)-H(03B)	0.98	C(26)-C(21)-P(2)	111.6(3)
C(03)-H(03C)	0.98	C(22)-C(21)-H(21)	106
C(04)-C(05)	1.427(6)	C(26)-C(21)-H(21)	106
C(04)-H(04)	0.87(6)	P(2)-C(21)-H(21)	106
C(05)-O(03)	1.248(6)	C(21)-C(22)-C(23)	112.7(4)
C(05)-C(06)	1.509(7)	C(21)-C(22)-H(22A)	109.1
C(06)-H(06A)	0.98	C(23)-C(22)-H(22A)	109.1
C(06)-H(06B)	0.98	C(21)-C(22)-H(22B)	109.1
C(06)-H(06C)	0.98	C(23)-C(22)-H(22B)	109.1
C(11)-C(16)	1.529(6)	H(22A)-C(22)-H(22B)	107.8
C(11)-C(12)	1.530(6)	C(24)-C(23)-C(22)	112.5(4)
C(11)-P(2)	1.839(4)	C(24)-C(23)-H(23A)	109.1
C(11)-H(11)	1	C(22)-C(23)-H(23A)	109.1
C(12)-C(13)	1.527(6)	C(24)-C(23)-H(23B)	109.1
C(12)-H(12A)	0.99	C(22)-C(23)-H(23B)	109.1
C(12)-H(12B)	0.99	H(23A)-C(23)-H(23B)	107.8
C(13)-C(14)	1.526(6)	C(25)-C(24)-C(23)	112.8(4)
C(13)-H(13A)	0.99	C(25)-C(24)-H(24A)	109
C(13)-H(13B)	0.99	C(23)-C(24)-H(24A)	109
C(14)-C(15)	1.524(7)	C(25)-C(24)-H(24B)	109
C(14)-H(14A)	0.99	C(23)-C(24)-H(24B)	109
C(14)-H(14B)	0.99	H(24A)-C(24)-H(24B)	107.8
C(15)-C(16)	1.536(7)	C(24)-C(25)-C(26)	112.3(4)
C(15)-H(15A)	0.99	C(24)-C(25)-H(25A)	109.2
C(15)-H(15B)	0.99	C(26)-C(25)-H(25A)	109.2

APPENDIX I

C(16)-H(16A)	0.99	C(24)-C(25)-H(25B)	109.2
C(16)-H(16B)	0.99	C(26)-C(25)-H(25B)	109.2
C(21)-C(22)	1.514(6)	H(25A)-C(25)-H(25B)	107.9
C(21)-C(26)	1.528(6)	C(25)-C(26)-C(21)	111.4(4)
C(21)-P(2)	1.850(4)	C(25)-C(26)-H(26A)	109.3
C(21)-H(21)	1	C(21)-C(26)-H(26A)	109.3
C(22)-C(23)	1.518(6)	C(25)-C(26)-H(26B)	109.3
C(22)-H(22A)	0.99	C(21)-C(26)-H(26B)	109.3
C(22)-H(22B)	0.99	H(26A)-C(26)-H(26B)	108
C(23)-C(24)	1.503(7)	C(32)-C(31)-C(36)	118.3(4)
C(23)-H(23A)	0.99	C(32)-C(31)-P(2)	123.0(4)
C(23)-H(23B)	0.99	C(36)-C(31)-P(2)	118.4(4)
C(24)-C(25)	1.501(8)	C(33)-C(32)-C(31)	120.5(5)
C(24)-H(24A)	0.99	C(33)-C(32)-H(32)	119.7
C(24)-H(24B)	0.99	C(31)-C(32)-H(32)	119.7
C(25)-C(26)	1.516(6)	C(32)-C(33)-C(34)	118.6(6)
C(25)-H(25A)	0.99	C(32)-C(33)-H(33)	120.7
C(25)-H(25B)	0.99	C(34)-C(33)-H(33)	120.7
C(26)-H(26A)	0.99	C(35)-C(34)-C(33)	121.3(5)
C(26)-H(26B)	0.99	C(35)-C(34)-H(34)	119.4
C(31)-C(32)	1.393(7)	C(33)-C(34)-H(34)	119.4
C(31)-C(36)	1.401(6)	C(34)-C(35)-C(36)	120.3(5)
C(31)-P(2)	1.829(5)	C(34)-C(35)-H(35)	119.9
C(32)-C(33)	1.392(7)	C(36)-C(35)-H(35)	119.9
C(32)-H(32)	0.95	C(35)-C(36)-C(31)	120.9(5)
C(33)-C(34)	1.404(8)	C(35)-C(36)-H(36)	119.6
C(33)-H(33)	0.95	C(31)-C(36)-H(36)	119.6
C(34)-C(35)	1.340(9)	C(42)-C(41)-C(46)	109.3(4)
C(34)-H(34)	0.95	C(42)-C(41)-P(1)	111.9(3)
C(35)-C(36)	1.379(7)	C(46)-C(41)-P(1)	111.3(3)
C(35)-H(35)	0.95	C(42)-C(41)-H(41)	108.1
C(36)-H(36)	0.95	C(46)-C(41)-H(41)	108.1
C(41)-C(42)	1.528(6)	P(1)-C(41)-H(41)	108.1

APPENDIX I

C(41)-C(46)	1.541(6)	C(41)-C(42)-C(43)	110.1(4)
C(41)-P(1)	1.841(4)	C(41)-C(42)-H(42A)	109.6
C(41)-H(41)	1	C(43)-C(42)-H(42A)	109.6
C(42)-C(43)	1.528(7)	C(41)-C(42)-H(42B)	109.6
C(42)-H(42A)	0.99	C(43)-C(42)-H(42B)	109.6
C(42)-H(42B)	0.99	H(42A)-C(42)-H(42B)	108.2
C(43)-C(44)	1.516(6)	C(44)-C(43)-C(42)	112.3(4)
C(43)-H(43A)	0.99	C(44)-C(43)-H(43A)	109.1
C(43)-H(43B)	0.99	C(42)-C(43)-H(43A)	109.1
C(44)-C(45)	1.518(7)	C(44)-C(43)-H(43B)	109.1
C(44)-H(44A)	0.99	C(42)-C(43)-H(43B)	109.1
C(44)-H(44B)	0.99	H(43A)-C(43)-H(43B)	107.9
C(45)-C(46)	1.525(8)	C(43)-C(44)-C(45)	110.8(4)
C(45)-H(45A)	0.99	C(43)-C(44)-H(44A)	109.5
C(45)-H(45B)	0.99	C(45)-C(44)-H(44A)	109.5
C(46)-H(46A)	0.99	C(43)-C(44)-H(44B)	109.5
C(46)-H(46B)	0.99	C(45)-C(44)-H(44B)	109.5
C(51)-C(56)	1.391(8)	H(44A)-C(44)-H(44B)	108.1
C(51)-C(52)	1.397(7)	C(44)-C(45)-C(46)	111.6(4)
C(51)-P(1)	1.830(5)	C(44)-C(45)-H(45A)	109.3
C(52)-C(53)	1.397(7)	C(46)-C(45)-H(45A)	109.3
C(52)-H(52)	0.95	C(44)-C(45)-H(45B)	109.3
C(53)-C(54)	1.371(10)	C(46)-C(45)-H(45B)	109.3
C(53)-H(53)	0.95	H(45A)-C(45)-H(45B)	108
C(54)-C(55)	1.376(10)	C(45)-C(46)-C(41)	110.1(5)
C(54)-H(54)	0.95	C(45)-C(46)-H(46A)	109.6
C(55)-C(56)	1.387(7)	C(41)-C(46)-H(46A)	109.6
C(55)-H(55)	0.95	C(45)-C(46)-H(46B)	109.6
C(56)-H(56)	0.95	C(41)-C(46)-H(46B)	109.6
C(61)-C(62)	1.525(6)	H(46A)-C(46)-H(46B)	108.2
C(61)-C(66)	1.531(7)	C(56)-C(51)-C(52)	118.8(5)
C(61)-P(1)	1.857(5)	C(56)-C(51)-P(1)	118.9(4)
C(61)-H(61)	1	C(52)-C(51)-P(1)	122.1(4)

APPENDIX I

C(62)-C(63)	1.527(7)	C(53)-C(52)-C(51)	119.7(6)
C(62)-H(62A)	0.99	C(53)-C(52)-H(52)	120.2
C(62)-H(62B)	0.99	C(51)-C(52)-H(52)	120.2
C(63)-C(64)	1.514(8)	C(54)-C(53)-C(52)	120.4(6)
C(63)-H(63A)	0.99	C(54)-C(53)-H(53)	119.8
C(63)-H(63B)	0.99	C(52)-C(53)-H(53)	119.8
C(64)-C(65)	1.521(8)	C(53)-C(54)-C(55)	120.2(5)
C(64)-H(64A)	0.99	C(53)-C(54)-H(54)	119.9
C(64)-H(64B)	0.99	C(55)-C(54)-H(54)	119.9
C(65)-C(66)	1.532(7)	C(54)-C(55)-C(56)	120.0(6)
C(65)-H(65A)	0.99	C(54)-C(55)-H(55)	120
C(65)-H(65B)	0.99	C(56)-C(55)-H(55)	120
C(66)-H(66A)	0.99	C(55)-C(56)-C(51)	120.7(6)
C(66)-H(66B)	0.99	C(55)-C(56)-H(56)	119.7
C(71)-O(70)	1.208(13)	C(51)-C(56)-H(56)	119.7
C(71)-C(72)#1	1.383(14)	C(62)-C(61)-C(66)	111.1(4)
C(71)-C(72)	1.383(14)	C(62)-C(61)-P(1)	112.1(3)
C(72)-H(72A)	0.98	C(66)-C(61)-P(1)	114.9(3)
C(72)-H(72B)	0.98	C(62)-C(61)-H(61)	106
C(72)-H(72C)	0.98	C(66)-C(61)-H(61)	106
O(02)-Ir(1)	2.071(3)	P(1)-C(61)-H(61)	106
P(2)-Ir(1)	2.3291(11)	C(61)-C(62)-C(63)	110.6(4)
P(1)-Ir(1)	2.3327(11)	C(61)-C(62)-H(62A)	109.5
C(81)-O(80A)	1.326(13)	C(63)-C(62)-H(62A)	109.5
C(81)-H(81A)	0.98	C(61)-C(62)-H(62B)	109.5
C(81)-H(81B)	0.98	C(63)-C(62)-H(62B)	109.5
C(81)-H(81C)	0.98	H(62A)-C(62)-H(62B)	108.1
C(82)-H(82A)	0.98	C(64)-C(63)-C(62)	111.7(4)
C(82)-H(82B)	0.98	C(64)-C(63)-H(63A)	109.3
C(82)-H(82C)	0.98	C(62)-C(63)-H(63A)	109.3
O(01)-C(01)-Ir(1)	178.4(4)	C(64)-C(63)-H(63B)	109.3
O(02)-C(02)-C(04)	123.6(4)	C(62)-C(63)-H(63B)	109.3
O(02)-C(02)-C(03)	113.3(4)	H(63A)-C(63)-H(63B)	107.9

APPENDIX I

C(04)-C(02)-C(03)	123.0(4)	C(63)-C(64)-C(65)	111.3(4)
C(02)-C(03)-H(03A)	109.5	C(63)-C(64)-H(64A)	109.4
C(02)-C(03)-H(03B)	109.5	C(65)-C(64)-H(64A)	109.4
H(03A)-C(03)-H(03B)	109.5	C(63)-C(64)-H(64B)	109.4
C(02)-C(03)-H(03C)	109.5	C(65)-C(64)-H(64B)	109.4
H(03A)-C(03)-H(03C)	109.5	H(64A)-C(64)-H(64B)	108
H(03B)-C(03)-H(03C)	109.5	C(64)-C(65)-C(66)	113.0(5)
C(02)-C(04)-C(05)	127.2(4)	C(64)-C(65)-H(65A)	109
C(02)-C(04)-H(04)	119(4)	C(66)-C(65)-H(65A)	109
C(05)-C(04)-H(04)	113(4)	C(64)-C(65)-H(65B)	109
O(03)-C(05)-C(04)	124.6(5)	C(66)-C(65)-H(65B)	109
O(03)-C(05)-C(06)	119.1(4)	H(65A)-C(65)-H(65B)	107.8
C(04)-C(05)-C(06)	116.2(4)	C(61)-C(66)-C(65)	111.7(4)
C(05)-C(06)-H(06A)	109.5	C(61)-C(66)-H(66A)	109.3
C(05)-C(06)-H(06B)	109.5	C(65)-C(66)-H(66A)	109.3
H(06A)-C(06)-H(06B)	109.5	C(61)-C(66)-H(66B)	109.3
C(05)-C(06)-H(06C)	109.5	C(65)-C(66)-H(66B)	109.3
H(06A)-C(06)-H(06C)	109.5	H(66A)-C(66)-H(66B)	107.9
H(06B)-C(06)-H(06C)	109.5	O(70)-C(71)-C(72)#1	113.8(10)
C(16)-C(11)-C(12)	109.4(4)	O(70)-C(71)-C(72)	113.8(10)
C(16)-C(11)-P(2)	111.7(3)	C(72)#1-C(71)-C(72)	132.4(19)
C(12)-C(11)-P(2)	112.3(3)	C(71)-C(72)-H(72A)	109.5
C(16)-C(11)-H(11)	107.7	C(71)-C(72)-H(72B)	109.5
C(12)-C(11)-H(11)	107.7	H(72A)-C(72)-H(72B)	109.5
P(2)-C(11)-H(11)	107.7	C(71)-C(72)-H(72C)	109.5
C(13)-C(12)-C(11)	110.1(4)	H(72A)-C(72)-H(72C)	109.5
C(13)-C(12)-H(12A)	109.6	H(72B)-C(72)-H(72C)	109.5
C(11)-C(12)-H(12A)	109.6	C(02)-O(02)-Ir(1)	131.1(3)
C(13)-C(12)-H(12B)	109.6	C(31)-P(2)-C(11)	104.2(2)
C(11)-C(12)-H(12B)	109.6	C(31)-P(2)-C(21)	103.3(2)
H(12A)-C(12)-H(12B)	108.2	C(11)-P(2)-C(21)	105.17(19)
C(14)-C(13)-C(12)	111.9(4)	C(31)-P(2)-Ir(1)	111.77(15)
C(14)-C(13)-H(13A)	109.2	C(11)-P(2)-Ir(1)	119.12(14)

APPENDIX I

C(12)-C(13)-H(13A)	109.2	C(21)-P(2)-Ir(1)	111.86(15)
C(14)-C(13)-H(13B)	109.2	C(51)-P(1)-C(41)	104.4(2)
C(12)-C(13)-H(13B)	109.2	C(51)-P(1)-C(61)	103.6(2)
H(13A)-C(13)-H(13B)	107.9	C(41)-P(1)-C(61)	105.9(2)
C(15)-C(14)-C(13)	112.0(4)	C(51)-P(1)-Ir(1)	112.35(17)
C(15)-C(14)-H(14A)	109.2	C(41)-P(1)-Ir(1)	117.53(15)
C(13)-C(14)-H(14A)	109.2	C(61)-P(1)-Ir(1)	111.83(15)
C(15)-C(14)-H(14B)	109.2	C(01)-Ir(1)-O(02)	179.71(18)
C(13)-C(14)-H(14B)	109.2	C(01)-Ir(1)-P(2)	90.50(15)
H(14A)-C(14)-H(14B)	107.9	O(02)-Ir(1)-P(2)	89.62(9)
C(14)-C(15)-C(16)	111.8(4)	C(01)-Ir(1)-P(1)	90.86(15)
C(14)-C(15)-H(15A)	109.3	O(02)-Ir(1)-P(1)	89.08(9)
C(16)-C(15)-H(15A)	109.3	P(2)-Ir(1)-P(1)	167.94(4)
C(14)-C(15)-H(15B)	109.3	H(82A)-C(82)-H(82B)	109.5
C(16)-C(15)-H(15B)	109.3	H(82A)-C(82)-H(82C)	109.5
H(15A)-C(15)-H(15B)	107.9	H(82B)-C(82)-H(82C)	109.5
C(11)-C(16)-C(15)	109.7(4)		
C(11)-C(16)-H(16A)	109.7		

Symmetry transformations used to generate equivalent atoms:
 #1 -x+1,y,-z+3/2

Table 1-3. Anisotropic displacement parameters ($\text{\AA}^2 \times 10^3$) for $[\text{Ir}(\text{acac-}O)(\text{CO})(\text{PPhCy}_2)_2]$. The anisotropic displacement factor exponent takes the form: $-2\pi^2 [h^2 a^{*2} U^{11} + \dots + 2 h k a^* b^* U^{12}]$.

	U11	U22	U33	U23	U13	U12
C(01)	20(2)	21(2)	25(2)	0(2)	7(2)	0(2)
C(02)	23(2)	15(2)	32(2)	0(2)	14(2)	-1(2)
C(03)	30(2)	25(2)	34(3)	-2(2)	17(2)	6(2)
C(04)	23(2)	15(2)	31(2)	-2(2)	13(2)	1(2)
C(05)	21(2)	17(2)	45(3)	0(2)	10(2)	-4(2)
C(06)	30(3)	35(3)	45(3)	9(3)	3(2)	3(2)
C(11)	22(2)	14(2)	19(2)	0(2)	8(2)	1(2)
C(12)	24(2)	26(2)	20(2)	-3(2)	5(2)	9(2)
C(13)	20(2)	45(3)	19(2)	0(2)	2(2)	6(2)
C(14)	27(2)	35(3)	17(2)	-2(2)	3(2)	-3(2)

APPENDIX I

C(15)	46(3)	32(3)	22(2)	-7(2)	7(2)	6(2)
C(16)	32(2)	32(3)	22(2)	-2(2)	8(2)	10(2)
C(21)	21(2)	24(2)	18(2)	3(2)	7(2)	1(2)
C(22)	26(2)	27(2)	27(2)	-1(2)	13(2)	-1(2)
C(23)	33(2)	32(3)	31(3)	7(2)	20(2)	7(2)
C(24)	41(3)	36(3)	27(2)	1(2)	21(2)	8(2)
C(25)	37(3)	36(3)	15(2)	4(2)	4(2)	5(2)
C(26)	26(2)	23(2)	18(2)	4(2)	8(2)	5(2)
C(31)	25(2)	21(2)	29(2)	9(2)	12(2)	7(2)
C(32)	41(3)	26(2)	27(2)	3(2)	9(2)	8(2)
C(33)	62(4)	28(3)	41(3)	6(2)	22(3)	15(3)
C(34)	60(4)	35(3)	29(3)	2(2)	8(3)	30(3)
C(35)	31(3)	49(4)	38(3)	12(3)	6(2)	21(3)
C(36)	26(2)	32(3)	26(2)	2(2)	5(2)	11(2)
C(41)	20(2)	24(2)	18(2)	1(2)	7(2)	-2(2)
C(42)	37(3)	24(2)	21(2)	0(2)	13(2)	9(2)
C(43)	50(3)	16(2)	23(2)	1(2)	7(2)	3(2)
C(44)	37(3)	28(2)	19(2)	-3(2)	8(2)	0(2)
C(45)	46(3)	57(4)	28(3)	7(3)	21(2)	19(3)
C(46)	50(3)	37(3)	24(2)	1(2)	16(2)	20(3)
C(51)	22(2)	32(3)	24(2)	-2(2)	3(2)	6(2)
C(52)	25(2)	56(4)	34(3)	3(3)	9(2)	3(2)
C(53)	24(2)	80(5)	39(3)	-6(3)	11(2)	9(3)
C(54)	33(3)	71(4)	33(3)	-19(3)	2(2)	26(3)
C(55)	42(3)	43(3)	41(3)	-2(3)	-2(3)	21(3)
C(56)	28(3)	28(2)	36(3)	-3(2)	0(2)	9(2)
C(61)	26(2)	23(2)	20(2)	-2(2)	5(2)	1(2)
C(62)	32(2)	30(3)	20(2)	2(2)	5(2)	3(2)
C(63)	38(3)	45(3)	20(2)	-2(2)	6(2)	1(2)
C(64)	40(3)	44(3)	28(3)	-8(2)	5(2)	8(3)
C(65)	44(3)	35(3)	31(3)	-8(2)	4(2)	-6(2)
C(66)	35(3)	31(3)	25(2)	-4(2)	7(2)	-8(2)
C(71)	53(6)	80(7)	87(8)	0	-13(5)	0

APPENDIX I

C(72)	53(6)	80(7)	87(8)	0	-13(5)	0
O(01)	32(2)	31(2)	38(2)	-9(2)	21(2)	2(2)
O(02)	23(2)	21(2)	24(2)	2(1)	9(1)	6(1)
O(03)	36(2)	33(2)	55(2)	-3(2)	10(2)	15(2)
O(70)	68(6)	56(6)	380(20)	0	-39(9)	0
P(2)	17(1)	17(1)	17(1)	3(1)	6(1)	3(1)
P(1)	18(1)	18(1)	19(1)	0(1)	6(1)	2(1)
Ir(1)	16(1)	16(1)	17(1)	2(1)	6(1)	3(1)
C(81)	25(4)	20(3)	89(7)	13(4)	1(4)	-1(3)
O(80A)	180(7)	570(20)	317(11)	-110(13)	-12(7)	60(11)
C(82)	25(4)	20(3)	89(7)	13(4)	1(4)	-1(3)
O(80B)	180(7)	570(20)	317(11)	-110(13)	-12(7)	60(11)

Table 1-4. Hydrogen coordinates ($\times 10^4$) and isotropic displacement parameters ($\text{\AA}^2 \times 10^3$) for [Ir(acac-O)(CO)(PPhCy₂)₂].

	x	y	z	U(eq)
H(03A)	8172	3772	7848	42
H(03B)	8423	3170	8329	42
H(03C)	8894	3733	8309	42
H(06A)	9778	3090	10851	56
H(06B)	9101	3237	10996	56
H(06C)	9563	3791	10912	56
H(11)	8973	6205	9921	21
H(12A)	9032	4946	10420	28
H(12B)	9367	5190	9804	28
H(13A)	10101	5161	10984	34
H(13B)	10026	5850	10663	34
H(14A)	9468	5380	11782	32
H(14B)	9995	5909	11892	32
H(15A)	9277	6610	11203	40
H(15B)	8960	6321	11811	40
H(16A)	8332	5651	10923	34
H(16B)	8217	6349	10631	34

APPENDIX I

H(21)	8666	5113	8602	25
H(22A)	9261	6007	8858	31
H(22B)	8713	6399	8324	31
H(23A)	9463	6191	7679	36
H(23B)	9469	5471	7878	36
H(24A)	8481	6116	6882	39
H(24B)	8903	5573	6676	39
H(25A)	8418	4845	7243	36
H(25B)	7876	5231	6690	36
H(26A)	7639	5081	7849	27
H(26B)	7672	5800	7660	27
H(32)	8401	6975	9446	37
H(33)	7828	7892	9103	50
H(34)	6768	7829	8418	51
H(35)	6275	6897	8169	48
H(36)	6830	5987	8518	34
H(41)	6213	3369	9977	24
H(42A)	7564	3492	10428	32
H(42B)	7200	2976	9866	32
H(43A)	6794	2527	10797	36
H(43B)	7548	2560	11077	36
H(44A)	7487	3419	11810	34
H(44B)	7048	2885	12007	34
H(45A)	6522	3861	11858	50
H(45B)	6139	3359	11290	50
H(46A)	6938	4300	10924	43
H(46B)	6181	4297	10660	43
H(52)	5337	3850	9547	46
H(53)	4350	4345	9240	57
H(54)	4195	5201	8472	56
H(55)	5057	5689	8200	53
H(56)	6051	5225	8528	39
H(61)	6960	3397	8611	28

APPENDIX I

H(62A)	6790	4270	7843	33
H(62B)	6042	4159	7663	33
H(63A)	6437	3736	6705	42
H(63B)	6929	3319	7284	42
H(64A)	6075	2699	6703	46
H(64B)	5585	3174	6910	46
H(65A)	6460	2411	7924	45
H(65B)	5706	2357	7737	45
H(66A)	5625	3267	8371	36
H(66B)	6142	2844	8909	36
H(72A)	5562	7246	6848	119
H(72B)	5690	7838	7375	119
H(72C)	5092	7825	6679	119
H(81A)	4092	7851	5311	70
H(81B)	4335	7775	4579	70
H(81C)	4833	7832	5363	70
H(82A)	5251	6668	5544	70
H(82B)	4950	6922	6182	70
H(82C)	5247	7394	5703	70
H(04)	8510(20)	4010(30)	10030(30)	28(14)

Table 1-5. Torsion angles [°] for [Ir(acac-O)(CO)(PPhCy₂)₂].

O(02)-C(02)-C(04)-C(05)	-178.9(4)
C(03)-C(02)-C(04)-C(05)	0.3(7)
C(02)-C(04)-C(05)-O(03)	-3.2(8)
C(02)-C(04)-C(05)-C(06)	175.5(5)
C(16)-C(11)-C(12)-C(13)	-60.5(5)
P(2)-C(11)-C(12)-C(13)	174.9(3)
C(11)-C(12)-C(13)-C(14)	56.2(6)
C(12)-C(13)-C(14)-C(15)	-52.1(6)
C(13)-C(14)-C(15)-C(16)	52.2(6)
C(12)-C(11)-C(16)-C(15)	60.5(5)
P(2)-C(11)-C(16)-C(15)	-174.5(3)

APPENDIX I

C(14)-C(15)-C(16)-C(11)	-56.5(6)
C(26)-C(21)-C(22)-C(23)	-52.9(5)
P(2)-C(21)-C(22)-C(23)	178.8(3)
C(21)-C(22)-C(23)-C(24)	51.4(6)
C(22)-C(23)-C(24)-C(25)	-51.0(6)
C(23)-C(24)-C(25)-C(26)	52.8(6)
C(24)-C(25)-C(26)-C(21)	-54.3(5)
C(22)-C(21)-C(26)-C(25)	54.2(5)
P(2)-C(21)-C(26)-C(25)	-175.5(3)
C(36)-C(31)-C(32)-C(33)	4.0(7)
P(2)-C(31)-C(32)-C(33)	177.4(4)
C(31)-C(32)-C(33)-C(34)	-3.3(8)
C(32)-C(33)-C(34)-C(35)	2.2(9)
C(33)-C(34)-C(35)-C(36)	-1.7(9)
C(34)-C(35)-C(36)-C(31)	2.4(8)
C(32)-C(31)-C(36)-C(35)	-3.5(7)
P(2)-C(31)-C(36)-C(35)	-177.2(4)
C(46)-C(41)-C(42)-C(43)	58.4(5)
P(1)-C(41)-C(42)-C(43)	-177.9(3)
C(41)-C(42)-C(43)-C(44)	-56.8(6)
C(42)-C(43)-C(44)-C(45)	54.3(6)
C(43)-C(44)-C(45)-C(46)	-54.7(7)
C(44)-C(45)-C(46)-C(41)	57.7(6)
C(42)-C(41)-C(46)-C(45)	-59.2(6)
P(1)-C(41)-C(46)-C(45)	176.8(4)
C(56)-C(51)-C(52)-C(53)	-2.9(8)
P(1)-C(51)-C(52)-C(53)	-177.2(4)
C(51)-C(52)-C(53)-C(54)	5.0(9)
C(52)-C(53)-C(54)-C(55)	-6.0(10)
C(53)-C(54)-C(55)-C(56)	4.9(9)
C(54)-C(55)-C(56)-C(51)	-2.9(9)
C(52)-C(51)-C(56)-C(55)	1.9(8)
P(1)-C(51)-C(56)-C(55)	176.4(4)

APPENDIX I

C(66)-C(61)-C(62)-C(63)	-56.5(5)
P(1)-C(61)-C(62)-C(63)	173.4(3)
C(61)-C(62)-C(63)-C(64)	57.7(6)
C(62)-C(63)-C(64)-C(65)	-55.0(6)
C(63)-C(64)-C(65)-C(66)	52.1(6)
C(62)-C(61)-C(66)-C(65)	53.4(6)
P(1)-C(61)-C(66)-C(65)	-177.9(4)
C(64)-C(65)-C(66)-C(61)	-51.5(6)
C(04)-C(02)-O(02)-Ir(1)	3.8(6)
C(03)-C(02)-O(02)-Ir(1)	-175.4(3)
C(32)-C(31)-P(2)-C(11)	26.5(5)
C(36)-C(31)-P(2)-C(11)	-160.1(4)
C(32)-C(31)-P(2)-C(21)	-83.2(4)
C(36)-C(31)-P(2)-C(21)	90.2(4)
C(32)-C(31)-P(2)-Ir(1)	156.4(4)
C(36)-C(31)-P(2)-Ir(1)	-30.2(4)
C(16)-C(11)-P(2)-C(31)	67.4(4)
C(12)-C(11)-P(2)-C(31)	-169.2(3)
C(16)-C(11)-P(2)-C(21)	175.7(3)
C(12)-C(11)-P(2)-C(21)	-60.9(4)
C(16)-C(11)-P(2)-Ir(1)	-58.0(3)
C(12)-C(11)-P(2)-Ir(1)	65.4(3)
C(22)-C(21)-P(2)-C(31)	63.1(4)
C(26)-C(21)-P(2)-C(31)	-65.0(4)
C(22)-C(21)-P(2)-C(11)	-45.8(4)
C(26)-C(21)-P(2)-C(11)	-173.9(3)
C(22)-C(21)-P(2)-Ir(1)	-176.5(3)
C(26)-C(21)-P(2)-Ir(1)	55.4(3)
C(56)-C(51)-P(1)-C(41)	160.1(4)
C(52)-C(51)-P(1)-C(41)	-25.6(5)
C(56)-C(51)-P(1)-C(61)	-89.2(4)
C(52)-C(51)-P(1)-C(61)	85.1(5)
C(56)-C(51)-P(1)-Ir(1)	31.7(5)

APPENDIX I

C(52)-C(51)-P(1)-Ir(1)	-154.0(4)
C(42)-C(41)-P(1)-C(51)	172.3(3)
C(46)-C(41)-P(1)-C(51)	-65.2(4)
C(42)-C(41)-P(1)-C(61)	63.3(4)
C(46)-C(41)-P(1)-C(61)	-174.2(3)
C(42)-C(41)-P(1)-Ir(1)	-62.5(4)
C(46)-C(41)-P(1)-Ir(1)	60.1(4)
C(62)-C(61)-P(1)-C(51)	64.5(4)
C(66)-C(61)-P(1)-C(51)	-63.6(4)
C(62)-C(61)-P(1)-C(41)	174.1(3)
C(66)-C(61)-P(1)-C(41)	46.0(4)
C(62)-C(61)-P(1)-Ir(1)	-56.7(3)
C(66)-C(61)-P(1)-Ir(1)	175.2(3)
O(01)-C(01)-Ir(1)-O(02)	25(47)
O(01)-C(01)-Ir(1)-P(2)	-88(16)
O(01)-C(01)-Ir(1)-P(1)	104(16)
C(02)-O(02)-Ir(1)-C(01)	-23(37)
C(02)-O(02)-Ir(1)-P(2)	90.3(4)
C(02)-O(02)-Ir(1)-P(1)	-101.7(4)
C(31)-P(2)-Ir(1)-C(01)	-46.4(2)
C(11)-P(2)-Ir(1)-C(01)	75.3(2)
C(21)-P(2)-Ir(1)-C(01)	-161.6(2)
C(31)-P(2)-Ir(1)-O(02)	133.92(19)
C(11)-P(2)-Ir(1)-O(02)	-104.44(18)
C(21)-P(2)-Ir(1)-O(02)	18.66(17)
C(31)-P(2)-Ir(1)-P(1)	50.1(3)
C(11)-P(2)-Ir(1)-P(1)	171.8(2)
C(21)-P(2)-Ir(1)-P(1)	-65.1(2)
C(51)-P(1)-Ir(1)-C(01)	45.3(2)
C(41)-P(1)-Ir(1)-C(01)	-75.9(2)
C(61)-P(1)-Ir(1)-C(01)	161.4(2)
C(51)-P(1)-Ir(1)-O(02)	-134.96(19)
C(41)-P(1)-Ir(1)-O(02)	103.83(18)

APPENDIX I

C(61)-P(1)-Ir(1)-O(02)	-18.93(18)
C(51)-P(1)-Ir(1)-P(2)	-51.1(3)
C(41)-P(1)-Ir(1)-P(2)	-172.3(2)
C(61)-P(1)-Ir(1)-P(2)	64.9(2)

Symmetry transformations used to generate equivalent atoms:
#1 -x+1,y,-z+3/2

Table 1-6. Hydrogen bonds for [Ir(acac-O)(CO)(PPhCy₂)₂] [Å and °].

D-H...A	d(D-H)	d(H...A)	d(D...A)	<(DHA)
C(26)-H(26A)...O(02)	0.99	2.4	3.124(6)	129
C(62)-H(62A)...O(02)	0.99	2.46	3.154(6)	126.3
C(81)-H(81C)...O(03)#2	0.98	1.78	2.709(12)	157.5
C(82)-H(82B)...O(70)	0.98	2.47	3.442(14)	169.5
C(82)-H(82C)...O(03)#2	0.98	1.78	2.738(11)	165.9

Symmetry transformations used to generate equivalent atoms:
#1 -x+1,y,-z+3/2 #2 -x+3/2,y+1/2,-z+3/2

2 Crystal Data for [Ir(acac)(CO)(PCy₃)₂]

Table 2-1. Atomic coordinates ($\times 10^4$) and equivalent isotropic displacement parameters ($\text{\AA}^2 \times 10^3$) for [Ir(acac)(CO)(PCy₃)₂]. U(eq) is defined as one third of the trace of the orthogonalized U^{ij} tensor.

	x	y	z	U(eq)
C(02)	248(7)	-886(15)	2041(8)	41(4)
C(03)	219(8)	-2430(20)	2121(10)	51(2)
C(04)	475(7)	-362(17)	1605(9)	42(4)
C(05)	549(7)	1008(15)	1462(7)	32(3)
C(06)	802(9)	1390(20)	918(10)	49(4)
C(01)	0	3700(12)	2500	51(2)
C(11A)	1490(4)	790(8)	3846(5)	41(1)
C(12A)	1249(9)	20(20)	4274(11)	41(1)
C(13A)	1562(4)	-1273(8)	4590(5)	41(1)
C(14A)	1757(5)	-2100(8)	4093(5)	41(1)
C(15A)	2081(4)	-1290(8)	3765(5)	41(1)
C(16A)	1760(9)	-26(19)	3459(10)	41(1)
C(11B)	1490(4)	790(8)	3846(5)	41(1)

APPENDIX I

C(12B)	1078(9)	-147(19)	4137(11)	41(1)
C(13B)	1562(4)	-1273(8)	4590(5)	41(1)
C(14B)	1757(5)	-2100(8)	4093(5)	41(1)
C(15B)	2081(4)	-1290(8)	3765(5)	41(1)
C(16B)	1601(9)	-90(20)	3282(10)	41(1)
C(31A)	946(4)	3194(8)	4136(4)	38(1)
C(32A)	679(4)	4600(9)	3951(4)	38(1)
C(33A)	521(10)	5291(19)	4471(9)	38(1)
C(34A)	1063(3)	5180(6)	5241(3)	38(1)
C(35A)	1488(8)	3983(17)	5479(8)	38(1)
C(36A)	1530(4)	3245(8)	4850(4)	38(1)
C(31B)	946(4)	3194(8)	4136(4)	38(1)
C(32B)	679(4)	4600(9)	3951(4)	38(1)
C(33B)	482(10)	5030(20)	4574(9)	38(1)
C(34B)	1063(3)	5180(6)	5241(3)	38(1)
C(35B)	1282(8)	3724(18)	5412(9)	38(1)
C(36B)	1530(4)	3245(8)	4850(4)	38(1)
C(21)	1536(5)	3164(9)	3078(6)	47(1)
C(22)	2205(4)	3419(10)	3649(5)	47(1)
C(23)	2639(4)	3941(10)	3320(5)	47(1)
C(24)	2379(4)	5214(10)	2890(5)	47(1)
C(25)	1715(4)	4977(10)	2346(5)	47(1)
C(26)	1276(4)	4457(10)	2672(5)	47(1)
O(02)	0	-189(9)	2500	51(2)
O(03)	384(6)	1906(12)	1753(8)	51(2)
O(01)	0	4810(20)	2500	2000(500)
P(1)	1006(1)	2262(2)	3397(1)	21(1)
Ir(1)	0	1941(1)	2500	25(1)

Table 2-2. Bond lengths [Å] and angles [°] for [Ir(acac)(CO)(PCy₃)₂].

Bond	Distance (Å)	Bond Angle	Angle (°)
C(02)-C(04)	1.33(3)	C(15A)-C(14A)-C(13A)	112.0(7)
C(02)-O(02)	1.48(2)	C(15A)-C(14A)-H(14A)	109.2

APPENDIX I

C(02)-C(03)	1.55(3)	C(13A)-C(14A)-H(14A)	109.2
C(03)-H(03A)	0.98	C(15A)-C(14A)-H(14B)	109.2
C(03)-H(03B)	0.98	C(13A)-C(14A)-H(14B)	109.2
C(03)-H(03C)	0.98	H(14A)-C(14A)-H(14B)	107.9
C(04)-C(05)	1.43(2)	C(14A)-C(15A)-C(16A)	114.1(11)
C(04)-H(04)	0.95	C(14A)-C(15A)-H(15A)	108.7
C(05)-O(03)	1.229(18)	C(16A)-C(15A)-H(15A)	108.7
C(05)-C(06)	1.52(2)	C(14A)-C(15A)-H(15B)	108.7
C(06)-H(06A)	0.98	C(16A)-C(15A)-H(15B)	108.7
C(06)-H(06B)	0.98	H(15A)-C(15A)-H(15B)	107.6
C(06)-H(06C)	0.98	C(11A)-C(16A)-C(15A)	120.0(15)
C(01)-O(01)	1.10(2)	C(11A)-C(16A)-H(16A)	107.3
C(01)-Ir(1)	1.755(12)	C(15A)-C(16A)-H(16A)	107.3
C(11A)-C(12A)	1.45(2)	C(11A)-C(16A)-H(16B)	107.3
C(11A)-C(16A)	1.46(2)	C(15A)-C(16A)-H(16B)	107.3
C(11A)-P(1)	1.852(8)	H(16A)-C(16A)-H(16B)	106.9
C(11A)-H(11A)	1	H(12C)-C(12B)-H(12D)	109
C(12A)-C(13A)	1.49(2)	H(16C)-C(16B)-H(16D)	109.1
C(12A)-H(12A)	0.99	C(32A)-C(31A)-C(36A)	108.6(6)
C(12A)-H(12B)	0.99	C(32A)-C(31A)-P(1)	114.7(6)
C(13A)-C(14A)	1.530(12)	C(36A)-C(31A)-P(1)	118.4(6)
C(13A)-H(13A)	0.99	C(32A)-C(31A)-H(31A)	104.5
C(13A)-H(13B)	0.99	C(36A)-C(31A)-H(31A)	104.5
C(14A)-C(15A)	1.456(12)	P(1)-C(31A)-H(31A)	104.5
C(14A)-H(14A)	0.99	C(33A)-C(32A)-C(31A)	117.0(9)
C(14A)-H(14B)	0.99	C(33A)-C(32A)-H(32A)	108
C(15A)-C(16A)	1.47(2)	C(31A)-C(32A)-H(32A)	108
C(15A)-H(15A)	0.99	C(33A)-C(32A)-H(32B)	108
C(15A)-H(15B)	0.99	C(31A)-C(32A)-H(32B)	108
C(16A)-H(16A)	0.99	H(32A)-C(32A)-H(32B)	107.3
C(16A)-H(16B)	0.99	C(32A)-C(33A)-C(34A)	112.2(14)
C(12B)-H(12C)	0.99	C(32A)-C(33A)-H(33A)	109.2
C(12B)-H(12D)	0.99	C(34A)-C(33A)-H(33A)	109.2

APPENDIX I

C(16B)-H(16C)	0.99	C(32A)-C(33A)-H(33B)	109.2
C(16B)-H(16D)	0.99	C(34A)-C(33A)-H(33B)	109.2
C(31A)-C(32A)	1.518(11)	H(33A)-C(33A)-H(33B)	107.9
C(31A)-C(36A)	1.541(11)	C(35A)-C(34A)-C(33A)	122.0(10)
C(31A)-P(1)	1.851(8)	C(35A)-C(34A)-H(34A)	106.8
C(31A)-H(31A)	1	C(33A)-C(34A)-H(34A)	106.8
C(32A)-C(33A)	1.45(2)	C(35A)-C(34A)-H(34B)	106.8
C(32A)-H(32A)	0.99	C(33A)-C(34A)-H(34B)	106.8
C(32A)-H(32B)	0.99	H(34A)-C(34A)-H(34B)	106.7
C(33A)-C(34A)	1.577(18)	C(34A)-C(35A)-C(36A)	111.7(11)
C(33A)-H(33A)	0.99	C(34A)-C(35A)-H(35A)	109.3
C(33A)-H(33B)	0.99	C(36A)-C(35A)-H(35A)	109.3
C(34A)-C(35A)	1.498(18)	C(34A)-C(35A)-H(35B)	109.3
C(34A)-H(34A)	0.99	C(36A)-C(35A)-H(35B)	109.3
C(34A)-H(34B)	0.99	H(35A)-C(35A)-H(35B)	107.9
C(35A)-C(36A)	1.538(18)	C(35A)-C(36A)-C(31A)	119.4(9)
C(35A)-H(35A)	0.99	C(35A)-C(36A)-H(36A)	107.5
C(35A)-H(35B)	0.99	C(31A)-C(36A)-H(36A)	107.5
C(36A)-H(36A)	0.99	C(35A)-C(36A)-H(36B)	107.5
C(36A)-H(36B)	0.99	C(31A)-C(36A)-H(36B)	107.5
C(33B)-H(33C)	0.99	H(36A)-C(36A)-H(36B)	107
C(33B)-H(33D)	0.99	H(33C)-C(33B)-H(33D)	108.3
C(35B)-H(35C)	0.99	H(35C)-C(35B)-H(35D)	108.5
C(35B)-H(35D)	0.99	C(26)-C(21)-C(22)	109.3(7)
C(21)-C(26)	1.522(13)	C(26)-C(21)-P(1)	115.9(7)
C(21)-C(22)	1.538(14)	C(22)-C(21)-P(1)	114.6(7)
C(21)-P(1)	1.859(9)	C(26)-C(21)-H(21)	105.3
C(21)-H(21)	1	C(22)-C(21)-H(21)	105.3
C(22)-C(23)	1.528(12)	P(1)-C(21)-H(21)	105.3
C(22)-H(22A)	0.99	C(23)-C(22)-C(21)	111.1(8)
C(22)-H(22B)	0.99	C(23)-C(22)-H(22A)	109.4
C(23)-C(24)	1.526(13)	C(21)-C(22)-H(22A)	109.4
C(23)-H(23A)	0.99	C(23)-C(22)-H(22B)	109.4

APPENDIX I

C(23)-H(23B)	0.99	C(21)-C(22)-H(22B)	109.4
C(24)-C(25)	1.508(13)	H(22A)-C(22)-H(22B)	108
C(24)-H(24A)	0.99	C(24)-C(23)-C(22)	111.8(8)
C(24)-H(24B)	0.99	C(24)-C(23)-H(23A)	109.3
C(25)-C(26)	1.533(11)	C(22)-C(23)-H(23A)	109.3
C(25)-H(25A)	0.99	C(24)-C(23)-H(23B)	109.3
C(25)-H(25B)	0.99	C(22)-C(23)-H(23B)	109.3
C(26)-H(26A)	0.99	H(23A)-C(23)-H(23B)	107.9
C(26)-H(26B)	0.99	C(25)-C(24)-C(23)	110.0(7)
O(02)-C(02)#1	1.48(2)	C(25)-C(24)-H(24A)	109.7
O(02)-Ir(1)	2.126(9)	C(23)-C(24)-H(24A)	109.7
O(03)-Ir(1)	2.090(16)	C(25)-C(24)-H(24B)	109.7
P(1)-Ir(1)	2.3310(16)	C(23)-C(24)-H(24B)	109.7
Ir(1)-O(03)#1	2.090(16)	H(24A)-C(24)-H(24B)	108.2
Ir(1)-P(1)#1	2.3310(16)	C(24)-C(25)-C(26)	112.8(8)
C(04)-C(02)-O(02)	128.8(14)	C(24)-C(25)-H(25A)	109
C(04)-C(02)-C(03)	120.6(16)	C(26)-C(25)-H(25A)	109
O(02)-C(02)-C(03)	110.6(14)	C(24)-C(25)-H(25B)	109
C(02)-C(03)-H(03A)	109.5	C(26)-C(25)-H(25B)	109
C(02)-C(03)-H(03B)	109.5	H(25A)-C(25)-H(25B)	107.8
H(03A)-C(03)-H(03B)	109.5	C(21)-C(26)-C(25)	110.3(8)
C(02)-C(03)-H(03C)	109.5	C(21)-C(26)-H(26A)	109.6
H(03A)-C(03)-H(03C)	109.5	C(25)-C(26)-H(26A)	109.6
H(03B)-C(03)-H(03C)	109.5	C(21)-C(26)-H(26B)	109.6
C(02)-C(04)-C(05)	129.6(16)	C(25)-C(26)-H(26B)	109.6
C(02)-C(04)-H(04)	115.2	H(26A)-C(26)-H(26B)	108.1
C(05)-C(04)-H(04)	115.2	C(02)-O(02)-C(02)#1	123.9(15)
O(03)-C(05)-C(04)	120.4(16)	C(02)-O(02)-Ir(1)	118.1(7)
O(03)-C(05)-C(06)	118.6(16)	C(02)#1-O(02)-Ir(1)	118.1(7)
C(04)-C(05)-C(06)	121.0(15)	C(05)-O(03)-Ir(1)	134.1(13)
C(05)-C(06)-H(06A)	109.5	C(31A)-P(1)-C(11A)	102.7(4)
C(05)-C(06)-H(06B)	109.5	C(31A)-P(1)-C(21)	110.1(4)
H(06A)-C(06)-H(06B)	109.5	C(11A)-P(1)-C(21)	102.0(4)

APPENDIX I

C(05)-C(06)-H(06C)	109.5	C(31A)-P(1)-Ir(1)	109.6(3)
H(06A)-C(06)-H(06C)	109.5	C(11A)-P(1)-Ir(1)	119.6(3)
H(06B)-C(06)-H(06C)	109.5	C(21)-P(1)-Ir(1)	112.2(3)
O(01)-C(01)-Ir(1)	180.000(5)	C(01)-Ir(1)-O(03)	91.0(3)
C(12A)-C(11A)-C(16A)	114.0(13)	C(01)-Ir(1)-O(03)#1	91.0(3)
C(12A)-C(11A)-P(1)	114.7(9)	O(03)-Ir(1)-O(03)#1	178.1(7)
C(16A)-C(11A)-P(1)	118.5(9)	C(01)-Ir(1)-O(02)	180.000(2)
C(12A)-C(11A)-H(11A)	102.1	O(03)-Ir(1)-O(02)	89.0(3)
C(16A)-C(11A)-H(11A)	102.1	O(03)#1-Ir(1)-O(02)	89.0(3)
P(1)-C(11A)-H(11A)	102.1	C(01)-Ir(1)-P(1)	82.11(4)
C(11A)-C(12A)-C(13A)	118.9(15)	O(03)-Ir(1)-P(1)	89.8(4)
C(11A)-C(12A)-H(12A)	107.6	O(03)#1-Ir(1)-P(1)	90.4(4)
C(13A)-C(12A)-H(12A)	107.6	O(02)-Ir(1)-P(1)	97.89(4)
C(11A)-C(12A)-H(12B)	107.6	C(01)-Ir(1)-P(1)#1	82.11(4)
C(13A)-C(12A)-H(12B)	107.6	O(03)-Ir(1)-P(1)#1	90.4(4)
H(12A)-C(12A)-H(12B)	107	O(03)#1-Ir(1)-P(1)#1	89.8(4)
C(12A)-C(13A)-C(14A)	113.4(11)	O(02)-Ir(1)-P(1)#1	97.89(4)
C(12A)-C(13A)-H(13A)	108.9	P(1)-Ir(1)-P(1)#1	164.23(8)
C(14A)-C(13A)-H(13A)	108.9		
C(12A)-C(13A)-H(13B)	108.9		
C(14A)-C(13A)-H(13B)	108.9		
H(13A)-C(13A)-H(13B)	107.7		

Symmetry transformations used to generate equivalent atoms:
 #1 -x,y,-z+1/2

Table 2-3. Anisotropic displacement parameters ($\text{\AA}^2 \times 10^3$) for $[\text{Ir}(\text{acac})(\text{CO})(\text{PCy}_3)_2]$. The anisotropic displacement factor exponent takes the form: $-2\pi^2 [h^2 a^{*2} U^{11} + \dots + 2 h k a^* b^* U^{12}]$.

	U11	U22	U33	U23	U13	U12
C(02)	29(7)	29(7)	37(8)	1(6)	-14(6)	0(6)
C(03)	36(3)	52(4)	44(3)	-17(4)	-2(3)	14(4)
C(04)	29(7)	40(8)	42(8)	-7(7)	0(6)	1(6)
C(05)	28(6)	33(7)	25(6)	-3(5)	2(5)	8(5)
C(06)	47(10)	55(11)	44(9)	9(8)	19(8)	3(8)
C(01)	36(3)	52(4)	44(3)	-17(4)	-2(3)	14(4)

APPENDIX I

C(11A)	45(3)	29(2)	46(3)	8(2)	16(3)	7(2)
C(12A)	45(3)	29(2)	46(3)	8(2)	16(3)	7(2)
C(13A)	45(3)	29(2)	46(3)	8(2)	16(3)	7(2)
C(14A)	45(3)	29(2)	46(3)	8(2)	16(3)	7(2)
C(15A)	45(3)	29(2)	46(3)	8(2)	16(3)	7(2)
C(16A)	45(3)	29(2)	46(3)	8(2)	16(3)	7(2)
C(11B)	45(3)	29(2)	46(3)	8(2)	16(3)	7(2)
C(12B)	45(3)	29(2)	46(3)	8(2)	16(3)	7(2)
C(13B)	45(1)	29(1)	46(1)	8(1)	16(1)	7(1)
C(14B)	45(1)	29(1)	46(1)	8(1)	16(2)	7(1)
C(15B)	45(1)	29(2)	46(1)	8(1)	16(2)	7(1)
C(16B)	45(3)	29(2)	46(3)	8(2)	16(3)	7(2)
C(31A)	38(3)	44(3)	26(2)	-3(2)	6(2)	5(2)
C(32A)	38(3)	44(3)	26(2)	-3(2)	6(2)	5(2)
C(33A)	38(3)	44(3)	26(2)	-3(2)	6(2)	5(2)
C(34A)	38(3)	44(3)	26(2)	-3(2)	6(2)	5(2)
C(35A)	38(3)	44(3)	26(2)	-3(2)	6(2)	5(2)
C(36A)	38(3)	44(3)	26(2)	-3(2)	6(2)	5(2)
C(31B)	38(3)	44(3)	26(2)	-3(2)	6(2)	5(2)
C(32B)	38(1)	44(2)	26(1)	-3(1)	6(1)	5(1)
C(33B)	38(1)	44(1)	26(1)	-3(1)	6(2)	5(1)
C(34B)	38(1)	44(2)	26(1)	-3(1)	6(1)	5(1)
C(35B)	38(3)	44(3)	26(2)	-3(2)	6(2)	5(2)
C(36B)	38(1)	44(2)	26(1)	-3(1)	6(2)	5(1)
C(21)	40(2)	50(2)	51(2)	12(2)	19(2)	-6(2)
C(22)	40(2)	50(2)	51(2)	12(2)	19(2)	-6(2)
C(23)	40(2)	50(2)	51(2)	12(2)	19(2)	-6(2)
C(24)	40(2)	50(2)	51(2)	12(2)	19(2)	-6(2)
C(25)	40(2)	50(2)	51(2)	12(2)	19(2)	-6(2)
C(26)	40(2)	50(2)	51(2)	12(2)	19(2)	-6(2)
O(02)	36(3)	52(4)	44(3)	-17(4)	-2(3)	14(4)
O(03)	36(3)	52(4)	44(3)	-17(4)	-2(3)	14(4)
P(1)	17(1)	24(1)	17(1)	2(1)	2(1)	0(1)

APPENDIX I

Ir(1)	19(1)	26(1)	21(1)	0	-1(1)	0
-------	-------	-------	-------	---	-------	---

Table 2-4. Hydrogen coordinates ($\times 10^4$) and isotropic displacement parameters ($\text{\AA}^2 \times 10^3$) for [Ir(acac)(CO)(PCy₃)₂].

	x	y	z	U(eq)
H(03A)	-221	-2707	1972	76
H(03B)	464	-2678	2616	76
H(03C)	397	-2872	1824	76
H(04)	607	-995	1353	50
H(06A)	472	1257	441	73
H(06B)	1167	830	984	73
H(06C)	930	2336	981	73
H(11A)	1874	1220	4215	49
H(12A)	799	-176	3977	49
H(12B)	1264	602	4666	49
H(13A)	1270	-1811	4721	49
H(13B)	1942	-1080	5029	49
H(14A)	2037	-2837	4364	49
H(14B)	1376	-2504	3720	49
H(15A)	2126	-1824	3387	49
H(15B)	2511	-1084	4125	49
H(16A)	2065	543	3366	49
H(16B)	1415	-240	2994	49
H(11B)	1899	1067	4238	49
H(12C)	921	378	4436	49
H(12D)	714	-549	3740	49
H(13C)	1938	-852	4963	49
H(13D)	1361	-1859	4821	49
H(14C)	2037	-2837	4364	49
H(14D)	1376	-2504	3720	49
H(15C)	2213	-1862	3461	49
H(15D)	2464	-885	4136	49
H(16C)	1801	439	3027	49

APPENDIX I

H(16D)	1199	-471	2934	49
H(31A)	623	2693	4240	46
H(32A)	989	5155	3859	46
H(32B)	293	4552	3504	46
H(33A)	129	4904	4467	46
H(33B)	441	6248	4338	46
H(34A)	1338	5973	5311	46
H(34B)	861	5277	5574	46
H(35A)	1327	3361	5735	46
H(35B)	1915	4275	5810	46
H(36A)	1656	2309	5000	46
H(36B)	1878	3659	4764	46
H(31B)	623	2693	4240	46
H(32C)	307	4606	3489	46
H(32D)	1001	5221	3926	46
H(33C)	248	5889	4453	46
H(33D)	204	4339	4635	46
H(34C)	968	5583	5621	46
H(34D)	1384	5734	5168	46
H(35C)	927	3152	5388	46
H(35D)	1624	3662	5895	46
H(36C)	1846	3882	4827	46
H(36D)	1727	2348	4976	46
H(21)	1592	2545	2730	56
H(22A)	2186	4082	3993	56
H(22B)	2379	2574	3906	56
H(23A)	3061	4128	3700	56
H(23B)	2688	3242	3009	56
H(24A)	2381	5952	3210	56
H(24B)	2650	5480	2651	56
H(25A)	1724	4319	1994	56
H(25B)	1542	5827	2094	56
H(26A)	1236	5141	2996	56

APPENDIX I

H(26B)	851	4291	2293	56
--------	-----	------	------	----

Table 2-5. Torsion angles [°] for [Ir(acac)(CO)(PCy₃)₂].

O(02)-C(02)-C(04)-C(05)	1(3)
C(03)-C(02)-C(04)-C(05)	-179.2(15)
C(02)-C(04)-C(05)-O(03)	-1(3)
C(02)-C(04)-C(05)-C(06)	-177.9(15)
C(16A)-C(11A)-C(12A)-C(13A)	32(2)
P(1)-C(11A)-C(12A)-C(13A)	173.0(11)
C(11A)-C(12A)-C(13A)-C(14A)	-39.8(18)
C(12A)-C(13A)-C(14A)-C(15A)	47.1(13)
C(13A)-C(14A)-C(15A)-C(16A)	-48.2(13)
C(12A)-C(11A)-C(16A)-C(15A)	-33(2)
P(1)-C(11A)-C(16A)-C(15A)	-172.6(10)
C(14A)-C(15A)-C(16A)-C(11A)	42.8(18)
C(36A)-C(31A)-C(32A)-C(33A)	-55.3(13)
P(1)-C(31A)-C(32A)-C(33A)	169.8(10)
C(31A)-C(32A)-C(33A)-C(34A)	46.8(16)
C(32A)-C(33A)-C(34A)-C(35A)	-31.1(19)
C(33A)-C(34A)-C(35A)-C(36A)	24.4(18)
C(34A)-C(35A)-C(36A)-C(31A)	-34.2(16)
C(32A)-C(31A)-C(36A)-C(35A)	48.4(12)
P(1)-C(31A)-C(36A)-C(35A)	-178.5(9)
C(26)-C(21)-C(22)-C(23)	-57.7(11)
P(1)-C(21)-C(22)-C(23)	170.2(7)
C(21)-C(22)-C(23)-C(24)	56.8(11)
C(22)-C(23)-C(24)-C(25)	-54.3(11)
C(23)-C(24)-C(25)-C(26)	54.9(11)
C(22)-C(21)-C(26)-C(25)	57.2(11)
P(1)-C(21)-C(26)-C(25)	-171.4(7)
C(24)-C(25)-C(26)-C(21)	-57.5(11)
C(04)-C(02)-O(02)-C(02)#1	179.3(16)
C(03)-C(02)-O(02)-C(02)#1	-0.9(8)

APPENDIX I

C(04)-C(02)-O(02)-Ir(1)	-0.7(16)
C(03)-C(02)-O(02)-Ir(1)	179.1(8)
C(04)-C(05)-O(03)-Ir(1)	2(2)
C(06)-C(05)-O(03)-Ir(1)	178.7(12)
C(32A)-C(31A)-P(1)-C(11A)	168.7(6)
C(36A)-C(31A)-P(1)-C(11A)	38.3(7)
C(32A)-C(31A)-P(1)-C(21)	60.7(7)
C(36A)-C(31A)-P(1)-C(21)	-69.7(7)
C(32A)-C(31A)-P(1)-Ir(1)	-63.2(7)
C(36A)-C(31A)-P(1)-Ir(1)	166.5(6)
C(12A)-C(11A)-P(1)-C(31A)	54.4(11)
C(16A)-C(11A)-P(1)-C(31A)	-166.1(11)
C(12A)-C(11A)-P(1)-C(21)	168.5(10)
C(16A)-C(11A)-P(1)-C(21)	-52.1(11)
C(12A)-C(11A)-P(1)-Ir(1)	-67.2(11)
C(16A)-C(11A)-P(1)-Ir(1)	72.3(11)
C(26)-C(21)-P(1)-C(31A)	-71.7(8)
C(22)-C(21)-P(1)-C(31A)	57.1(8)
C(26)-C(21)-P(1)-C(11A)	179.8(8)
C(22)-C(21)-P(1)-C(11A)	-51.4(8)
C(26)-C(21)-P(1)-Ir(1)	50.6(8)
C(22)-C(21)-P(1)-Ir(1)	179.4(6)
O(01)-C(01)-Ir(1)-O(03)	-42(100)
O(01)-C(01)-Ir(1)-O(03)#1	138(100)
O(01)-C(01)-Ir(1)-O(02)	0(25)
O(01)-C(01)-Ir(1)-P(1)	47(100)
O(01)-C(01)-Ir(1)-P(1)#1	-133(100)
C(05)-O(03)-Ir(1)-C(01)	178.4(15)
C(05)-O(03)-Ir(1)-O(03)#1	-1.6(15)
C(05)-O(03)-Ir(1)-O(02)	-1.6(15)
C(05)-O(03)-Ir(1)-P(1)	96.3(15)
C(05)-O(03)-Ir(1)-P(1)#1	-99.5(15)
C(02)-O(02)-Ir(1)-C(01)	138(100)

APPENDIX I

C(02)#1-O(02)-Ir(1)-C(01)	-42(100)
C(02)-O(02)-Ir(1)-O(03)	0.8(7)
C(02)#1-O(02)-Ir(1)-O(03)	-179.2(7)
C(02)-O(02)-Ir(1)-O(03)#1	-179.2(7)
C(02)#1-O(02)-Ir(1)-O(03)#1	0.8(7)
C(02)-O(02)-Ir(1)-P(1)	-88.9(6)
C(02)#1-O(02)-Ir(1)-P(1)	91.1(6)
C(02)-O(02)-Ir(1)-P(1)#1	91.1(6)
C(02)#1-O(02)-Ir(1)-P(1)#1	-88.9(6)
C(31A)-P(1)-Ir(1)-C(01)	60.7(3)
C(11A)-P(1)-Ir(1)-C(01)	178.8(3)
C(21)-P(1)-Ir(1)-C(01)	-61.9(3)
C(31A)-P(1)-Ir(1)-O(03)	151.7(4)
C(11A)-P(1)-Ir(1)-O(03)	-90.2(5)
C(21)-P(1)-Ir(1)-O(03)	29.1(5)
C(31A)-P(1)-Ir(1)-O(03)#1	-30.2(4)
C(11A)-P(1)-Ir(1)-O(03)#1	87.9(5)
C(21)-P(1)-Ir(1)-O(03)#1	-152.8(5)
C(31A)-P(1)-Ir(1)-O(02)	-119.3(3)
C(11A)-P(1)-Ir(1)-O(02)	-1.2(3)
C(21)-P(1)-Ir(1)-O(02)	118.1(3)
C(31A)-P(1)-Ir(1)-P(1)#1	60.7(3)
C(11A)-P(1)-Ir(1)-P(1)#1	178.8(3)
C(21)-P(1)-Ir(1)-P(1)#1	-61.9(3)

Symmetry transformations used to generate equivalent atoms:

#1 -x,y,-z+1/2

Table 2-6. Hydrogen bonds for [Ir(acac)(CO)(PCy₃)₂] [Å and °].

D-H...A	d(D-H)	d(H...A)	d(D...A)	<(DHA)
C(12A)-H(12A)...O(02)	0.99	2.85	3.63(2)	136
C(26)-H(26B)...O(01)	0.99	2.26	2.864(9)	118.5
C(32A)-H(32B)...O(01)	0.99	1.92	2.770(8)	141.9
C(32A)-H(32B)...O(01)	0.99	1.92	2.770(8)	141.9

Symmetry transformations used to generate equivalent atoms:

#1 -x,y,-z+1/2

APPENDIX II

SUPPLEMENTARY DATA TO THE KINETIC STUDY

Table 2-1: k_{obs} values for the different runs for the 1st reaction between [Ir(acac)(CO)₂] and PPh₃ followed *via* Stopped-flow spectroscopy with different concentrations of PPh₃ in MeOH at -10 °C, k_{obs1} represents the 1st reaction.

(10 ³) [PPh ₃] (M)	k_{obs1} (s ⁻¹)				
	Run 1	Run 2	Run 3	Run 4	Ave
1.0	89.3(7)	96.1(1)	91.3(8)	108(2)	92(2)
1.5	139(2)	134(1)	132(2)	142(3)	137(4)
2.0	180(3)	183(2)	192(2)	181(2)	184(4)
2.5	229(5)	237(2)	228(4)	233(2)	232(7)
3.0	280(3)	281(4)	264(2)	294(5)	280(8)

Table 2-2: k_{obs} values for the different runs for the 1st and 2nd reaction between [Ir(acac)(CO)₂] and PPh₃ followed *via* Stopped-flow spectroscopy with different concentrations of PPh₃ in MeOH at -20 °C, k_{obs1} represents the 1st reaction and k_{obs2} the second.

(10 ³) [PPh ₃] (M)	k_{obs1} (s ⁻¹)				
	Run 1	Run 2	Run 3	Run 4	Ave
1.0	67.4(4)	66.1(2)	64.3(3)	65.3(4)	65.8(7)
1.5	113(1)	109(1)	101.9(6)	107.6(9)	108(2)
2.0	138(1)	144(2)	-	141(2)	141(2)
2.5	201(2)	193(2)	200(2)	198(2)	198(4)
3.0	251(4)	237(3)	242(2)	254(2)	246(6)
(10 ³) [PPh ₃] (M)	k_{obs2} (s ⁻¹)				
	Run 1	Run 2	Run 3	Run 4	Ave
1.0	18.4(4)	15.4(3)	16.4(4)	15.3(5)	16(1)
1.5	30(3)	24(3)	24(1)	19(4)	24(5)
2.0	28(2)	29(4)	-	29(5)	29(7)
2.5	34(1)	35(2)	34(1)	34(1)	34(3)
3.0	47(6)	42(4)	39(1)	39(1)	42(7)

APPENDIX II

Table 2-3: k_{obs} values for the different runs for the 1st and 2nd reaction between [Ir(acac)(CO)₂] and PPh₃ followed via Stopped-flow spectroscopy with different concentrations of PPh₃ in MeOH at -30 °C, k_{obs1} represents the 1st reaction and k_{obs2} the second.

	$k_{\text{obs1}} \text{ (s}^{-1}\text{)}$				
$(10^3) [\text{PPh}_3] \text{ (M)}$	Run 1	Run 2	Run 3	Run 4	Ave
1.0	63(2)	56(1)	59.8(3)	55(1)	59(3)
1.5	87.7(3)	85.3(3)	86.7(2)	83.1(3)	86(1)
2.0	132(1)	121(1)	119(1)	114(1)	122(3)
2.5	163(2)	183(2)	186(2)	160(3)	173(5)
3.0	221(3)	204(3)	205(4)	205(5)	209(8)
5.0	341(5)	330(9)	342(4)	314(9)	332(8)
	$k_{\text{obs2}} \text{ (s}^{-1}\text{)}$				
$(10^3) [\text{PPh}_3] \text{ (M)}$	Run 1	Run 2	Run 3	Run 4	Ave
1.0	31(1)	27(2)	31.7(2)	26(2)	29(3)
1.5	37(1)	32(1)	31(1)	36(1)	34(1)
2.0	39(2)	34(3)	24(3)	22(5)	30(7)
2.5	38(3)	45(2)	60(2)	38(5)	45(6)
3.0	55(3)	45(3)	45(5)	34(9)	45(9)
5.0	62(1)	63(3)	68(1)	66(4)	65(5)

Table 2-4: k_{obs} values for the different runs for the 1st and 2nd reaction between [Ir(acac)(CO)₂] and PPh₃ followed via Stopped-flow spectroscopy with different concentrations of PPh₃ in MeOH at -40 °C, k_{obs1} represents the 1st reaction and k_{obs2} the second.

	$k_{\text{obs1}} \text{ (s}^{-1}\text{)}$				
$(10^3) [\text{PPh}_3] \text{ (M)}$	Run 1	Run 2	Run 3	Run 4	Ave
1.0	48(2)	42(1)	44(1)	45(1)	44(3)
1.5	70(2)	69(1)	79(2)	67(1)	71(3)
2.0	111(1)	111(1)	113(1)	119(2)	114(3)
2.5	149(1)	152(2)	143(1)	142(1)	147(3)
3.0	188(1)	188(1)	187(3)	188(1)	188(3)
5.0	309(3)	290(4)	284(3)	288(3)	293(7)

APPENDIX II

$(10^3) [\text{PPh}_3] \text{ (M)}$	$k_{\text{obs}2} \text{ (s}^{-1}\text{)}$				
	Run 1	Run 2	Run 3	Run 4	Ave
1.0	21(1)	17(1)	18(2)	20(1)	19(3)
1.5	20(3)	13(2)	31(2)	19(2)	21(5)
2.0	26(1)	25(1)	30(2)	37(2)	29(3)
2.5	30(1)	34(2)	27(1)	27(1)	29(3)
3.0	31(1)	32(1)	38(2)	30(1)	33(3)
5.0	33.9(3)	34.6(3)	36.4(3)	35.2(3)	35(1)

Table 2-5: $\ln(k_1/T)$ and $1/T$ values as used for the Eyring plot (Figure 6-6) for the first reaction observed on Stopped-flow spectroscopy for the reaction between $[\text{Ir}(\text{acac})(\text{CO})_2]$ and PPh_3 .

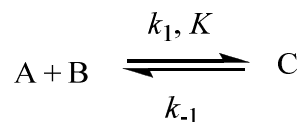
$\ln(k_1/T)$	$1/T \text{ (K}^{-1}\text{)}$
5.863082	0.003802281
5.724172	0.003952569
5.608706	0.004115226
5.523237	0.004291845

Table 2-6: $\ln(k_3/T)$ and $1/T$ values as used for the Eyring plot (Figure 6-8) for the second reaction observed on Stopped-flow spectroscopy for the reaction between $[\text{Ir}(\text{acac})(\text{CO})_2]$ and PPh_3 .

$\ln(k_3/T)$	$1/T \text{ (K}^{-1}\text{)}$
-0.34383	0.003952569
-0.93378	0.004115226
-1.59838	0.004291845

Derivation of Eq. 6.2.

Consider the reaction:



The rate of the reaction above can be expressed as

$$\text{Rate} = k_1[\text{A}][\text{B}] - k_{-1}[\text{C}] \quad 2.1$$

where [A] = concentration of reactant A

[B] = concentration of reactant B

[C] = concentration of product C

Under pseudo-first order conditions where [B] >> [A], Eq 2.1 simplifies to

$$-\frac{d[A]}{dt} = \frac{d[C]}{dt} = k'_1[A] - k_{-1}[C] \quad 2.2$$

where $k'_1 = k_1[B]$

If the reaction reaches equilibrium, the following equation would be true

$$-\frac{d[A]_{eq}}{dt} = \frac{d[C]_{eq}}{dt} = 0 \quad 2.3$$

where [A] = concentration of reactant A at equilibrium

[C] = concentration of product C at equilibrium

From Eq. 2.1 and 2.3 we get

$$\frac{k'_1}{k_{-1}} = \frac{[C]_{eq}}{[A]_{eq}} \quad 2.4$$

If the initial concentration of A is given the value of A_0 we can manipulate Eq. 2.4 to

$$\frac{k'_1}{k_{-1}} = \frac{[A]_0 - [A]_{eq}}{[A]_{eq}}$$

$$[A]_{eq} = \left(\frac{k_{-1}}{k'_1 + k_{-1}} \right) [A]_0 \quad 2.5$$

We also apply this manipulation to Eq. 2.2

$$\frac{d[A]}{dt} = -k'_1[A] + k_{-1}([A]_0 - [A])$$

$$\begin{aligned}
 &= -k'_1[A] + k_{-1}[A]_0 - k_{-1}[A] \\
 &= -(k'_1 + k_{-1})[A] + k_{-1}[A]_0 \\
 &= -(k'_1 + k_{-1}) \left([A] - \frac{k_{-1}}{k'_1 k_{-1}} [A]_0 \right) \qquad \qquad \qquad \mathbf{2.6}
 \end{aligned}$$

From Eq. 2.5 and 2.6 we get

$$\frac{d[A]}{dt} = -(k'_1 + k_{-1})([A] - [A]_{eq}) \qquad \qquad \qquad \mathbf{2.7}$$

By grouping the variables in Eq. 2.7, we can then integrate to remove the differential signs

$$\begin{aligned}
 \frac{d[A]}{[A] - [A]_{eq}} &= -(k'_1 + k_{-1}) \\
 \int_{[A]_0}^{[A]} \frac{d[A]}{[A] - [A]_{eq}} &= -(k'_1 + k_{-1}) \int_{t=0}^{t=t} dt \\
 \ln ([A] - [A]_{eq}) \Big|_{[A]_0}^{[A]} &= -(k'_1 + k_{-1}) [t]_{t=0}^{t=t} \\
 \ln \left(\frac{[A]_0 - [A]_{eq}}{[A] - [A]_{eq}} \right) &= (k'_1 + k_{-1}) t \qquad \qquad \qquad \mathbf{2.8}
 \end{aligned}$$

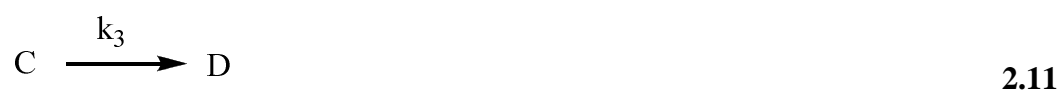
The sum of the two constants ($k'_1 + k_{-1}$) is also a constant. By definition this constant is the observed rate, k_{obs} . Thus we have

$$k_{obs} = k'_1 + k_{-1}$$

Therefore

$$k_{\text{obs}} = k_1[\text{B}] + k_{-1} \quad 2.9$$

Derivation of Eq. 6.9.



The rate of Eq. 2.11 can be expressed as:

$$k_{\text{obs}} = k_3[\text{C}] \quad 2.12$$

where $[\text{C}]$ = concentration of reactant C

The equilibrium constant, K_2 , can be written as

$$K_2 = \frac{[\text{C}]}{[\text{A}][\text{B}]} \quad 2.13$$

where $[\text{A}]$ = concentration of reactant A, $[\text{B}]$ = concentration of reactant B and $[\text{C}]$ = concentration of reactant C

Eq. 2.13 can be easily manipulated to produce Eq. 2.14.

$$[\text{A}] = \frac{[\text{C}]}{K_2[\text{B}]} \quad 2.14$$

Because the exact concentration of the activated complex is unknown the total metal concentration is given with all possible metal complexes present:

APPENDIX II

$$[M]_{tot} = [A] + [C] \quad 2.15$$

Combination of Eq. 2.14 and 2.15 giving the total metal concentration in equilibrium as

$$[M]_{tot} = \frac{[C]}{K_2[B]} + [C] \quad 2.16$$

That can be rewritten as

$$[C] = \frac{K_2[B]}{1+K_2[B]} [M]_{tot} \quad 2.17$$

By substitution of Eq. 2.17 into Eq. 2.12 the metal concentration is given in terms of the reaction rate as

$$Rate = \frac{k_3 K_2 [B]}{1 + K_2 [B]} [M]_{tot} = k_{obs} [M]_{tot} \quad 2.18$$

and k_{obs} as

$$k_{obs} = \frac{k_3 K_2 [B]}{1 + K_2 [B]} \quad 2.19$$